INSTITUTE OF BIOLOGY, BIOTECHNOLOGY
AND ENVIRONMENTAL PROTECTION
FACULTY OF NATURAL SCIENCES
UNIVERSITY OF SILESIA IN KATOWICE

NIKOLINA SKOWROŃSKA

Album number: 8457

DOCTORAL DISSERTATION

FORMATION OF VASCULAR PATTERN IN *ARABIDOPSIS* LEAF PRIMORDIA

THESIS SUPERVISOR:
dr hab. Agata Burian, prof. UŚ

Katowice 2023

Key words: *Arabidopsis thaliana*, vascular system, leaf, auxin, anatomy

Oświadczenie (Declaration)

Oświadczam, że ww. praca dyplomowa:

• nie narusza praw autorskich w rozumieniu ustawy z dnia 4 lutego 1994 r. o prawie autorskim i prawach pokrewnych (tekst jednolity Dz. U. z 2006 r. Nr 90, poz. 631, z poźn. zm.) oraz dóbr osobistych chronionych prawem cywilnym,

• nie zawiera danych i informacji, które uzyskałem/łam w sposób niedozwolony,

• nie była podstawą nadania dyplomu uczelni wyższej lub tytułu zawodowego ani mnie, ani innej osobie.

Oświadczam również, że treść pracy dyplomowej zamieszczonej przeze mnie w Archiwum Prac Dyplomowych jest identyczna z treścią zawartą w wydrukowanej wersji pracy.

Jestem świadoma odpowiedzialności karnej za złożenie fałszywego oświadczenia.

data podpis autora pracy

Podziękowania (Acknowledgements)

W sposób szczególny składam serdeczne podziękowania
Pani dr hab. Agacie Burian, prof. UŚ za opiekę naukową,
nieocenioną pomoc oraz za cenne uwagi merytoryczne,
które przyczyniły się do powstania niniejszej rozprawy doktorskiej.
Dziękuję także za możliwość poszerzenia wiedzy,
wsparcie oraz wyrozumiałość.

Pragnę także podziękować mojej Rodzinie,
przede wszystkim za ich ogromne wsparcie i cierpliwość
oraz wiarę w moje możliwości.

This work was supported by the research grant SONATA BIS6 (2016/22/E/NZ3/00342) from the National Science Centre, Poland.

Contents:

1. INTRODUCTION 6

1.1. The vascular system in leaves 6

1.2. Shoot apical meristem organization 7

1.3. Auxin biosynthesis, transport, and signaling 10

1.4. Leaf initiation at the shoot apical meristem. The formation of leaf midvein 14

1.5. Mechanisms of polar auxin transport 16

1.6. The formation of higher order vascular strands in leaf primordia 19

1.7. Experimental testing the role of auxin transport in the formation of vascular pattern 24

1.8. The role of auxin sources and auxin sink in the formation of vascular pattern 26

1.9. The role of auxin biosynthesis in development of leaf vascular system 28

1.10. Cellular basis of vascular strand differentiation 30

2. AIMS 34

3. MATERIAL AND METHODS 35

3.1. Plant material and growth conditions 35

3.2.1. Plant dissection and live imaging 36

3.2.2. Clearing of leaf primordia 37

3.2.3. Auxin microapplication and global treatment 38

3.2.4. Suppression of polar auxin transport by the NPA treatment 39

3.2.5. Cell ablations 39

3.2.6. Laser confocal microscopy 40

3.2.7. Image analysis 41

4. RESULTS 44

4.1. Visualization of vascular system initiation by different transgenic lines 44

4.2. Quantification of the DR5v2 expression at apical and lateral auxin sources 47

4.3. Expression patterns of auxin biosynthesis genes 49

4.4. Development of procambial cells 52

4.5. Development of procambial strand pattern 57

4.6. Auxin transcriptional response and the differentiation of procambial cells 60

4.7. Chemical disturbing of auxin sources – auxin microapplication 63

4.8. Chemical disturbing of auxin sources – global auxin treatment 68

4.9. Suppression of polar auxin transport – NPA treatment 74

4.10. Genetic disturbance of auxin sources – *pin1* and *cuc2 cuc3* mutants 80

4.11. Mechanical disturbance of auxin sources and pre-existing strands – cell ablations 83

5. DISCUSSION 95

5.1. Methods in studying the formation of leaf vasculature in *Arabidopsis* 95

5.2. The generation and maintenance of auxin sources at leaf primordia 98

5.3. The midvein development 100

5.4. Development of higher-order strands and loops 102

5.5. The relation between vascular pattern development and primordium growth 106

6. CONCLUSIONS 109

7. REFERENCES 111

8. SUMMARY 124

9. STRESZCZENIE 125

1. INTRODUCTION

1.1. The vascular system in leaves

Plant vascular system plays a crucial role in transport of substances and communication between distant regions of a plant body. Vascular tissues are organized in a network of strands which contains two conducting tissues: phloem and xylem (Esau 1965). Water and mineral nutrients are moved from the roots towards the shoot *via* xylem, while carbohydrates produced in photosynthetic tissues are distributed to different plant organs *via* phloem. The vascular system is also responsible for the propagation of signalling molecules such as hormones, proteins, or small RNAs. Beside the long-distance transport, the vasculature provides a mechanical support for a plant body.

One of the most striking feature of the plant vascular system is its continuity. To maintain its continuity during plant ontogeny and in the interaction with the environment, the vascular system need to be plastic (Dengler 2000; Scarpella 2017). For example, new vascular strands and their connections are constantly formed during organogenesis and afterwards during subsequent organ development. Furthermore, after a tissue wounding, new strands are formed *de novo* bypassing the wounding site to restore vascular continuity (Sachs 1981).

Especially in leaves, vascular patterns draw an attention due to their variability and beauty. In dicots (like *Arabidopsis*), leaf vasculature forms a hierarchical branching system, where new veins diverge from the pre-existing ones. In particular, the primary vein (midvein), which is continuous with the underlying vasculature of the stem, extends along proximo-distal leaf axis (**Fig. 1.1A**). The second-order veins branch from the midvein, and the third-order veins branch from the second-order veins. This pattern is iterated through even several orders in some plants (Nelson and Dengler 1997). The second- or higher-order veins can connect to the other veins forming vascular loops, or remain free-ending. In contrast to the vasculature in dicots, veins in monocot leaves (like *Zea mays*) diverge already at the leaf base, then extend parallel along entire leaf blade, and converge at apical leaf region (**Fig. 1.1B**). During leaf development, multiple minor transverse connection veins are formed between the parallel veins. Although, the general organization of the vasculature in leaves is predictable, the precise arrangement of vascular strands and their connections show some variability (especially in dicots) as they strongly depend on local signals (Scarpella and Meijer 2010).

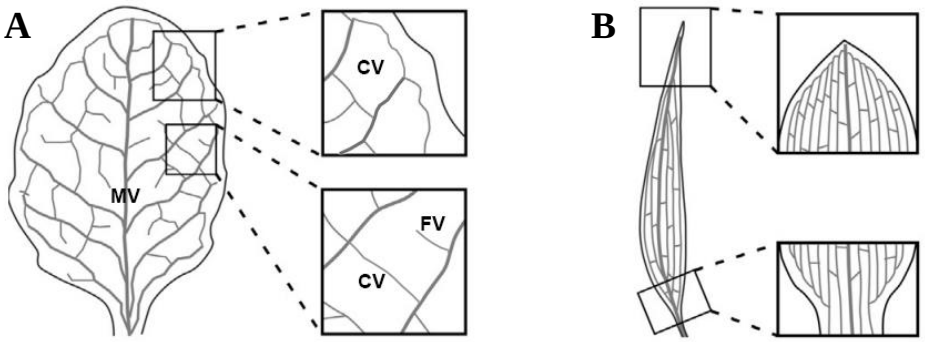

Fig. 1.1. Vascular patterns in dicot and monocot leaves.

(**A**) In a typical dicot leaf, the higher-order veins branch from lower-order veins. For example, the second-order veins branch from the single primary vein (MV, midvein). The higher-order veins either connect to the other veins (connected veins, CV) or stay free-ending (FV). (**B**) In a typical monocot leaf, veins extend parallel to each other along most of a leaf blade and are connected to each other through minor transverse veins (Linh et al. 2018, modified).

Vascular cells differentiate from a primary meristematic tissue called procambium, which serves as a precursor to both phloem and xylem tissues. Thus, the first step in the vasculature development and in the generation of vascular patterns is the specification of procambial cells within the ground tissues. The mechanism of this process has been extensively studied in the recent years especially in *Arabidopsis* leaves. All these studies indicate that the main factor controlling the initiation of veins is auxin (Berleth et al. 2000; Smith and Bayer 2009; Biedroń and Banasiak 2018; Perico et al. 2022). There is also a general agreement that the vasculature initiation and leaf formation are closely related (Dengler 2006; Banasiak and Gola 2023). Namely, the first element of a leaf vasculature - the midvein - is initiated almost simultaneously with the emergence of leaf primordia at the shoot apical meristem.

1.2. Shoot apical meristem organization

The shoot apical meristem (SAM) located at the tip of shoots is the center of organization of plant development. In *Arabidopsis*, the SAM can be composed of few hundreds small constantly growing and dividing cells, that ultimately differentiate and form different organs such as stem, leaves or flowers through the entire plant lifetime. Throughout the vegetative phase of plant development, the SAM produces primordia which give rise to leaves, while

during the reproductive phase the SAM produces floral meristems, i.e. the primordia which give rise to flowers (Ha et al. 2010).

Generally, the SAM structure is maintained despite highly dynamic cell behavior, which involves constant displacement of cells from the meristem center into the periphery (Kwiatkowska 2004). The SAM in *Arabidopsis* (as in other dicots) has a layered structure, that means that cells close to the SAM surface are organized into layers and form so called tunica (Aichinger et al. 2012). Usually, the tunica consists of two cell layers. The outermost layer (L1) gives rise to the epidermis, while the below lying L2 layer contributes to subepidermal tissues and germ cells. The layered structure of the SAM is a consequence of anticlinal (perpendicular to the surface) cell divisions. In contrast, in inner cells forming so called corpus (L3), cell division plane is not restricted and cells are dividing anticlinally and periclinally (parallel to the surface). These cells ultimately give rise to vascular tissues and the pith. Thus, the SAM structure can determine cell fates.

The SAM can be also divided into distinct functional zones: central and peripheral zones, and the rib meristem zone (**Fig. 1.2**). The central zone is located at the SAM summit and forms a niche for a slowly dividing initial cells (Lyndon 1990). These cells have a capacity for both self-renewing and the generation of cells which further form new tissues (Heidstra and Sabatini 2014). Thus, initial cells are a source of cells at the SAM. After the division of a initial cell, one descendent cell maintains the position at the SAM summit and retains the identity of initial cell, while the other descendent cell "leaves" the summit, and due to the SAM growth is displaced to the periphery, where it enters the differentiation pathway (Burian 2021).

The central zone is surrounding by the peripheral zone, which consists of rapidly growing and dividing cells. The peripheral zone is a place, where cell fates are specified into the formation of a stem or lateral organs such as leaves or flowers, and primordia of these organs are initiated. The rib meristem zone localized below the central and peripheral zones, also consists of fast growing and dividing cells (Kwiatkowska 2004). This zone generates longitudinal files of cells (ribs) due to cell divisions perpendicular to the long shoot axis (Esau 1965). Between initial cells in the central zone and the rib meristem zone, there is a small group of cells forming so called organizing center, which is a source of signals for the maintenance of initial cells (Zhang et al. 2021).

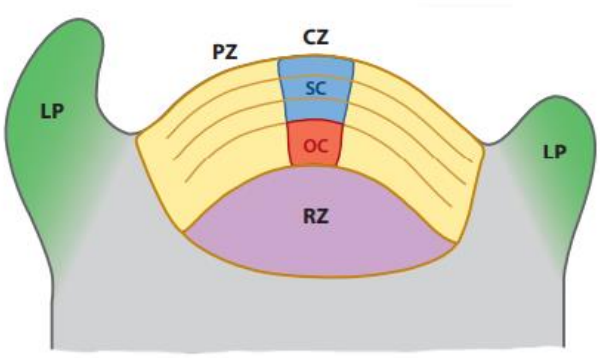

Fig. 1.2. The shoot apical meristem organization.

The figure illustrates the SAM structure: CZ - central zone; SC – initial cells; PZ – peripheral zone; RZ – rib meristem zone; OC – organizing center; LP- leaf primordia (Aichinger et al. 2012, modified).

The functioning of meristematic cells is genetically regulated by transcription factors. The maintenance of initial cells and their self-renewal is controlled by a negative feedback loop between *CLAVATA* (*CLV*) and *WUSCHEL* (*WUS*) genes. The *CLV* genes are expressed in initial cells and their closest neighbors, and encode a receptor-like kinase (CLV1) and a small peptide (CLV3) (Carles and Fletcher 2003). The CLV3 is thought to specify initial cells, but only in the presence of other factors inducing the SAM formation, and to regulate the functioning of initial cells related to the entering the differentiation pathway (Schoof et al. 2000). The *WUS* gene encodes a homeodomain transcription factor, which is expressed in the organizing center underlying the initial cells. The WUS is involved in the maintenance of initial cells and prevents their premature differentiation (Mayer et al. 1998). This transcription factor is moving through plasmodesmata to the above *CLV*-expressing domain, where it induces the *CLV3* expression. The CLV1, in turn, after binding the CLV3 peptide inhibits the *WUS* expression. Thus, this negative feedback loops enables to balance the amount of initial cells at the SAM. Independently of *CLV* and *WUS* genes, meristematic cells are also regulated by other transcription factor – SHOOTMERISTEMLESS (STM), which maintains meristematic cell identity and inhibits their differentiation (Endrizzi et al. 1996). In contrast to *CLV* and *WUS*, the *STM* is expressed in all meristematic cells and its downregulation at the peripheral zone is the first landmark of cell specification into lateral organs.

The process of organ formation at the SAM peripheral zone is closely related to plant hormone auxin. Local high concentrations of auxin at the SAM surface specify the position of new organs well ahead any physical signs of organogenesis (Reinhardt et al. 2003).

1.3. Auxin biosynthesis, transport, and signaling

Auxin (IAA, indole-3acetic acid) is synthesized in above-ground parts of plants such as shoot apices, young leaves or flowers, and seeds in a tryptophan (TRP)-dependent or -independent pathways (Wang et al. 2015). The TRP-independent pathway is not fully understood, but instead four TRP-dependent pathways have been identified. The best known is the two step tryptophan aminotransferase (TAA) / YUCCA (YUC) pathway (**Fig. 1.3**). In this pathway, first, TAA enzymes removes the amino group from TRP and form indole-3-pyruvate (IPA). Then, the IPA is decarboxylated by YUC enzymes to produce IAA (Zhao 2014). In *Arabidopsis*, 4 *TAA* and 11 *YUC* genes have been identified (Cao et al. 2019).

Fig. 1.3. Tryptophan-dependent auxin biosynthesis pathway (Perico et al. 2021, modified).

Auxin, which is synthesized in source organs, is then transported passively or actively to the different parts of plants, or to different regions within the same organs. Long-distance auxin transport occurs *via* the mature phloem together with photosynthetic assimilates, while short-distance directional auxin transport (or polar auxin transport, PAT) occurs from cell-to-cell passively by diffusion through the plasma membranes and plasmodesmata, or actively by carrier proteins (Friml and Wiśniewska 2005; Adamowski and Friml 2015; Perico et al. 2021). Passive auxin transport through plasma membranes is strongly affected by a local pH. Namely, in acidic environment, for example, in the apoplast where pH is about 5.5, auxin is partially protonated to lipophilic form IAAH, and in this form it can easily diffuse across the lipid plasma membrane from the apoplast to the cell interior (auxin influx) (**Fig. 1.4**). However, in the cell cytoplasm, where the pH is more alkaline (pH 7), auxin occurs in unprotonated hydrophilic form IAA^-, which cannot cross the membrane. Thus, auxin transport from the cytoplasm to the apoplast (auxin efflux) needs to be mediated by carrier proteins. Auxin carrier proteins can also

participate in auxin influx, as an additional mechanism of auxin transport from the apoplast to the cytoplasm.

Several auxin efflux and influx carrier proteins were identified in *Arabidopsis*. Among auxin efflux carriers, the best known is PIN-FORMED1 (PIN1), which regulates the polar auxin transport in several developmental processes such as embryogenesis, lateral organ formation in the shoot and root, the initiation and differentiation of the vascular system (Petrasek and Friml 2009). In many cells, the localization of PIN1 in the plasma membrane is polar, which determines the direction of auxin flow (Wiśniewska et al. 2006). While the PIN1 acts as auxin efflux in the plasma membrane, other carrier proteins can be localized in the endoplasmic reticulum and participate in both auxin influx and efflux. There are PIN-LIKES (PILS) carriers at the endoplasmic reticulum, which maintain intracellular auxin homeostasis, but only by auxin influx (Barbez et al. 2012). The *PIN1* gene is one out of 8 other *PIN* genes belonging to the *PIN* family, which differs in the length of hydrophilic loop and also in the cellular localization. The PIN1, PIN2, PIN3, PIN4, and PIN7 proteins with long hydrophilic loops are localized in cell plasma membranes, while PIN5, PIN6, and PIN8 which have short hydrophilic loops are localized in the membrane of the endoplasmic reticulum. The latter possibly maintain a balance of auxin levels in the cell cytoplasm by the regulation auxin exchange between the endoplasmic reticulum and the cytoplasm (Zažímalová et al. 2010).

The other carriers which play a role in auxin efflux, are ATP-binding cassette subfamily B (ABCB)-type transporters (Petrasek and Friml 2009). Some of these proteins have a binding affinity to the auxin transport inhibitor 1-naphthylphthalamic acid (NPA) (Murphy et al. 2002). However, ABCB proteins probably do not have a direct effect on the polar auxin transport due to the lack of polar localization in the plasma membrane (Keneda et al. 2011). Nonetheless, they have been reported to regulate embryogenesis, root development or leaf shape (Petrasek and Friml 2009).

In addition to auxin diffusion into the cell cytoplasm, auxin influx can be facilitated by plasma membrane-localized AUXIN RESISTANT1/LIKE-AUX (AUX1/LAX) carrier proteins (Petrasek and Friml 2009; Peret et al. 2012). In *Arabidopsis*, 4 auxin influx carriers have been described: AUX1, LAX1, LAX2, and LAX3. All of them play role in the regulation of phyllotaxis, while AUX1 and LAX3 play also a role in lateral root development.

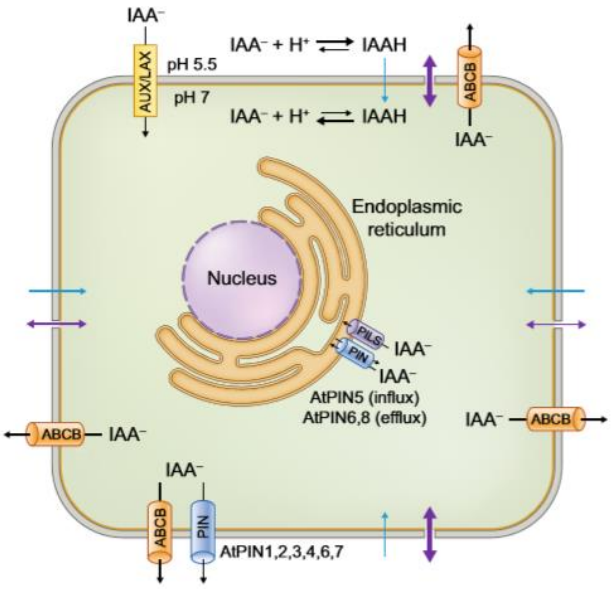

Fig 1.4. Auxin transport pathways in an *Arabidopsis* cell.

Purple arrows indicate bidirectional auxin movement into and out of a cell *via* plasmodesmata; blue arrows indicate auxin diffusion *via* the plasma membrane. Auxin efflux and influx carrier proteins are shown: PIN transporters (blue); ABCB transporters (orange), PIN-LIKES (PILS) transporters (purple), AUX/LAX transporters (yellow) (Perico et al. 2021, modified).

Once auxin enters the cell interior, it triggers diverse and context-dependent responses by changing the expression of auxin-regulated genes. These genes contain Auxin Response Elements (AREs), which in turn are bound by Auxin Response Factors (ARFs) transcription factors (Leyser 2018). The best understood signal transduction pathway from auxin to gene expression involves TRANSPORT INHIBITOR RESPONSE/AUXIN F-BOX (TIR1/AFB)-mediated ubiquitination of AUX/IAA transcriptional repressor family (**Fig. 1.5**) (Kubes and Napier 2019). At low auxin concentration, AUX/IAA repressors together with TOPLESS (TPL) co-repressors interact with ARFs and inhibit their activity. When auxin concentration is high, auxin binds to the TIR1/AFB that increases the affinity of this protein for AUX/IAA repressors. Consequently, this process leads to the ubiquitination and degradation of AUX/IAAs and releasing ARFs to regulate auxin-responsive genes. In *Arabidopsis* there are 23 identified ARFs that bind to specific AREs with the sequence TGTCTC in the promoters of auxin-regulated genes (Vernoux et al. 2011). Despite the fact, that auxin usually activates transcription, most of ARFs act as transcriptional repressors and only five of them (ARF5/MONOPTEROS, ARF6, ARF7, ARF8, ARF19) are activators.

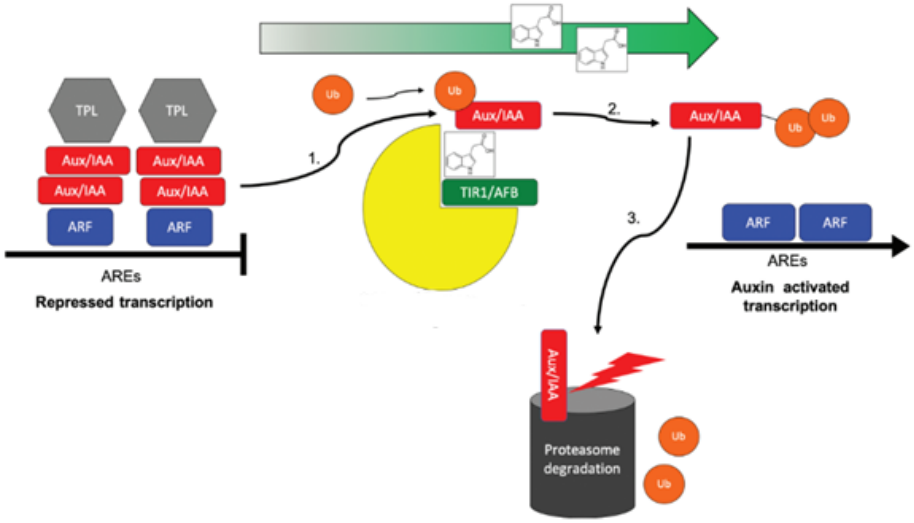

Fig. 1.5. Canonical TIR1/AFB-dependent auxin signaling pathway.

The green arrow indicates increasing auxin concentrations (Kubes and Napier 2019, modified).

This canonical mechanism of auxin perception was used to generate auxin reporters, such as DR5, which enables the visualization of auxin distribution and auxin transcriptional response in plant cells, tissues, and organs (Sabatini et al. 1999; Benkova et al. 2003). The DR5 is the most commonly used auxin reporter applied in *Arabidopsis*, maize, soybean, tomato, poplar and many other plant species (Chen et al. 2013). This synthetic auxin-induced promoter contains several ARF-binding sites driving the expression of a reporter gene. The DR5 is expressed in cells with a high auxin concentration, for example in lateral root primordia, flower or leaf primordia at the SAM, and in initiating vascular strands (Jedlickova et al. 2022). It needs to be noted, however, that the DR5 expression shows indirectly auxin levels, because its expression depends also on the activity of several upstream elements in auxin signaling pathway (TIR1/AFB, AUX/IAAs, ARFs). The original version of the DR5 promoter has been modified to increase its affinity to auxin, and in consequence, to detect auxin accumulation and response in cells or tissues, where the expression of the original DR5 was low (Liao et al. 2015). In comparison to the original DR5, the new DR5 version (DR5v2) was highly and more broadly expressed in *Arabidopsis* embryos (in particular in incipient cotyledons and vasculature), roots (metaxylem, pericycle, lateral root cap, epidermal cells), and shoot apex (meristem L1 and surrounding cells, leaf incipient midvein).

1.4. Leaf initiation at the shoot apical meristem. The formation of leaf midvein

The process of leaf formation in dicots can be divided into four stages (**Fig. 1.6**) (Du et al. 2018). At the first stage, a small group of cells at the SAM peripheral zone are specified and form so called incipient (future) primordium (**Fig. 1.6A**). At the second stage, the primordium after its initiation is growing in the distal direction that leads to the establishment of leaf proximal-distal axis (**Fig. 1.6B**). In the next stage, a leaf blade and a petiole are initiated, and the growth is especially high along the margins that leads to the blade outgrowth (**Fig. 1.6C**). At the final stage, the growth of leaf blade occurs in the whole blade region (intercalary growth) resulting in overall leaf expansion (**Fig. 1.6D**).

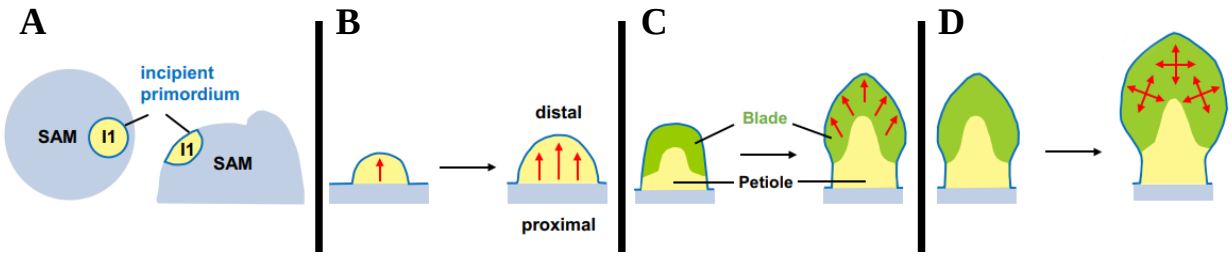

Fig. 1.6. Leaf morphogenesis in dicots.

(**A**) Stage 1: Cell specification at the SAM peripheral zone. The top (left) and front (right) views of the SAM . I1, the oldest incipient primordium. (**B**) Stage 2: Distal primordium growth. (**C**) Stage 3: Blade and petiole initiation. (**D**) Stage 4: Intercalary primordium growth. Arrows indicate growth direction (Du et al. 2018, modified).

The formation of leaves at the SAM peripheral zone is triggered by local auxin maxima, which are generated due to the polar auxin transport (Kuhlemeier 2007; Reinhardt and Gola 2022). Although the auxin transport through plant tissues can be mediated by different auxin influx and efflux carrier proteins, the efflux carrier PIN1 is a major regulator of auxin transport at the SAM. According to the model proposed by Reinhardt et al. (2003) for *Arabidopsis*, that was further developed for tomato (Bayer et al. 2009), auxin is transported acropetally at the SAM (towards the SAM summit) *via* PIN1 proteins, which are polarly localized at L1 cell layer, in particular at the apical side of these cells (**Fig. 1.7A**). At the SAM surface, auxin transport is affected by pre-existing leaf primordia, where auxin is directed from the L1 to inner cells, that in a consequence results in auxin depletion from the cells surrounding primordia (**Fig. 1.7A**, P_1, P_2). At a certain distance from pre-existing primordia, the PIN1 localization is convergent

(forming so called convergence points), that leads to local auxin accumulation marking the sites of incipient primordia (**Fig. 1.7A**, I_1). This process is also correlated with the local upregulation of the DR5 expression (Yoshida et al. 2011). Thus, PIN1-convergence points and local DR5 maxima at the SAM surface are the earliest landmarks of leaf initiation, that appear well ahead of other signs of primordium formation, such as physical bulging from the meristem surface.

The process of leaf formation is coupled with the initiation of leaf midvein, that at least in *Arabidopsis* and tomato always starts before the emergence of primordia. In particular, soon after the formation of local auxin maxima at the SAM surface, the PIN1 polarization at L1 is changing from the apical into basal, which gradually spreads also to underlying cells (**Fig. 1.7B**, left panel) (Bayer et al. 2009). This results in redirecting auxin transport into inner tissues and the formation of an auxin canal with a high auxin concentration, which specifies the future midvein (**Fig. 1.7B**, right panel). Subsequently, the auxin canal extends downward and joins the pre-existing vasculature of the stem. Noteworthy, despite that the midvein is initiating by the basipetal auxin transport from the SAM surface, the differentiation of the midvein proceeds acropetally (Dengler 2006).

Furthermore, it has to be noted, that although the PIN1 was proposed to be major regulator of the polar auxin transport in the specification of incipient primordia and the midvein, the PIN1 is not absolutely necessary in these processes. Despite the lack of properly functioning PIN1, in the *pin1* mutant the leaves with well-developed vasculature are formed (Mattson et al. 1999; Berleth et al. 2000; Scarpella et al. 2006; Guenot et al. 2012; Verna et al. 2019). On the other hand, PIN1 carriers are necessary for the regular arrangement of leaves (phyllotaxy) at the SAM and the proper pattern of the leaf vasculature.

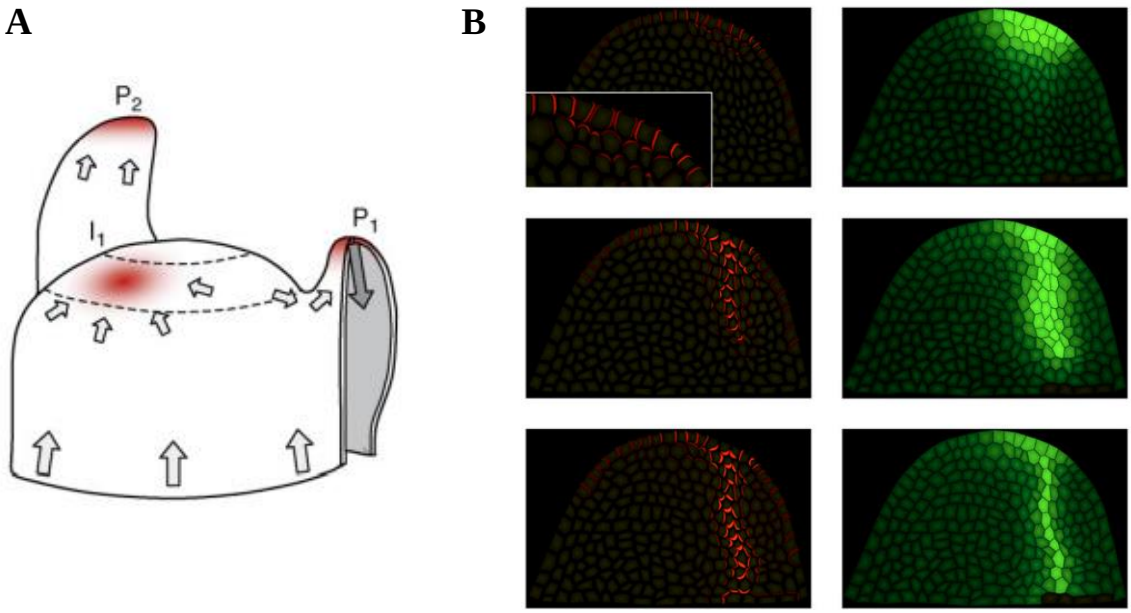

Fig. 1.7. Models of leaf primordia initiation and the formation of leaf midvein.

(**A**) The initiation of leaf primordia at the SAM. The polarization of the PIN1 directs the polar auxin transport (arrows), which leads to the auxin accumulation (red) at the sites of primordium initiation (I1). The PIN1 polarization is basipetal in emerging primordia (P_1, P_2), which drains auxin into inner cells (Kuhlemeier 2007, modified). (**B**) The formation of the leaf midvein. Images from upper to bottom show events at different time points. Left panel: The PIN1 polarization (red) is acropetal at the SAM surface (upper) and subsequently changes into basipetal (middle and bottom). Right panel: Auxin (light green) is accumulated at the SAM surface (upper) and subsequently is canalized into inner cells (middle and bottom) towards pre-existing stem vasculature (dark grey cells at the bottom right corner) (Bayer et al. 2009, modified).

1.5. Mechanisms of polar auxin transport

To explain phyllotaxis and the formation of leaf vasculature, two mechanisms of polar auxin transport have been hypothesized: up-the-gradient and with-the-flux. According to the up-the-gradient hypothesis, the auxin efflux carrier (PIN1) localizes in the cell plasma membrane toward the cells of higher auxin concentration (Jonsson et al. 2006; Smith et al. 2006; Merks et al. 2007). This hypothesis states that cells can somehow sense the concentration of auxin in nearby cells, and direct the PIN1 proteins, where auxin concentration is higher. It is assumed that at initial conditions, there are some cells with a slightly higher auxin concentration due to random fluctuations, that polarizes the PIN1 proteins towards these cells. The resultant

additional polar auxin transport further increases auxin concentration, and in a positive feedback creates more polarized PIN1 pattern. This proposed mechanism can explain the generation of PIN1 convergence points and auxin accumulation at the SAM peripheral zone triggering leaf initiation (**Fig. 1.7A**). Furthermore, it can also explain the formation of a proper spacing between leaf primordia, that is fundamental for phyllotaxis. The PIN1 convergence pattern leads to auxin depletion from the surrounding cells, preventing the generation of other convergence points nearby. Thus, in this way emerging leaf primordia inhibit new organ formation in their neighborhood, that is in the agreement with a classical concept proposed by W. Hofmeister in 1868 (Smith and Bayer 2009; Reinhardt and Gola 2022).

In turn, the with-the-flux hypothesis explains a mechanism on how auxin feeds back on its own transport, that is a core of more general concept called canalization (Ravichandran et al. 2020). The canalization hypothesis has been proposed by Tsvi Sachs (Sachs 1969; 1981) who suggested that cell's ability to transport auxin (or auxin-dependent signal) increases with the auxin flux. In a consequence, this positive feedback leads to the generation of narrow 'canals', that are cell files with the highest ability to transport auxin (auxin flux).

In Sachs' experiments, auxin which has been applied to segments of mature stems or roots, leads to the generation of new vascular strands (**Fig. 1.8A**) (Ravichandran et al. 2020). These vascular strands connect the site of auxin application (acting as auxin source) and the pre-existing vasculature of the stem (acting as auxin sink). Sachs explained this phenomenon by auxin diffusion from the site of auxin application and the positive feedback between auxin and its own transport, that leads to locally more polarized auxin transport (**Fig. 1.8B**). Initially, the most polarized auxin transport occurs in cells nearby the pre-existing vascular strand, which is already highly polarized. Gradually, an auxin canal is formed, that finally reaches auxin application site and initiates the differentiation of a new vascular strand.

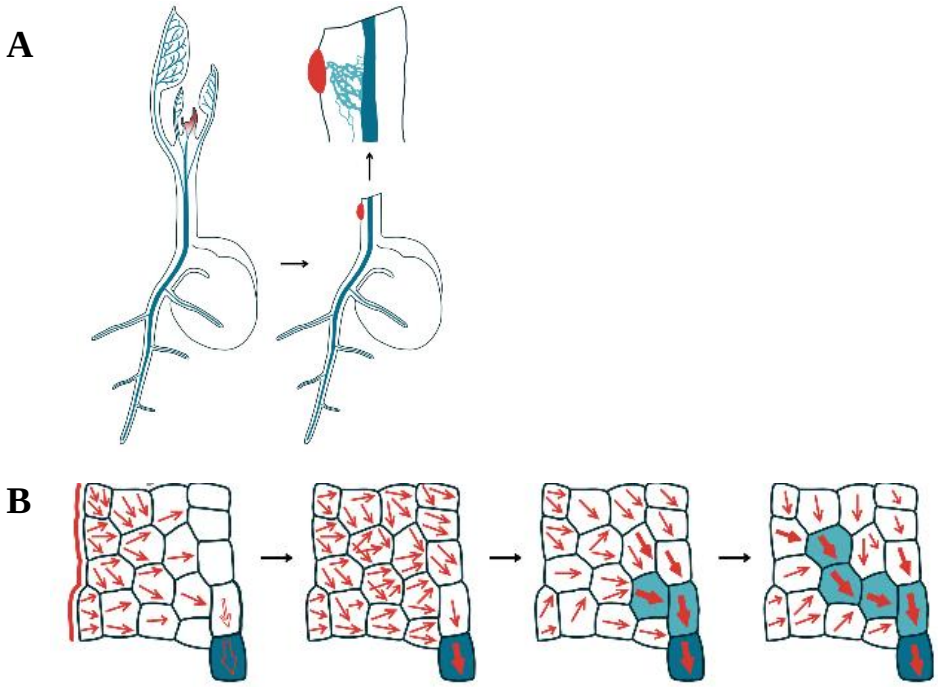

Fig. 1.8. The induction of new vascular strand by a local auxin application according to canalization hypothesis.

(**A**) The application of auxin (red) to the stem segments, where all above leaves have been removed, leads to the formation of new vascular strands (light blue) connected to the pre-existing stem vasculature (dark blue). (**B**) A model of consecutive stages of vascular strand formation predicted by canalization hypothesis. Initially, auxin transport *via* diffusion from the site of auxin application (red line on the left) occurs in different directions (thin arrows). Subsequently, due to a positive feedback, auxin transport become more polarized (thicker arrows), first, close to the pre-existing vascular strand (dark blue), which is already highly polarized (empty arrows). Consequently, auxin transport is directed toward this the pre-existing strand. Finally, a canal of highly polarized auxin transport is generated (light blue) (Ravihandran et al. 2020, modified).

Sachs' canalization model has been further extended by different molecular mechanisms (Smith and Bayer 2009). Namely, it has been proposed that auxin can be canalized by facilitated diffusion, where some passive channels (e.g. plasmodesmata) increase the auxin diffusion rate from cell to cell. The other mechanism relies on the PIN1-mediated polar auxin transport (with-the-flux hypothesis). By using computer simulations, the latter mechanism has been shown to generate PIN1 polarity directed away from the auxin maximum (auxin source) towards auxin minimum (auxin sink), which reproduces acropetal formation of the leaf midvein (Roland-Lagan and Prusinkiewicz 2005). Accordingly, auxin is moving basipetally from the sites of

auxin accumulation (auxin sources) localized at SAM surface (or subsequently at the primordium tip) towards the pre-existing vasculature of the stem (auxin sink). The canalization hypothesis contributes also to the understanding of further stages of vasculature development in a leaf, such as the formation of second-order vascular strands (see below), or effects of suppressing auxin transport on the structure of vascular strands (Roland-Lagan and Prusinkiewicz 2005).

On the other hand, some aspects of the canalization hypothesis are still controversial, such as predicted low auxin concentration in the pre-existing vascular strands (auxin sink) resulting from high auxin flux (Ravichandran et al. 2020). In contrast to this prediction, experimental data show high activity of auxin-related reporters (MP, PIN1, ARF3, DR5) in initiating and differentiating vascular strands, which indicate high auxin concentration (Mattsson et al. 2003; Scarpella et al. 2006; Wenzel et al. 2007; Husbands et al. 2015). However, theoretical models show that this controversy might be solved by taking into account additional factors, such as specific dynamics of auxin flux and efflux carrier proteins in a cell plasma membrane, or the modulation of auxin source strength (Feugier et al. 2005; Feller et al. 2015). High auxin concentration in vascular strands predicted from experimental data can be also achieved by localized auxin production (see the below section **1.8. The role of auxin biosynthesis in development of leaf vascular system**).

1.6. The formation of higher-order vascular strands in leaf primordia

During shoot development, *Arabidopsis* leaves change their size and shape demonstrating a phenomenon called heteroblasty. These changes can also include the localization and density of trichomes or the amount of hydathodes and serrations (Kang and Dengler 2004). For example, the shape of cotyledons is rounded and they do not have any trichomes (Sieburth 1999). Juvenile leaves (including the first true leaves) are also rounded or slightly elongated, and have trichomes only at adaxial side of the leaf blade. In turn, adult leaves are more elongated, have trichomes also at the abaxial side, and several serrations at leaf margin (Lièvre et al. 2016).

Not only geometry, but also the pattern of vascular strands in *Arabidopsis* leaves depends on leaf developmental stage. The formation of vasculature in cotyledons is simple. After the midvein formation, a few second-order vascular strands branch from the midvein and form loops (**Fig. 1.9**). Usually, there are 4 second-order vascular strands and two pairs of loops

(Sieburth 1999). First, loops at apical (or distal) cotyledon region are formed, and then two other loops are formed below at basal (or proximal) region.

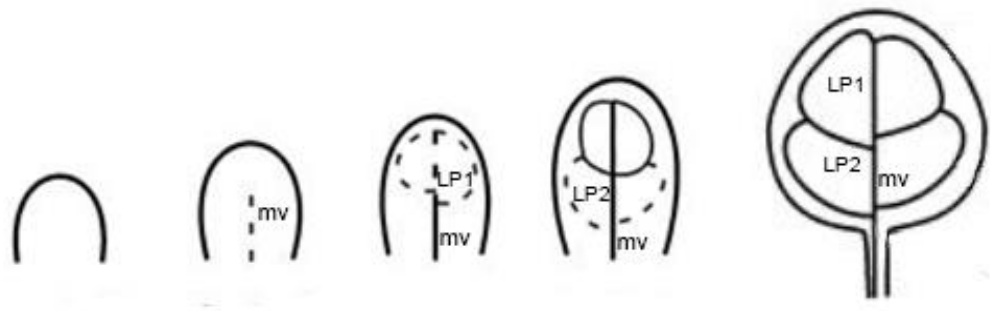

Fig. 1.9. Development of vascular pattern in cotyledons of *Arabidopsis*.

Early stages of vascular strand formation are indicated by dash lines, while later stages - by continuous lines. The midvein is marked by ‘mv, the first and second pairs of loops by LP1 and LP2, respectively (Sieburth 1999, modified).

The formation of vascular pattern is more complex at the first true rosette leaves, where mechanisms of vasculature initiation are the best recognized (Tsukaya et al. 2000; Scarpella et al. 2004; Sawchuk et al. 2008; Sack and Scoffoni 2013; Marcos and Berleth 2014; Krishna et al. 2021). After the midvein establishment, when the primordia attain elongated shape and a leaf blade begins to expand, the first two pairs of loops are generated in a similar way as in cotyledons: first, a pair of apical loops are formed. and then the next pair of loops is formed below (**Fig. 1.10A-C**). Subsequently, in contrast to cotyledons, the third pair of loops is formed at the basal region of the first true leaves (**Fig. 1.10D**). In addition, third-order vascular strands appear connecting strands from the neighboring loops. Finally, fourth-order strands branch from the lower-order strands and connects to other strands (**Fig. 1.10E**). Besides these connected strands, also free-ending strands can be formed.

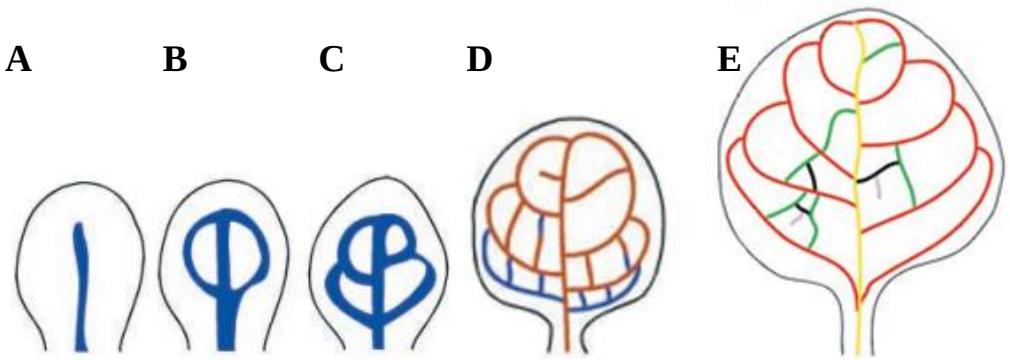

Fig. 1.10. Development of vascular pattern in first true leaves of *Arabidopsis*.

(**A**-**E**) Subsequent stages of the vascular pattern formation are shown. At (**A**-**D**) blue lines indicate early stages of vascular strand differentiation, while brown lines – later stages. At (**E**), the midvein (the primary strand) is marked by yellow line, the second-order strands – by red, the third-order strands – by green, the fourth-order strands– by black, and the fifth-order free-ending strands – by grey color (Scarpella et al. 2004, modified).

The formation of the vascular pattern in adult leaves is similar to that in juvenile leaves. However, in adult leaves, the density of vascular strands is higher than in juvenile leaves, and there is more higher-order strands and more strands with free ends (Lucas et al. 2013). Furthermore, there is a correlation between the formation and further extension of the second- or higher-order strands and the position of serrations at leaf margin (Kang and Dengler 2004).

As in the case of the midvein formation, auxin activity is crucial in the initiation of higher-order strands. Thus, to follow consecutive stages of leaf vasculature development, different auxin-related reporters are used. The midvein is already specified, when leaf primordia bulge from the SAM, and it is marked by the PIN1 and DR5 expression (Scarpella et al. 2006). The expression of both PIN1 and DR5 in the future midvein precedes the expression of vascular marker *ATHB8* (*ARABIDOPSIS THALIANA HOMEOBOX 8*). The ATHB8 is a transcription factor belonging to the HD-ZIP III family that regulates early stages of procambium specification (Donner et al. 2009). The expression of *ATHB8* depends on auxin signalling, in particular on the MP (one of auxin response factors) (Krishna et al. 2021). The PIN1, DR5, and ATHB8 expression also marks the initiation of higher-order vascular strands.

Soon after the establishment of the midvein in leaf primordia, the epidermal PIN1 convergence points (putative auxin sources) are generated at the primordium margin concomitantly to the formation of PIN1-expressing strands in inner cells (**Fig. 1.11A**) (Scarpella et al. 2006; Biedroń

and Banasiak 2018; Perico et al. 2022). These PIN1 strands connecting the convergence points and the midvein, are polarized towards the midvein and specify second-order veins forming lower part of the first loops. Next, upper PIN1 strands are formed, which are polarized towards the lower strands, and finally connect to the distal part of the midvein forming the first pair of loops at apical primordium region (**Fig. 1.11B**). The second pairs of loops are formed similarly, but the upper part of these loops is connected to the lower part of the first loops (**Fig. 1.11C**). In contrast to the second-order strands, the specification of third- or higher-order strands is not related to the PIN1 convergence points at the marginal epidermis. Namely, new PIN1-expressing strands extend from pre-existing strands and are polarized towards them without any connection to epidermis (**Fig. 1.11D**). These higher-order strands either connect to the other pre-existing strand or remain free-ending. Because PIN1 is always polarized towards pre-existing strands, whenever PIN1-expressing strands are connected to other strands, they contain cells of opposite polarity linking by a bipolar cell (**Fig. 1.11E**) (Scarpella et al. 2006; Marcos and Berleth 2014; Linh et al. 2018).

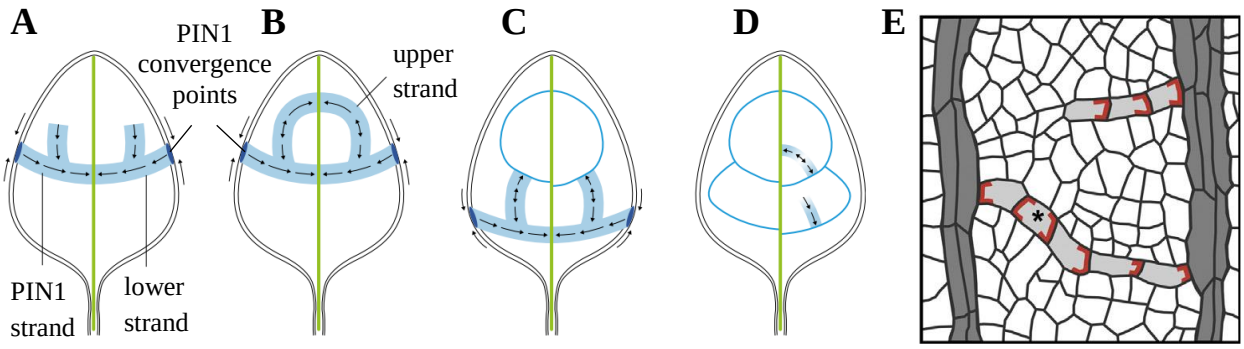

Fig. 1.11. Initiation of second- and higher-order vascular strands and loops in first true leaves of *Arabidopsis* marking by the PIN1 expression.

(A-D) Subsequent stages of vascular strand initiation are shown. First, epidermal PIN1 convergence points (dark blue) are formed at primordium margin together with PIN1-expressing strands (light blue) connecting them to the midvein (green). These strands mark future lower veins of the first loops (**A**). The PIN1 polarization directed towards the pre-existing strands is marked by arrows. Then, other PIN1-expressing strands are formed (future upper veins of the first loops), that connect lower strand to the distal part of the midvein (**A-B**). Second loops are formed in similar way below the first loops (**C**). Third-order strands are formed that either connect to other pre-existing strands or stay free-ending (**D**) (Perico et al. 2022, modified). (**E**) In the PIN1- expressing strands (light grey), that connect two other strands (dark grey), the PIN1 polarity (red) is opposite linking by a bipolar cell (asterisks) (Linh et al. 2018, modified).

There is a general agreement that the PIN1 is a regulator of the initiation of leaf vasculature. However, also other plasma-membrane PINs are expressed at future vascular strands. Namely, the expression of the PIN3, PIN4, and PIN7 is observed in the first-, second-, and higher-order vascular strands, however, this expression follows the expression of the PIN1 (Verna et al. 2019; Govindaraju et al. 2020). In addition, other plasma-membrane auxin efflux transporters – ABCB1 and ABCB19 are expressed at early stages of vasculature development (Verna et al. 2019). Among ER-localized PINs, the expression of PIN6 overlaps with the PIN1 expression in initiating strands (Sawchuk et al. 2013; Verna et al. 2015). In turn, the expression of other ER-localized PINs – PIN5 and PIN8 is restricted to very narrow sites of future vascular strands and this expression is observed much later in comparison to both PIN1 and PIN6.

The consecutive stages of second- and higher-order strand formation are also reflected by the DR5 expression. Similar to the PIN1, the DR5 expression marks the initiation of the first pair of loops at the apical primordium region, and then the formation of further loops in the basipetal direction in the relation to local DR5 maxima (putative auxin sources) at primordium margins corresponding to PIN1 convergence points (Mattsson et al. 2003; Scarpella et al. 2006; Marcos and Berleth 2014). Also, higher-order initiating strands both connected and free-ending are marked by the DR5 expression.

Comparing to the PIN1 and DR5, the expression of *ATHB8* is more specific. In contrast to the PIN1 and DR5, the *ATHB8* is not expressed at leaf epidermis at sites of putative auxin sources. Instead, it strictly marks early stages of initiating vascular strands (Scarpella et al. 2004; Donner et al. 2009; Marcos and Berleth 2014; Krishna et al. 2021). In particular, the *ATHB8*-expressing strands branch from the midvein, then develop acropetally, and finally connect to distal part of the midvein marking future second-order strands forming the first pair of loops. The *ATHB8* expression marks also the formation of further loops in a basipetal direction. The *ATHB8*-expressing strands (both second- and higher order) always extend from the pre-existing strands reflecting the direction of vascular strand differentiation, rather than the direction of auxin transport.

1.7. Experimental testing the role of auxin transport in the formation of vascular pattern

The expression of genes related to the polar auxin transport (*PIN1, PIN3, PIN4, PIN5, PIN6, PIN7, PIN8, ABCB*s) in cells which will differentiate into vascular tissues, suggests that the auxin transport is a crucial process determining the vascular pattern.

Indeed, numerous experiments show that non-specific suppression of the polar auxin transport with chemical inhibitors (such as NPA or TIBA) results in serious changes in the pattern of vascular strands in leaves (**Fig. 1.12A**). For example, the NPA treatment disrupts the PIN1 dynamics, and in a consequence leads to expanded PIN1 expression domains in future vascular strands. In a long-term it also leads to the formation of increased number of enlarged vascular strands, especially at the primordium center and nearby the margins (Mattsson et al. 1999; Sieburth 1999; Scarpella et al. 2006; Verna et al. 2019). Thus, to develop the proper vascular pattern, the polar auxin transport restricts vascular differentiation to narrow domains probably by local auxin drainage (Berleth et al. 2000).

Similar defects in the vascular pattern has been observed in the *pin1* mutant, although weaker in comparison with the NPA-treated plants (Mattsson et al. 1999). In particular, in the *pin1* mutant, an excess of vascular strands occurs especially at leaf margins and in proximal leaf regions (**Fig. 1.12B**). The weaker effect of single *pin1* mutation in comparison to the NPA treatment, might be explained by the redundancy among PIN proteins. Indeed, *pin1* mutant phenotype is enhanced in the combination with the *pin6* mutation (**Fig. 1.12B**), which suggests that the plasma-membrane (PIN1) and ER-localized (PIN6) proteins act redundantly (Sawchuk et al. 2013; Verna et al. 2015). Thus, it has been proposed, that not only the PIN1-dependent intercellular auxin transport, but also intracellular transport mediated by ER-localized PINs controls the formation of vascular pattern in *Arabidopsis* leaves. There is also the redundancy among plasma-membrane-localized PINs. The vascular pattern in triple *pin3 pin4 pin7* mutant is no different from the WT, while vascular defects appear in quadruple *pin1 pin3 pin4 pin7* mutant (**Fig. 1.12B**), which are even stronger than in single *pin1* mutant (Verna et al. 2019). Thus, also PIN3, PIN4, and PIN7 act redundantly with the PIN1 in the determination of leaf vascular pattern.

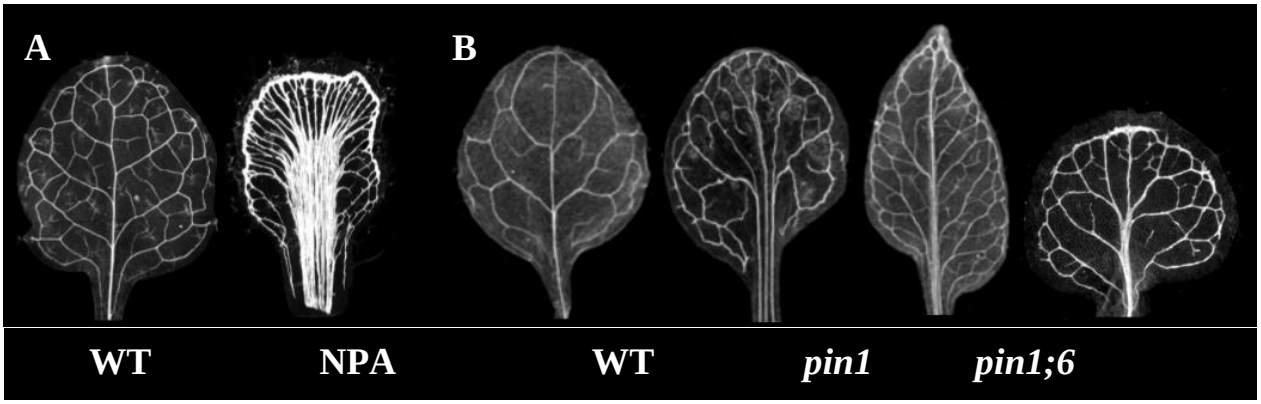

Fig. 1.12. Defects in the vascular pattern in *Arabidopsis* leaves after chemical or genetical suppression of the polar auxin transport.

(A) The second rosette leaves growing without (left, WT) or in the presence of 20 μM NPA (Mattsson et al. 1999, modified). (**B**) The first rosette leaves of (from left) WT, *pin1, pin1 pin6, pin1 pin3 pin4 pin7* plants (Verna et al. 2015; 2019, modified).

Nonetheless, in the WT leaves, which developed in the presence of auxin transport inhibitors or in the absence of functional PIN proteins or any other auxin transporters (ABCB, AUX1/LAX), vascular strands are formed in a very basic pattern and are oriented along the apical-basal leaf axis (Mattsson et al. 1999; Verna et al. 2019). This finding challenges the canalization hypothesis, which states that the formation of vascular strands depends on the feedback between auxin and its polar transport (Ravichandran et al. 2020). Still, it is possible that auxin transport depends on other unknown transporters.

Alternatively, the formation of vasculature pattern might be explained by other mechanisms. For example, auxin signalling might be involved, since its inhibition leads to decrease in the amount of vascular strands and reduced ability to produce loops (Verna et al. 2019; Ravichandran et al. 2020). Auxin signalling might in turn regulate auxin diffusion through the plasmodesmata. Indeed, the recent study shows that in the future vascular cells auxin-dependent plasmodesmata permeability in high, and this high permeability is maintained in the established vascular strands (Linh and Scarpella 2022). This indicate that during development of leaf vasculature cells are symplastically connected. Importantly, whenever any defects in the plasmodesmata aperture occur, they invariably leads to decreased amount of vascular strands or even to the formation of disconnected and discontinuous strands. Therefore, these and earlier findings lead to the model according which vasculature pattern is controlled by three pathways:

polar auxin transport, auxin signalling and the diffusion via plasmodesmata (Linh and Scarpella 2022).

1.8. The role of auxin sources and auxin sink in the formation of vascular pattern

There is a common observation that the suppression of the polar auxin transport by chemical inhibitors leads to the increased amount of vascular tissue nearby the leaf margins (Mattsson et al. 1999; Sieburth 1999; Scarpella et al. 2006). This might result from local auxin accumulation close to a putative auxin sources, which might be localized along leaf margins. Furthermore, a local auxin application to a leaf margin leads to the formation of new PIN1 convergence points in epidermis and extra vascular strands (Scarpella et al. 2006; Verna et al. 2019). Similar experiments have been performed earlier on other plant organs such as roots and stems, in which auxin local application to the organ surface also invariably led to the formation of new vascular strands (Sachs 1981; Sauer et al. 2009). This suggests an essential role of epidermal auxin sources with high auxin concentration at leaf margins in the induction of vascular strands. According to this scenario, auxin is transported *via* PIN1 from the epidermis to the inner cells, where it induces the formation of a new vascular strand (Linh et al. 2018). The PIN1-mediated polar auxin transport may also participate in the generation of auxin sources at early stages of primordium development (Scarpella et al. 2006). However, a recent study has questioned the importance of epidermal PIN1 expression in the formation of vasculature pattern. Specifically, that lack of epidermal PIN1 does not affect the pattern of vascular strands in *Arabidopsis l*eaves (Govindaraju et al. 2020). On the other hand, the presence of PIN1 in inner cells is essential for normal development of vasculature.

Alternatively, epidermal auxin sources might be generated or/and further maintained by local auxin production in the relation to the formation of serrations or hydathodes (structures involved in water release called guttation), which are localized at the serration tip (Aloni 2001, 2003; Yagi et al. 2021). Thus, during leaf primordium development, the number and spatial distribution of putative auxin sources requiring for the vascular strand formation would be changing. These auxin sources could be recognized for example by the DR5 expression (Aloni et al. 2003). Accordingly, just after leaf emergence, the major auxin source is localized at primordium tip (**Fig. 1.13A**). This apical auxin source develops at the time of leaf initiation due to PIN1-convergence pattern and resulting auxin accumulation at the SAM surface (Scarpella et al. 2006). Beside primordium tip, stipules (outgrows on both sides of a leaf base) are also a

source of auxin (**Fig. 1.3A**). Subsequently, new auxin sources are generated at primordium margin, for example in the relation to local auxin biosynthesis accompanying the formation of serrations and hydathodes (**Fig. 1.13B-C**) (Aloni 2003; Yagi et al. 2021). As the PIN1-mediated polar auxin transport is involved in the initiation of serrations (Bilsborough et al. 2011), the generation of these marginal (or lateral) auxin sources is also probably PIN1-dependent. Finally, a number of randomly distributed sites of local auxin production is generated in mesophyll cells, first more at the apical region and next at the basal region of primordia (**Fig. 1.13C-D**) (Aloni 2003). A role of auxin sources on resulting vascular pattern has been further demonstrated by computer simulations. Namely, higher number of regularly distributed auxin sources leads to the generation of more dense vascular network with smoother primary or second-order veins, and more uniform higher-order veins (Runions 2005). Also, lateral auxin sources added to the simulation on both sides of the initial source can induce realistic loops in a growing leaf (Rolland-Lagan and Prusinkiewicz 2005).

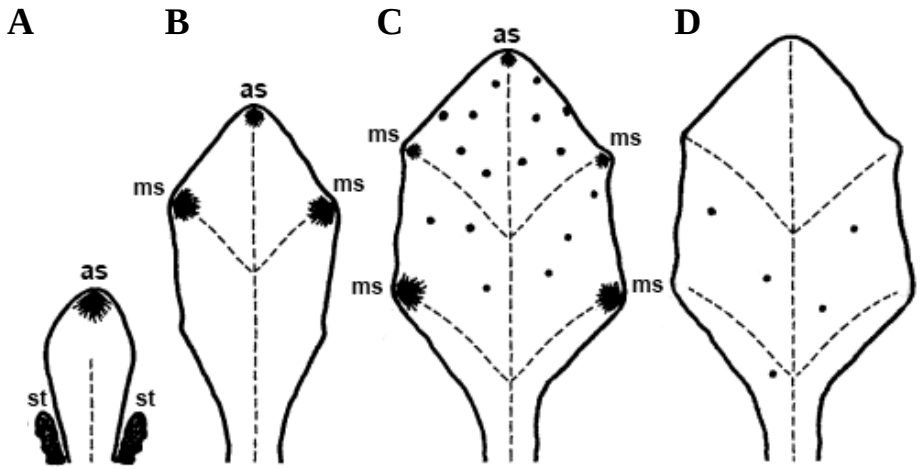

Fig. 1.13. Changes of auxin source distribution during leaf primordium development.

(**A**) Initially, auxin sources (apical source, as) are localized at stipules (st) and at primordium tip. (**B**) New auxin sources (marginal or lateral sources, ms) are generated at primordium margin at sites, where serrations and hydathodes are formed. (**C**) During further primordium development, more marginal sources are generated. In addition, random auxin sources (black dots) appear in mesophyll cells within a leaf blade at the apical primordium region. (**D**) Mesophyll auxin sources subsequently appear at more basal primordium region. The midvein and second-order vascular strands are indicated by dash lines (Aloni 2003, modified).

The fact that the PIN1 polarization in the initiating vascular strands is always directed towards pre-existing strands (Scarpella et al. 2006; Marcos and Berleth 2014) suggests that auxin is

depleted from the surrounding cells and transported into these pre-existing strands acting as auxin sinks in terms of auxin canalization hypothesis (Smith and Bayer 2009). Thus, beside auxin sources, pre-existing strands may also organize the pattern of vasculature in leaves, for example, by preventing the initiation of additional strands in a close proximity of existing strands. Also, theoretical models show that a concept of auxin sink can explain acropetal development of the midvein. Namely, assuming that the auxin sink is localized at the bottom of leaf primordia (which might corresponding to the pre-existing vasculature of the shoot), resulting auxin flux increases from the bottom to the top of primordia (i.e. in the acropetal direction), despite that the direction of auxin transport is basipetal (Rolland-Lagan and Prusinkiewicz 2005). Interestingly, the model also suggests that the acropetal development of the midvein may entirely depend on auxin sink, and the presence of auxin source is not necessary in this process.

1.9. The role of auxin biosynthesis in development of leaf vascular system

Since the PIN1-based polar auxin transport is crucial in the formation of a proper pattern of vascular network, the suppression of auxin transport in *pin* mutants or by chemical inhibitors of auxin transport has only a minor impact on vein initiation (Mattsson et al. 1999; Sieburth 1999; Carland et al., 2016; Verna et al. 2019; Govindaraju et al. 2020). This suggests that other aspects of auxin action upstream the auxin transport and canalization, are necessary for the initiation or/and further development of vascular strands. Auxin biosynthesis can be one of them. The importance of auxin local production in vascular system development has been demonstrated by several studies, which show that the disruption of auxin biosynthesis either by mutations or chemical inhibitors leads to a decrease in auxin levels and the generation of lower number of vein, disorganized or/and discontinuous vascular network (Stepanova et al. 2008; Stepanova et al. 2011; Nishimura et al. 2014).

The recent study more carefully explored the relation between auxin biosynthesis and *Arabidopsis* leaf vasculature (Kneuper et al. 2019). In particular, a detailed map of auxin synthetizing gene expression has been created in developing leaf primordium (**Fig. 1.14**). Generally, the *TAA* and *YUCCA* are expressed at partially overlapping domains at sites of future and present vascular strands. For example, the *TAA1, TAR2* and *YUC4* are expressed at early stage of midvein development, while the *YUC2* is expressed at later stages - mainly at the base of advanced midvein. The similar sequence of *TAA1, TAR2* , *YUC4,* and *YUC2* expression is

observed for the second-order vascular strands and loops. The *YUC4* is also initially expressed in a whole primordium, but later its expression is restricted to apical primordium region and primordium margins, where it overlaps with the *TAA1* and *YUC1* expression. In addition, the *TAA1* is strongly expressed in non-vascular cells between existing vascular strands.

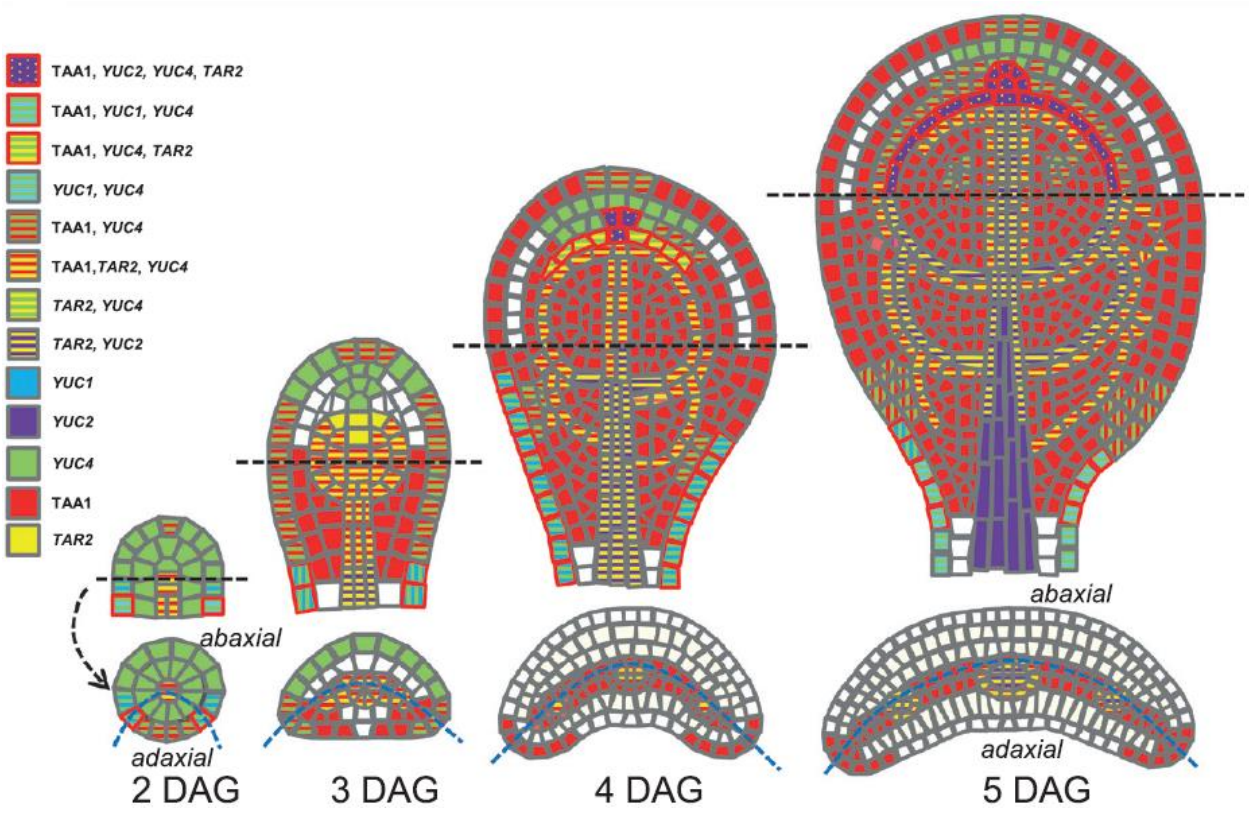

Fig. 1.14. A map of auxin synthetizing gene expression in developing *Arabidopsis* leaf primordium.

The expression domains of each auxin biosynthetic gene (*TAA1, TAR2, YUC1, YUC2, YUC4*) has been marked in different colors at 2, 3, 4 and 5 days after germination (DAG). Transverse sections across primordia are shown below. Blue dash line indicates the boundary between adaxial and abaxial primordium side (Kneuper et al. 2021, modified).

The observation that auxin is produced in future and present vascular strands explains controversy on canalization hypothesis, which, in contrast to experimental data, predicts low auxin concentration in vascular strands (see the section **1.5. Mechanisms of polar auxin transport**). Namely, high auxin levels can be maintained in developing vascular strands with high auxin flux due to local auxin production.

Furthermore, experimental data suggests that there is the relationship between auxin biosynthesis and the polar auxin transport (Kneuper et al. 2019). It is been shown that disrupted pattern of vascular strands resulting from genetic or chemical reduction of auxin biosynthesis can be rescued by the NPA treatment suppressing polar auxin transport. In particular, the reduction of auxin biosynthesis leads to decreased number of vascular strands and the absence of loops, while the suppression of auxin transport generates increased number of vascular strands and increased strand thickness. The former and latter abnormalities can be rescued and the normal vascular pattern is formed by simultaneous reduction in both auxin biosynthesis and transport. Thus, lower auxin production can be compensated by lower auxin flux.

Then, the question arises how auxin biosynthesis can be regulated in vascular strands? It is possible that auxin biosynthesis is positively regulated by the PIN1-mediated auxin flux (Burian et al. 2021). The *YUCCA* genes have been shown to be upregulated, when auxin levels decrease after the treatment of auxin biosynthesis inhibitor kynurenine (Suzuki et al. 2015). Accordingly, localized auxin production could balance the auxin depletion due to polar auxin transport. However, it needs to be further determined, whether auxin flux is sufficient to locally trigger the expression of *TAA* or/and *YUCCA* genes.

1.10. Cellular basis of vascular strand differentiation

Procambium is the primary tissue arranged in continuous strands, that develops from ground cells to ultimately differentiates into vascular tissues such as phloem or xylem (**Fig. 1.15A**) (Nelson and Dengler 1997). Procambial cells are elongated and narrow with a dense cytoplasm (Esau 1965), and thus can be recognized by its distinguished morphology from other cells (**Fig. 1.15A-B**). In leaves, procambial strands develop from strands of isodiametric pre-procambial cells, which morphologically are identical with the other surrounding cells, however, they are marked by a number of genetic markers such as MP, DR5, PIN1, and more specific – ATHB8 (**Fig. 1.15C**) (Scarpella and Meijer 2004).

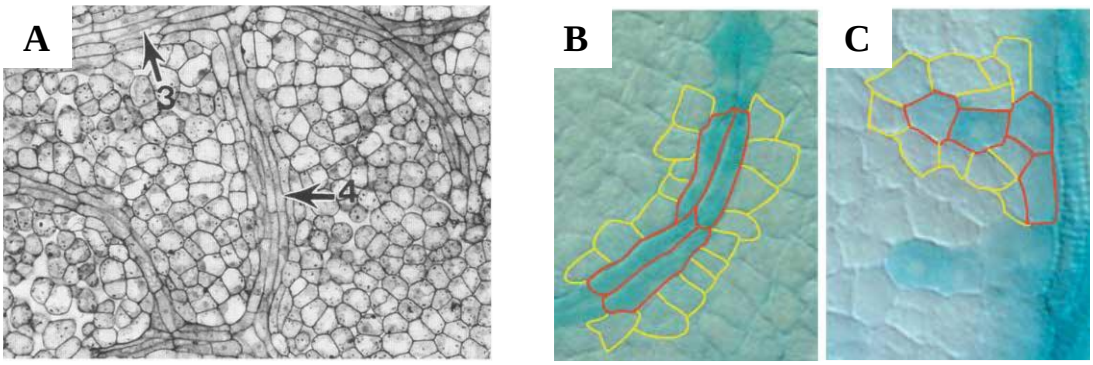

Fig. 1.15. Procambium development in *Arabidopsis* leaves.

(**A**) Procambium cells forming strands (three- and four-order strands are indicated by arrows and the number) (Nelson and Dengler 1997, modified). (**B**) Elongated procambial cells (outlined in red) are marked by the *ET1335-GUS* expression. (**C**) Isodiametric pre-procambial cells (outlined in red) are marked by the *ATHB8-GUS* expression (Scarpella et al. 2004, modified).

The specification of procambial cells is closely related to auxin and its polar transport through cells (see the sections **1.4** and **1.6**). After the specification, cells divide parallel to the axis of developing strands, but also the direction of maximal cell growth is along the same direction (in other words the growth is highly anisotropic). Consequently, procambial cells become narrow and highly elongated along the strand axis. However, it is not clear what is a sequence of these cellular process, and whether a characteristic elongated procambium shape is a primary result of cell divisions or anisotropic growth.

Interestingly, a number of theoretical studies demonstrate that both the orientation of cell division plane and the direction of cell growth can be regulated by mechanical stresses (**Fig. 1.16**). In particular, tissue-level compressive stresses can be generated due to differential growth in pre-procambial cells and surrounding mesophyll cells (Couder et al. 2002; Laguna et al. 2008; Corson et al. 2009). The difference in the growth rate might be in turn determined by local auxin biosynthesis. Accordingly, pre-procambial cells containing high auxin levels due to localized auxin production might promote the growth of surrounding cells, that consequently leads to generating of compressive stresses (Kneuper et al. 2021). Such mechanism may explain the formation of elongated narrow procambial cells in early leaf primordium. Mechanical stress can also affect the orientation of cell division plane in pre-procambial or/and procambial cells in agreement with the observation, that plant cells generally divide along the direction of maximal tension (Louveaux et al. 2016).

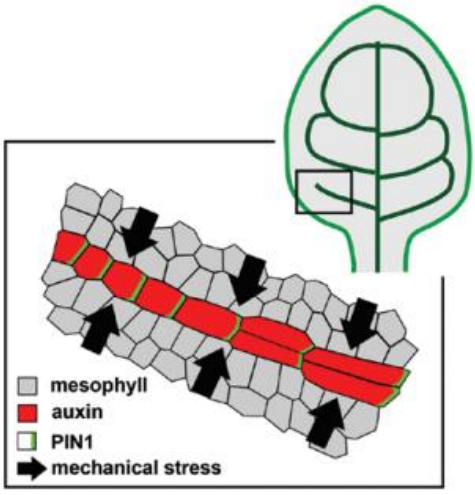

Fig. 1.16. Divisions and growth of pre-procambial and procambial cells can be regulated by mechanical stress.

Pre-procambial and procambial strands, containing high auxin levels due to putative positive feedback between auxin biosynthesis (red) and the PIN1-dependent auxin flux (green), stimulate the expansion of mesophyll cells. Resulting differential growth generates compressive stress, that determines the orientation of cell division plane and growth direction in pre-procambial and procambial cells (Burian et al. 2021, modified).

The other question is how the specification of pre-procambial and procambial cells is temporary and spatially coordinated. Several studies show that the specification of pre-procambial cells is progressive and in continuity with pre-existing vascular strands. Namely, the expression of pre-procambial markers, such as *ATHB8* or *J1721*, always extends away from other vascular strands (Kang and Dengler 2004; Scarpella et al. 2004; Sawchuk et al. 2007). In other words, a new pre-procambium strand branches from the pre-existing strand. For example, the formation of the first two loops in the first true *Arabidopsis* leaves is preceded by the branching of new pre-procambial strands from the midvein, i.e. new strands extend from primordium center to the margin (Sawchuk et al. 2007). However, in the case of the third loop, new strands can also branch from the second-order pre-existing strand localized in a close proximity of auxin response maxima (marking future serrations) at the primordium margin towards the midvein (Sawchuk et al. 2007).

In contrast to the pre-procambium, procambium develops very rapidly. Accordingly, the expression of procambium markers *ET1335* or *Q0990* is observed simultaneously along a given strand (Scarpella et al. 2004; Sawchuk et al. 2007; Marcos and Berleth 2014). An analysis of

cell morphology shows also that the expression of procambium markers is detected in elongated cells, but not in the cells that would divide parallel to the strand axis (Sawchuk et al. 2007). In addition, the expression of genes related to cell divisions (cyclin encoding genes) was not observed in the initial stages of procambial cells (Kang and Dengler 2002). Thus, these data suggests the pre-procambium differentiation into procambium results rather from synchronized cell elongation throughout the entire strand.

The pattern of vascular strands in leaves depends strongly on a leaf shape, that indicates a relationship between vascular patterning and leaf growth. Indeed, during undisturbed leaf growth, there is a continuous addition of new vascular strands and an increase in the complexity of the vascular pattern (Candela et al. 1999; Kang and Dengler 2004). Furthermore, the disruption of vascular pattern resulting from either mutations or chemical treatments is often accompanied by changes in the shape of a leaf blade (Mattsson et al. 1999; Sieburth 1999; Wenzel et al. 2021; Verna et al. 2019). Also, computer simulations shows that the shape and growth of a leaf have a strong impact on resulting vascular pattern (Runions et al. 2005). In particular, the growth rate can change the density of the vascular network and the shape of individual veins. And *vice versa*, leaf vasculature may as well affect the local growth rate leading to the diversity of leaf shapes (Runions et al. 2017). Thus, development of vascular system is plastic and coordinated with overall organ growth.

2. AIMS

In multicellular organisms like plants, the vascular system is absolutely necessary for the distribution of water and nutrients, for the propagation of signalling molecules that coordinate different processes within entire body, and for the mechanical support. The development of vascular system in dicot leaves is an example of patterning, which is formed hierarchically and in the continuity with the pre-existing stem vasculature. Moreover, the vascular system formation is strictly coordinated with leaf developmental program, and it is also plastic enough to respond to local disturbances. Since the leaf vascular system is initiated during the formation of leaves at the shoot apical meristem, experimental study of the earliest stages of vasculature development is difficult, especially in *Arabidopsis thaliana.* Usually, the development of the vascular system is studying in cotyledons or in the first rosette leaves with live imaging, but time-lapse imaging of leaf primordia is rare. Also, the majority of current studies focuses on molecular mechanisms of the vasculature formation, while there is little attention to mechanisms that control the pattern formation at cellular and tissue level.

The first aim of this study was to develop a protocol for *in vivo* studying the initiation of vascular system in growing *Arabidopsis* leaf primordia. This protocol should enable to monitor the earliest stages of vascular strand formation with using available auxin-related reporters, and allow to analyse anatomical details in initiating vascular strands, for example the morphology of procambial cells reflecting their differentiation status. This protocol should also allow for experimental manipulations such as chemical treatments or mechanical disruptions.

The formation of vascular strands and their pattern is usually explained in terms of canalization hypothesis, where the pathways of auxin flow from epidermal auxin sources to pre-existing vascular strands (auxin sink) specify future vascular strands. Thus, it is critical to test a role of auxin sources and existing vasculature in the formation of the vascular pattern in leaf primordia. The second aim of this study was to experimentally disturb auxin sources and signalling from pre-existing vascular strands with using different approaches (chemical, genetic, and mechanical disturbances), and to analyse effects of these manipulations on the differentiation of procambium in vascular strands and their pattern in leaf primordia. In addition, since there is a relationship between the vascular pattern and leaf growth, the further aim of this study was to analyse the initiation of the vascular system in the context of primordium development.

3. MATERIAL AND METHODS

3.1. Plant material and growth conditions

Arabidopsis thaliana plants were grown in the soil in short days conditions at 20-24 ˚C under 9 h of light (60 µmol m^2 s^{-1}) to prolong the vegetative phase of plant development. In all experiments leaf primordia from about two-month old vegetative rosettes were examined. The following transgenic lines were used: DR5v2:GFP (auxin response, nuclear localization, Liao et al. 2015), DR5v2:YFP (auxin response, the ER localization, Brackmann et al. 2018), pATHB8:YFP (procambium marker, Donner et al. 2009), pTAA1:TAA-GFP and pYUC4:GFP (auxin biosynthesis reporters, Stepanova et al. 2008; Robert et al. 2013), and single *pin1-7* mutant and double *cuc2 cuc3* mutant crossed with the DR5v2:YFP.

3.2. Methods

A scheme of methods used in this study is shown at the **Fig. 3.1**. The particular steps are described in details in below sections.

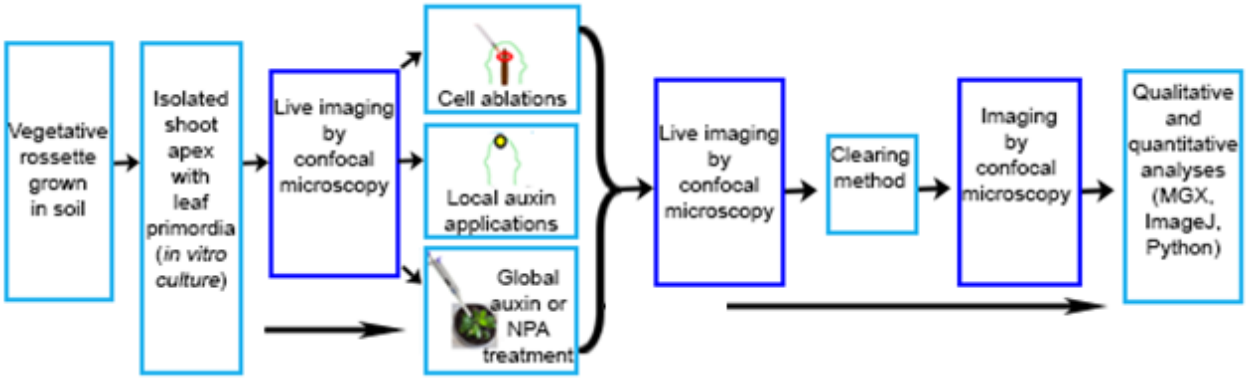

Fig. 3.1. A scheme of methods used to examine development of the vascular system in growing leaf primordia.

3.2.1. Plant dissection and live imaging

To make the youngest leaf primordia accessible for the imaging in a confocal microscope, plants were dissected with using a stereo-microscope (Nikon SMZ1000). Plants with about 15 or more rosette leaves (**Fig. 3.2A**) were transferred from the soil to a Petri dish filled with 1.5 % agar (bacterial agar, BTL, Łódź) to avoid water loss from the plant during the dissection. First, all older leaves and roots were cut off, and then also those younger leaves which cover the apex, until the shoot apical meristem with few youngest leaf primordia was visible. In this study, the earliest stages of leaf primordia (of length between 150 and 200 µm) were analyzed (**Fig.3.2B**). After the plant dissection, isolated shoot apices with few leaf primordia were transferred to another Petri dish filled with the growth medium containing Murashige and Skoog (MS) basal salt (0.46 g per 100 ml, Sigma), 1.5 % agarose (Duchefa), and 2 % sucrose (Chempur), supplemented with 0.01 µM gibberellic acid GA3 (Sigma), and 0.01 µM kinetin (Sigma) (the pH was adjusted to 5.8 with 1M KOH). To avoid the medium infection 1 µl/ml of PPM (Preservative for Plant Tissue Culture Media, Plant Cell Tech) was added. In this *in vitro* conditions, shoot apices with leaf primordia were growing normally at least during the next 3-4 days.

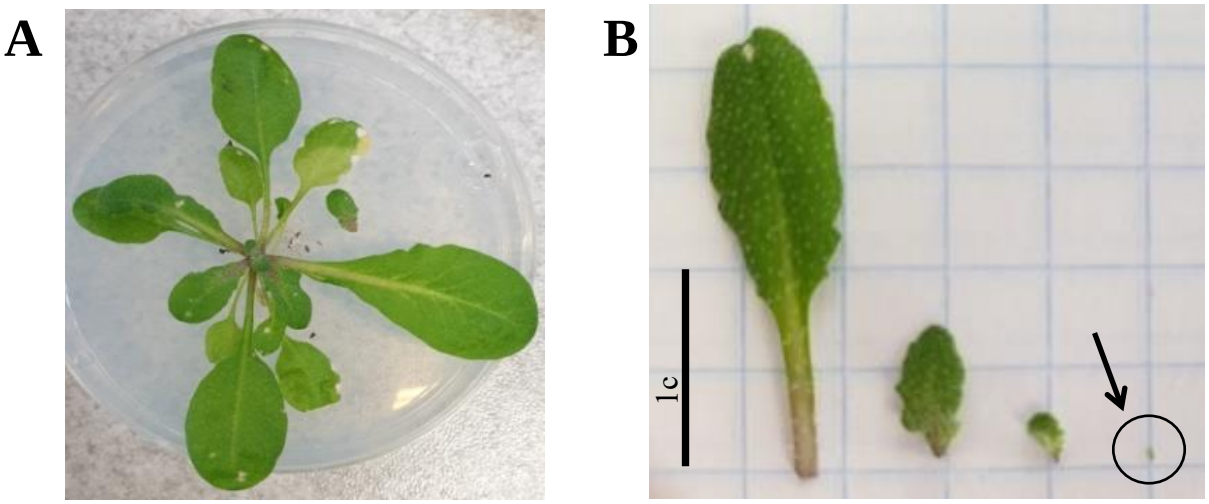

Fig. 3.2. Plant material used in this study.

(**A**) A 2-month old *Arabidopsis* rosette transferred to the Petri dish before the dissection. (**B**) A comparison of mature rosette leaves (from the left) and an exemplary isolated leaf primordium used for experiments and imaging (arrow, encircled) Scale bar: 1cm.

Growing leaf primordia were imaging with the laser confocal microscopy (see the below section **3.2.6. Laser confocal microscopy**) either at one-time point or two-time points with about 48 h time interval. Between the imaging, isolated shoot apices were kept in the same conditions as plants growing in the soil. For the imaging in inverted confocal microscope, the Petri dish with isolated apex was mounted upside down at the microscope stage, which was next adjusted to connect the apex with a drop of water at long-working distance objective.

3.2.2. Clearing of leaf primordia

The clearing method developed by Wuyts et al. (2010) was modified to visualize procambium strands in leaf primordia with a cellular resolution. In particular, isolated shoot apices with the youngest leaf primordia were fixed in the solution of ethanol and acetic acid or acetic anhydride (in the proportion 3:1) with a drop (50 µl) of Tween-20 (BioShop) under the vacuum for 1 h, and then left on a shaker for the next 24 h. Afterwards, the apices were rinsed in 50 % and 70 % ethanol, and treated with chloroform for 15 min. After washing in 70 % ethanol, the apices were progressive rehydrated. The apices were cleared in the solution of the SDS and NaOH (1% SDS and 200 mM NaOH) for 1.5 h, then rinsed in the water, and treated by 0.01 % amylase (Sigma) with the PBS buffer (prepared from the stock: 8 g NaCl, 0.2 g KCl, 1.44 g Na_2HPO_4, 0.24 g KH_2PO_4, pH 7.0, which was diluted 10 times in the water) during night at 37˚C. Next, after the rising in water, the apices were treated by 1 % periodic acid (Sigma) for 40 min, washing in water again, and stained in pseudo-Schiff-Propidium Iodide (0.01 % Propidium Iodide (PI) added to the pseudo-Schiff solution, Sigma) for 6 h followed by an overnight incubation in water. Finally, the apices were cleared in chloral hydrate (200 g chloral hydrate, 20 ml glycerol, and 30 ml of water) for 4 h.

During the entire clearing procedure, leaf primordia were still attached to shoot apices, otherwise they might be lost during treatments. Therefore, to image individual leaf primordia, the primordia were cut off from the isolated apices with using a stereo-microscope, mounted on a slide in Hoyer's solution (10 g Arabic gum, 40 ml MilliQ water, 10ml glycerol, and 100g chloral hydrate), and covered with a coverslip. Before the imaging in the confocal microscope, cleared primordia were checked with using brightfield light microscope (Nikon Elipse 80i) whether they are properly stained and mounted (**Fig. 3.3A**).

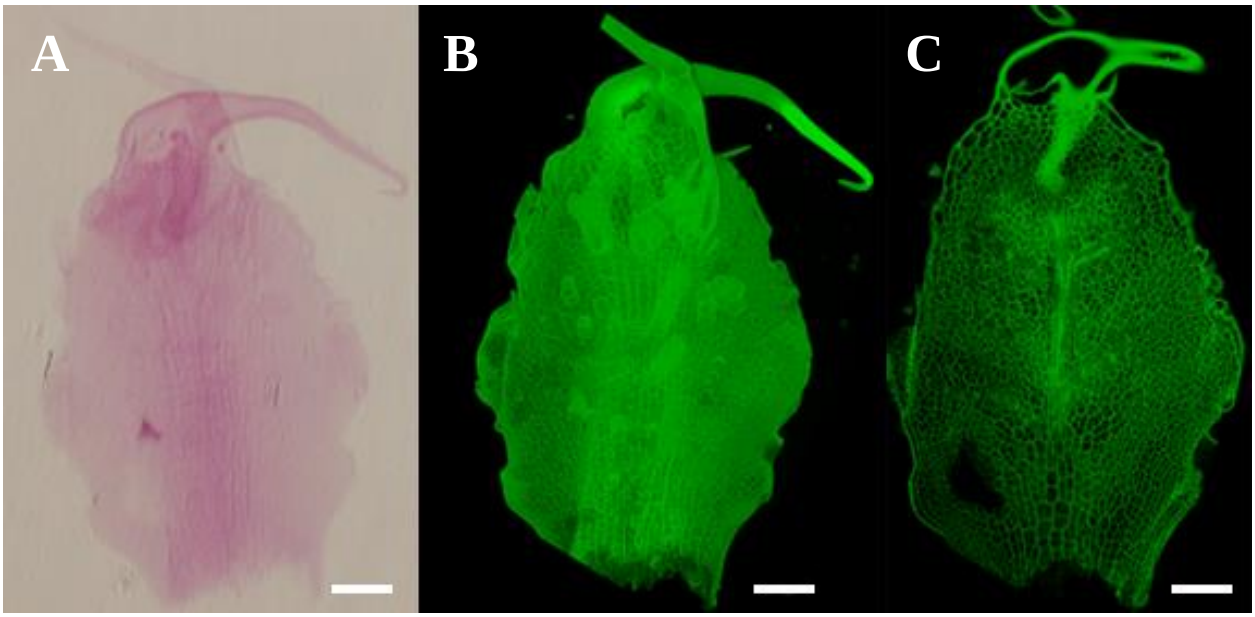

Fig. 3.3. Leaf primordia after the clearing procedure.

(**A-C**) Primordia were stained with the pseudo-Schiff - Propidium Iodide solution and imaged in the brightfield light microscope (**A**) or in the laser confocal microscope (**B-C**). A top view at the abaxial primordium side (**A, B**) and optical tangential section across the primordia (**C**). Both images (**B-C**) were obtained with using the MorphoGraphX software. Scale bars: 50 µm.

3.2.3. Auxin microapplication and global treatment

Before any auxin treatment, isolated shoot apices were imaged in the confocal microscope at first-time point (T_{0h}) (**Fig. 3.1**). Then, directly after the imaging, shoot apices were treated with auxin either by (1) a microapplication of 5 mM synthetic auxin NAA (1-Naphthaleneacetic acid, Sigma) solved in the lanolin paste with an addition of gel filtration medium Sephadex Superfine (Cytiva), or by (2) a global treatment of 5 mM natural auxin IAA (Indole-3-acetic acid, Sigma) solved in a sterile water. In the case of the microapplication, a drop of the paste with NAA was locally applied at the tip of leaf primordia. For the mock treatment, the paste without NAA was applied in the similar amount. In the case of global treatment, 100 µl of IAA water solution was applied at the primordia, and the treatment was repeated every day. For the mock treatment, only water was applied in the same amount. Then, the treated apices were grown in the short day conditions for the next 2 days, and afterwards, they were imaged again for the second time point (T_{+48h}). After this imaging, the isolated shoot apices were fixed and subjected to the clearing method (see the above the section **3.2.2 Clearing of leaf primordia**).

3.2.4. Suppression of polar auxin transport by the NPA treatment

To study the effect of polar auxin transport suppression on the vascular system, slightly different protocol was used that enabled longer plant treatment. In particular, vegetative rosettes, which were initially grown in the soil at bigger pots (about 15 x 7 cm), were moved into Petri dishes also filled with the soil (there was one plant per a dish, so that each plant was growing in the similar amount of soil, that helps to better control the NPA dose). After 5 days, few leaves that covered the apex were cut off, but all other leaves and roots remained intact. The NPA (1-N-Naphthylphthalamic acid, Supelco) at 100 mM concentration has been applied (in the amount of 200 µl) to the youngest primordia surrounding the apical meristem. Simultaneously, control plants were treated with the mock, i.e. the DMSO water solution at the same concentration and amount as used in the case of NPA treatment. Five days later, plants were dissected and apices with leaf primordia were isolated for live imaging in the confocal microscope. Afterwards, the apices were fixed and subjected to the clearing method.

3.2.5. Cell ablations

Before cell ablations isolated shoot apices were imaged at first-time point (T_{0h}) in the confocal microscope. After the imaging, cell ablations were performed manually by using very fine needles (0.3 mm x 13 mm, Microlance BD) at three different primordia sites (**Fig. 3.4A-C**). The aim of apical and lateral ablations was to disturb epidermal apical and lateral auxin sources marked by elevated DR5v2 expression with a puncture of primordium tip and margins (**Fig. 3.4A, B**). The puncture of the middle primordium region, which ablated epidermal, subepidermal and midvein cells, was to disrupt the midvein continuity (**Fig. 3.4C**). Then, the isolated apices were grown in the short day conditions for the next 2 days, and afterwards, they were imaged at second-time point (T_{+48h}). After this live imaging, the apices were fixed and subjected to the clearing method.

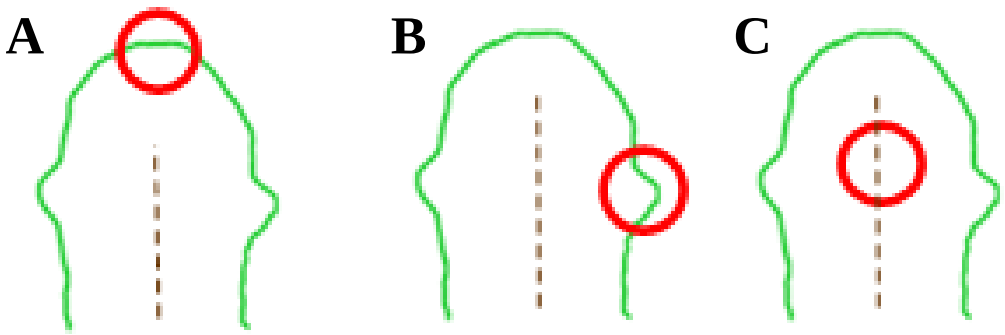

Fig. 3.4. Schemes of cell ablations at leaf primordia.

The apical ablation (**A**), lateral ablation (**B**), and the midvein ablation (**C**). Leaf primordia silhouette (green), the midvein (dashed brown line segment), the ablation site (red circle).

3.2.6. Laser confocal microscopy

The imaging of primordia was performed with using inverted confocal laser-scanning microscope (FV1000 Olympus) with long-working distance water-dipped 40x objectives for live imaging, or with 40x or 60x objectives with short-working distance and oil immersion for cleared material. To visualize cell walls for live imaging, shoot apices were treated with 0.1% Propidium Iodide (PI) solved in water for about 15-20 min before each imaging. Then, leaf primordia still attached to the apices were scanned in the microscope in the drop of water (live imaging). Leaf primordia after clearing procedure were mounted on a slide with a coverslip and scanned with oil immersion.

The following settings for the microscopy were used for live imaging: for GFP/YFP - excitation 488 nm, emission 505-540 nm, for PI - excitation 543 nm, emission 575-675 nm. Laser power was 15-20%. The imaging was performed at the resolution 512 x 512 pixels (live imaging) or 1024 × 1024 pixels (cleared material) with 8-bits, using one-directional scan mode and a scan speed 8.0 µs per pixel. The z-interval (z-step) which determines the resolution in z direction was 0.6 or 0.3 µm. Usually, the imaging took from 4 to 20 minutes due to different primordium size and applied settings.

3.2.7. Image analysis

The z-stacks from the confocal microscope were visualized and analyzed by using the MorphoGraphX (MGX) software (Barbier de Reuille et al., 2015; https://morphographx.org/), and by the ImageJ (https://imagej.nih.gov/ij/). Views on the whole leaf primordia and optical sections in different planes were performed in the MGX by adjusting 'opacity' for the signal intensity either for the PI alone or in the combination with different reporters (DR5v2, ATHB8, TAA1, YUC4). The signal intensity in a color scale was quantified with the MGX. First, a mask and then a mesh were created which overlapping with the surface of leaf primordia. Then, the signal was projected onto the mesh at a depth of 1-8 µm below the primordium surface corresponding to the epidermis.

The DR5v2 signal intensity at apical and lateral auxin sources or at inner tissues (including primary and second-order strands) shown at plots was measured by using the ImageJ software with 'multipoint selection' tool. Measurements of cell, strand or primordium dimensions (e.g. the width or length) were performed in the ImageJ with using 'straight line' tool. These parameters were measured at apical, middle, and basal primordium regions, which were designated according to a scheme shown at **Fig. 3.5**. Leaf primordia were cut off from the apex with a variable precision, so that sometimes the most proximal primordium region was not represented at images. Thus, the first serrations serve as reliable reference points to define the basal primordium region (**Fig. 3.5**). In particular, the basal region was set between the first serrations (**Fig. 3.5**, points 1 and 2). The very tip of primordia was represented by a trichome (point 7). The position of serrations and the trichome was a reference to set apical and middle regions. Namely, the apical region (between 5 and 6 points) was set at the half distance between the basal region (points 1 and 2) and the trichome (point 7). The middle regon (between 3 and 4 points), in turn, was set at the half distance between the basal and apical regions. The width of left and right primordium sides were measured from the points (1-6) at epidermis to the midvein, and summed to compute the overall primordium width. The primordium length was measured as a distance between a trichome (point 7) and the basal region (blue line). Because mature leaves in *Arabidopsis* can be asymmetric, meaning that left and right sides are different (Chitwood et al. 2012), the width of leaf primordia was first measured separately for these two sides.

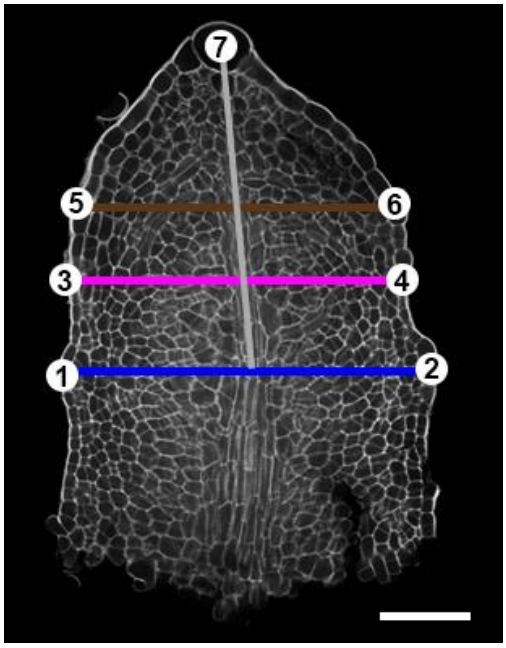

Fig. 3.5. A leaf primordium with marked apical, middle, and basal regions.

Line segments (brown, magenta, and blue) mark primordium regions (apical, middle, and basal respectively), where different cells/strand/primordium dimensions were measured. A grey line segment indicates the distance between the basal region and the trichome. Reference points at epidermis that define particular primordium regions are numbered from 1 to 6. The point 7 marks a trichome at the primordium tip. Scale bar: 50 µm.

The 3D reconstruction of procambium strands in primordia (shown at the **Fig. 4.7B-D, Fig. 4.16, Fig. 4.17, Fig. 4.21, Fig. 4.23**) was done with using a dedicated script written in Python (A. Kokosza, W. Pałubicki, unpublished). In this program, procambial cells were recognized by their elongation shape (the cell need to be at least 1.5 times longer than wider) and manually marked by points at individual slices of the confocal stacks from cleared primordia (**Fig. 3.6A**). Then, the points were joined into lines, which represented procambial strands (**Fig. 3.6B**).

Plots and statistical analyses were performed in Excel (Microsoft Office 365).

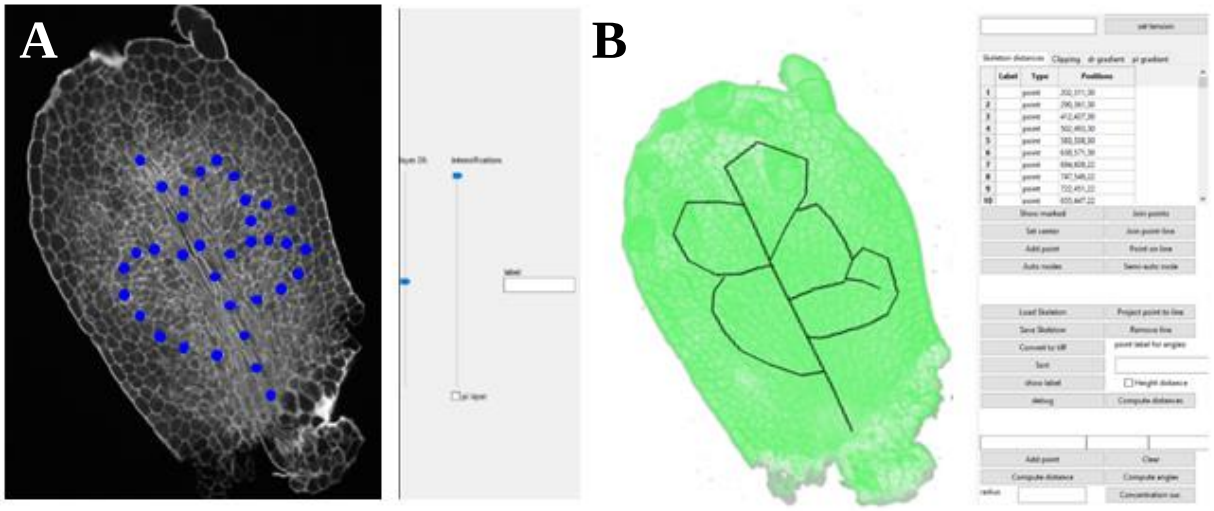

Fig. 3.6. The program written in the Python to reconstruct the pattern of procambial strands.

(**A**) Procambial cells (blue dots) were recognized at individual confocal stacks. **(B**) Points were jointed into the lines representing procambial strands.

4. RESULTS

4.1. Visualization of vascular system initiation by different transgenic lines

To visualize the initiation of vascular system in Arabidopsis leaf primordia, three transgenic lines were analyzed: pATHB8:YFP, DR5v2:GFP (nuclear localization), and DR5v2:YFP (localization in the endoplasmic reticulum) to select the one for further analyses and experiments.

Pre-procambial and procambial cells can be distinguished among other ground cells by using ATHB8:YFP reporter (Donner et al. 2009). In the earliest stages of leaf primordium development examined in this study, a strand of the ATHB8 expression is visible in the central region of primordia (**Fig. 4.1A**, asterisks). This strand is extended from the basal to apical primordium region and marks the future midvein. In next primordium stages, the ATHB8 expression is much weaker and restricted mainly to apical and middle primordium regions (**Fig. 4.1B-C**). The ATHB8-expressing strand marks the upper part of the midvein and future second-order veins forming loops (**Fig. 4.1B-C**, hash). In the oldest primordia, the ATHB8 expression is extremely weak, so that only strands corresponding to the midvein and second-order strands, which some are extended towards serrations, are observed (**Fig. 4.1D**, asterisks, hash). In all the stages, the ATHB8 expression is observed only in inner tissues but not in epidermal cells.

The localization of transcriptional auxin response related with the initiation of procambium can be monitored in different stages of leaf primordium development by using DR5v2:GFP and DR5v2:YFP reporters. These reporters also indirectly show auxin levels (Liao et al. 2015). Thus, the DR5v2 expression can reveal possible sites of local auxin accumulation (auxin maxima) corresponding to auxin sources and possible routes of auxin flow (auxin canals) marking pre-procambial and procambial cells at future veins.

In initial stages of primordium development, a strong expression of both DR5v2 reporters is observed in a strand corresponding to the future midvein (**Fig. 4.1E-F**, **I-J**, asterisks). Moreover, the strong DR5v2 expression is observed at the apical primordium region as well as at lateral regions (corresponding to future serrations), where the DR5v2 expression is localized mainly in epidermal, but also in subepidermal cells (**Fig. 4.1E-F**, **I-J**, arrows). These sites marked may be regarded as apical and lateral auxin sources, respectively. In next primordium stages, the DR5v2 expression marks also future second-order veins forming loops (**Fig. 4.1G**, **K**, hash). Finally, in the oldest primordia, the DR5v2 expression corresponding to the future

midvein gradually decreases in comparison to younger primordia (**Fig. 4.1H, L** compare with **4.1F-G, J-K,** asterisks). However, locally elevated DR5v2 expression in epidermal and subepidermal cells (corresponding to apical and lateral auxin sources) and the DR5v2 expression marking loops are still observed (**Fig. 4.1H, L** arrows and hash, respectively).

Summarizing, the initiation of the vascular system during early stages of leaf primordium development can be visualized by using different transgenic lines. The ATHB8 is a reliable marker of pre-procambial and procambial cell fate (Donner et al. 2009). However, in comparison to the DR5v2, the ATHB8 expression is much weaker in future vascular strands and less informative, because it does not reveal possible auxin sources. Also, it has been reported that other auxin-independent factors can have an impact on the ATHB8 expression (Marcos and Berleth, 2014). Therefore, the ATHB8:YFP line was not used in further experiments. Generally, the expression of DR5v2:GFP and DR5v2:YFP is similar and strong enough to distinguish initiating vascular strands during early primordium development. However, at the oldest primordia, the DR5v2 expression in both lines decreases in future veins, which is probably related with procambium differentiation and/or a weak penetration of the laser throughout tissues when primordia were scanned in the confocal microscope. Finally, the DR5v2:YFP line with the localization in the endoplasmic reticulum was selected for further experiments based on its more continuous fluorescent signal in initiating veins.

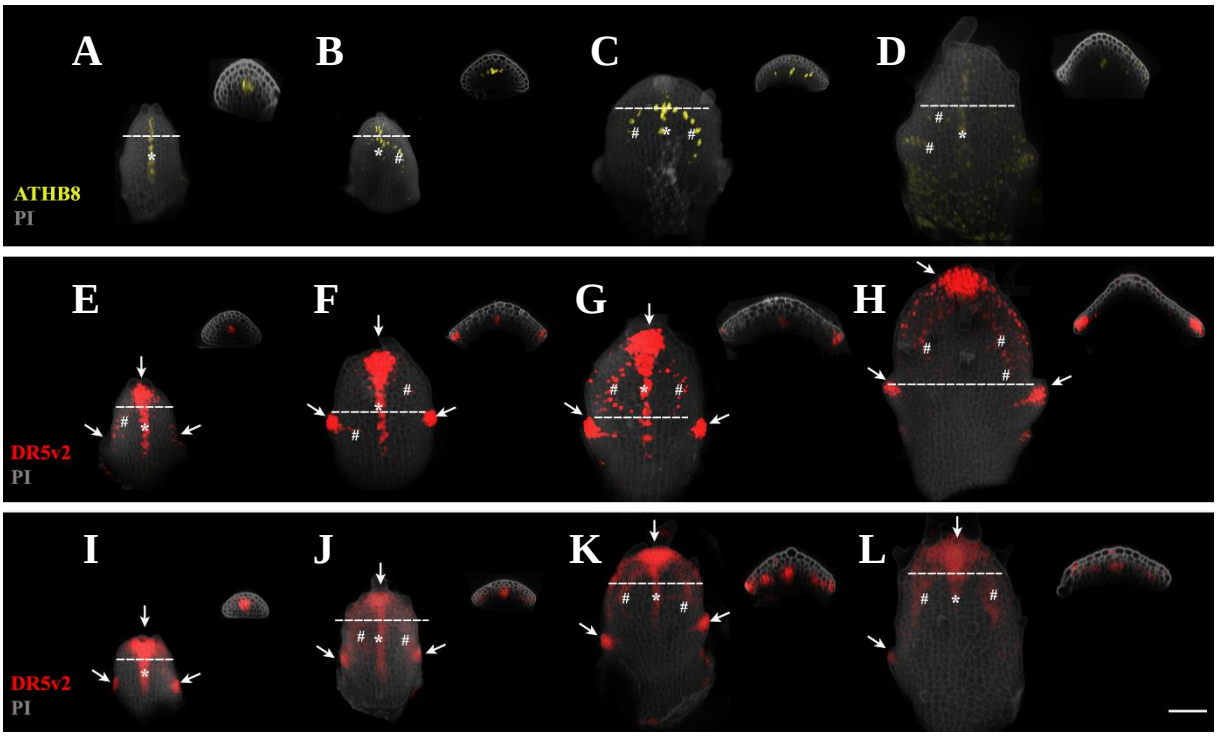

Fig. 4.1. Visualization of vascular system initiation at different primordium stages with using various transgenic lines.

(**A-D**) The ATHB8:YFP expression marking initiating vascular strands. (**E-L**) The DR5v2:GFP (nuclear localization, **E-H**) and DR5v2:YFP (endoplasmic reticulum localization, **I-L**) expression marking transcriptional auxin response and indirectly auxin levels in initiating vascular strands. Images show original confocal stacks (obtained from live imaging). Inserts show optical transverse sections across primordia indicated by a dashed line. Apical and lateral auxin sources are indicated by arrows. The future midvein is indicated by asterisks and future second-order veins and loops by a hash. Representative primordia are shown (out of 40 analyzed primordia). Scale bar: 50 μm.

4.2. Quantification of the DR5v2 expression at apical and lateral auxin sources

To study how the strength of apical and lateral auxin sources changes as leaf primordium develops, the DR5v2 expression was quantified in the DR5v2:YFP line. The DR5v2 signal projection and its quantification has been performed with using the MorphoGraphX (MGX) software. The DR5v2 signal was projected at the distance between 0 and 10 μm from the primordium surface, which corresponds to the epidermal cell layer. Even in the earliest stages of primordium development, both apical and lateral epidermal auxin sources are clearly visible marking by locally higher DR5v2 expression (**Fig. 4.2A**, arrows). Lateral sources are restricted to the region of primordia where the first pair of serrations will appear. In the oldest primordium stages, additional lateral sources above the pre-existing serrations are visible, probably marking successive serrations (**Fig. 4.2A**, asterisks).

To check whether there are differences in the signal strength between apical and lateral auxin sources at various primordium stages, the DR5v2 signal intensity was measured at different primordium sites by using ImageJ software and signal projection images obtained from the MGX. Then, the signal intensity has been plotted against the primordium length (**Fig. 4.2B-D**). In this case, the length of primordia serves as an indicator of their development stage. Statistical analysis of 12 examined primordia show that there is no correlation, or the correlation is very weak, between the DR5v2 signal intensity at apical or lateral (both right and left) auxin sources and primordium length (Pearson's correlation coefficient $r = 0.04$ for apical source; $r = -0.12$ for right lateral source; $r = -0.51$ for left lateral source) (**Fig. 4.2C-D**). Also, differences in the signal intensity between lateral and apical sources are not statistically significant (**Fig. 4.2E**).

Summarizing, quantitative analysis of the DR5v2 expression reveals that apical and lateral epidermal sources are present from the earliest stages of primordium development. However, there is no significant differences in the signal strength between apical and lateral sources, and the signal strength is not changing significantly during primordium growth.

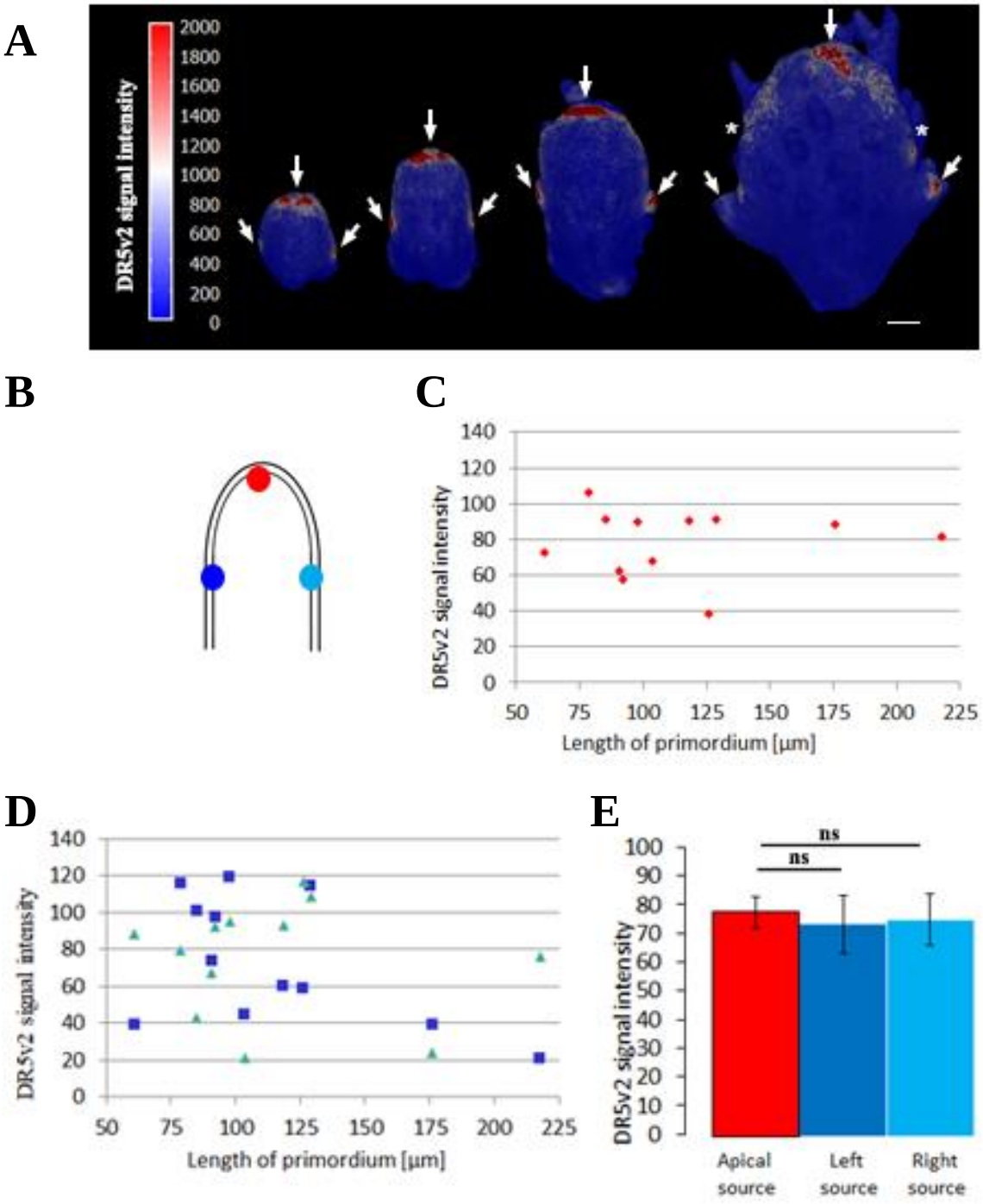

Fig. 4.2. Quantification of the DR5v2:YFP expression at different stages of primordium development.

(**A**) The DR5v2 signal projection and the quantification obtained with MGX software. Apical and lateral auxin sources marking by the epidermal DR5v2 expression are indicated by arrows; the expression above the first serrations is indicated by asterisks. (**B**) Schematic localizations of analyzed auxin sources. (**C**) The correlation between the DR5v2:YFP signal intensity at apical source (diamonds) and the length of primordia (measured as a distance between the position of first serrations and a trichome cell at apical

region of primordia). (**D**) The correlation between the DR5v2:YFP signal intensity at left (squares) and right (triangles) auxin source and primordium length. (**E**) Mean signal intensity of the DR5v2:YFP at apical and lateral sources. Apical auxin source (red); left (dark blue) and right (light blue) lateral sources. Error bars represent how the data are spread around the mean value (Standard Error, SE). Correlations (in **C** and **D**) are not significant at 0.05 level (Pearson's correlation significance test). Differences between mean values (in **E**) are not statistically significant (ns) at 0.05 level (Student's t test). N=12 primordia. Scale bar: 50µm.

4.3. Expression patterns of auxin biosynthesis genes

Sites of locally elevated auxin transcriptional response corresponding to auxin sources can be revealed by using DR5v2:GFP and DR5v2:YFP reporters. Thus, these sites may be related to a local auxin accumulation. Auxin accumulation can be in turn generated by the PIN1-mediated polar auxin transport, where PIN1 polarization forms epidermal convergence points at primordium margins (Scarpella et al. 2006). However, locally elevated auxin levels may be also a consequence of local auxin biosynthesis (Kneuper et al. 2021). Thus, the aim of further analysis was to check in which regions of leaf primordia auxin is synthesized, and what is the relationship between these regions and sites marked by the DR5v2 expression. Among genes involved in auxin biosynthesis, expression patterns of two genes *YUC4* and *TAA1* were analyzed (with using pYUC4:GFP and pTAA1:TAA-GFP transgenic lines) based on their activity at the shoot apex (Mano and Nemoto 2012).

The expression of *YUC4* is observed in the epidermis throughout the whole primordium from the earliest analyzed stages of leaf primordia (**Fig. 4.3A-B**, upper panel). The quantification of *YUC* signal intensity reveals that in these stages the signal intensity is already locally increased at the marginal region of primordia where future serrations will appear (**Fig. 4.3C-B**, middle and bottom panels, arrows). During subsequent primordium stages, a locally higher *YUC4* expression at the marginal region of primordia is even more clearly observed (**Fig. 4.3C**, arrows). In particular, the *YUC4* signal intensity is stronger, where the first pair of serrations are formed (**Fig. 4.3C**, dots), than at other primordium regions, where the signal is gradually decreasing. In the oldest analyzed primordia, the high *YUC4* expression is maintained at primordium margins (**Fig. 4.3D**, arrows), but the signal is observed above the existing first serrations (**Fig. 4.3D**, dots), probably corresponding to sites of future second serrations. Moreover, the *YUC4* expression almost completely disappears from other regions of primordia.

A similar expression pattern at marginal primordium region is observed in the case of *TAA1* gene. In particular, the *TAA1* is locally expressed at sites of future serrations from the earliest stages of primordia (**Fig. 4.3E-F**, arrows). Subsequently, when first serrations are formed (**Fig. 4.3G-H**, dots), the strong *TAA1* expression is observed above these serrations (**Fig. 4.3G-H**, arrows). On the other hand, there are some differences between the expression of *YUC4* and *TAA1*. First, the *TAA1* expression is not observed throughout the whole primordium like *YUC4*, but its expression is localized only at the marginal primordium region. Second, the *TAA1* expression is the strongest at later primordium stages. i.e. just before second serrations are formed (**Fig. 4.3G**), while the expression of *YUC4* is the strongest at earlier stages, i.e. before first serrations formation (**Fig. 4.3A**).

Taken together, the *YUC4* expression indicates that auxin can be initially synthesized in the whole leaf primordia. However, the expression of *YUC4* and *TAA1* at later stages suggests that during primordium growth, auxin synthesis is localized at primordium margins in a close relation to the formation of serrations. Thus, lateral auxin sources can be generated not only due to polar auxin transport, but also *via* localized auxin biosynthesis. However, based on obtained results, the increased DR5v2 expression marking auxin source at apical primordium region cannot be explained by localized auxin biosynthesis. Instead, this expression might be caused by the polar auxin transport or/and local upregulation of genes related with auxin signalization.

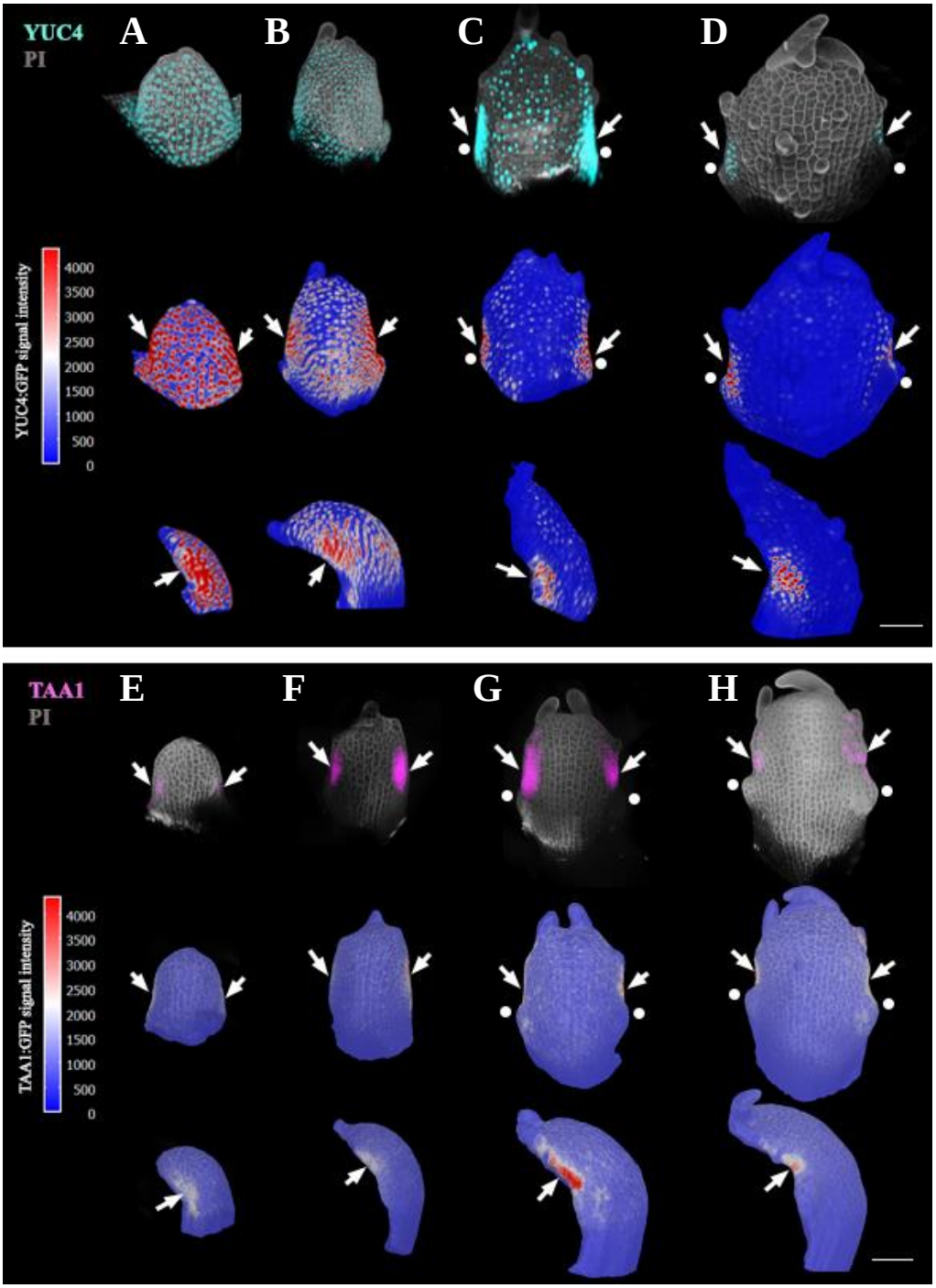

Fig. 4.3. Expression patterns of genes related with auxin biosynthesis pathway.

(**A-H**) The expression of *YUC4* (**A-D**) and *TAA1* (**E-H**) at different primordium stages. Original confocal images obtained from live imaging (upper panels). Signal projections obtained with MGX software: a view at abaxial primordium site and a side view (middle and bottom panels, respectively). Locally higher *YUC4* or *TAA1* expression is indicated by arrows. Serrations are indicated by dots. Representative primordia are shown (out of 12 analyzed primordia). Scale bar: 50 μm.

4.4. Development of procambial cells

To recognize cellular processes (i.e. cell growth, cell divisions) underlying the initiation of vascular system in leaf primordia, morphology of procambial cells has been analyzed in details in fixed cleared leaf primordia (see **Materials and Methods**). Gradual development of procambial strands has been described by "procambium differentiation levels" estimated based on the shape of procambial cells and new cell walls after cell divisions (**Fig. 4.4A-H**).

Initially, procambial cells were identified as cells which are slightly longer than wider (i.e. approximately 1.5 times longer than wider). This slightly elongated cell shape is obtained by a cell division of a nearly isodiametric cell (**Fig. 4.4A**, asterisks, a new cell wall was recognized by its lower PI signal). Thus, the initial shape of procambium cells is generated due to cell divisions, rather than from anisotropic growth. Subsequently, procambium cells become much more elongated (**Fig. 4.4B)**, and further cell divisions oriented along the long cell axis (and also the strand axis) lead to more elongated cell shapes (**Fig. 4.4C-D**, asterisks). Finally, several very elongated procambial cells are observed along the strand.

Next, a level of procambial cell differentiation was analysed in relation to primordium development (**Fig. 4.4E-H**). In agreement with the DR5v2 expression, a primary strand of procambial cells (i.e. the future midvein) is observed along primordia even at their very early developmental stages. All procambial cells in the future midvein are at early level of differentiation, showing their slightly elongated shapes (**Fig. 4.4E**). During later primordium development, further elongation of procambial cells is observed in the midvein (**Fig. 4.4F**). In addition, second-order procambial strands start to extend from the midvein towards lateral regions of primordia. Therefore, new procambium strands are branching (and they differentiate) from the pre-existing strand. Then, further second-order procambium strands are branching and finally form loops, first in the apical region and later also at the middle region of primordia (**Fig. 4.4G**, hash). Subsequently, more second-order strands are formed below the loops indicating basipetal direction of strand branching (**Fig. 4.4H**). Every loop is formed by joining the two second-order strands branching from the midvein, thus, also in the case of loops, the direction of procambium differentiation is from the pre-existing strand (**Fig. 4.4G**, hash, note less differentiated procambial strands marked in green linking more differentiated strands marked in yellow). Meanwhile, procambial cells in the midvein divide along the cell axis, so that they become extremely elongated (**Fig. 4.4G-H**). Finally, in the oldest analysed primordia a network of hierarchically arranged procambial strands is created, consisting of the primary

strand (midvein), second- and higher-order strands. Some of these strands form loops, while the other are free-ending.

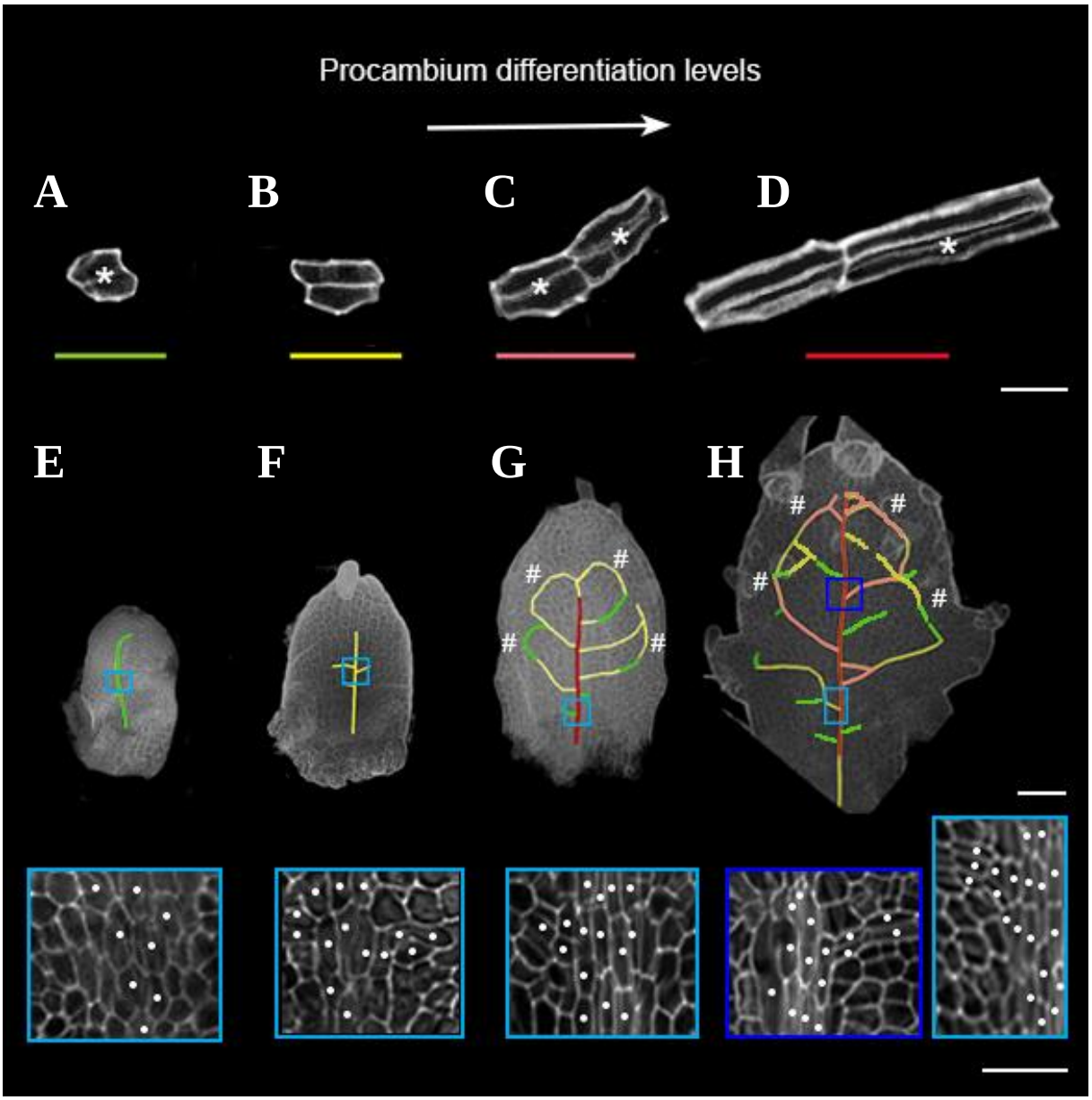

Fig. 4.4. Development of procambial cells.

(**A-D**) Procambium differentiation levels. Line segments of different colors indicate consecutive levels of procambium differentiation. Newly formed cell walls are marked with asterisks. (**E-H**) The color map of procambium differentiation levels at different developmental stages of primordia. Insertions at the bottom show the magnification of framed primordium regions. Dots indicate procambial cells at the future midvein and second-order veins. Loops are marked by a hash. Images show original confocal stacks (obtained from clearing method). Representative primordia are shown (out of 29 analyzed primordia). Scale bars: 5 µm (**A-D**), 50 µm (**E-H**), 10 µm (insertions).

So far, the data suggest that cell divisions are important in procambium formation. To further check the impact of cell divisions and cell growth in this process, cell number and cell shapes have been quantified in procambial strands during primordium development.

First, it has been investigated how the width of the primary procambial strand (the future midvein) changes during leaf primordium growth (determined by the length of primordia). To check this relation, the midvein width was measured in three primordium regions and plotted against the primordium length (**Fig. 4.5A**). Statistical analysis of 31 primordia showed a positive correlation between the midvein width and the primordium length in the apical primordium region (**Fig. 4.5A**, brown; Pearson's correlation coefficient r = 0.94), the middle region (**Fig. 4.5A**, magenta; Pearson's r = 0.73), and in the basal region corresponding to the level of first serrations (**Fig. 4.5A**, blue; Pearson's r = 0.69). Therefore, the midvein width increases during primordium growth.

In order to determinate how the midvein widens (i.e. either by cell divisions or cell growth, or by both), the number of procambial cells per midvein width, procambial cell width and length were measured in three previously designated primordium regions (**Fig. 4.5B-C**). Analysis of the procambial cell number per the midvein width shows a positive correlation between the cell number and the primordium length in all primordium regions: in the apical region (**Fig. 4.5B**, brown; Pearson's r = 0.51), in the middle region (**Fig. 4.5B**, magenta; Pearson's r = 0.57), and in the basal region (**Fig. 4.5B**, blue; Pearson's r = 0.72). Thus, the number of procambial cells increases as the midvein widens during primordium growth. Furthermore, the analysis of procambial cell morphology (cell width and length) also shows positive correlation between the cell length and the primordium length in the apical primordium region (**Fig. 4.5C**, brown triangles; Pearson's r = 0.53), in the middle region (**Fig. 4.5C**, magenta triangles; Pearson's r = 0.36), and in the basal region (**Fig. 4.5C**, blue triangles; Pearson's r = 0.38). However, there is no correlation between the cell width and the primordium length in apical, middle and basal regions (**Fig. 4.5C**, diamonds). Thus, the length of procambial cells increases, but their width remains constant during primordium growth.

In addition, analyzing the ratio of procambium cell length and width, a statistically significant difference is found in the mean ratio computed for different primordium regions (**Fig. 4.5F**). Namely, the mean ratio in the basal region is higher than in the middle region, while those in the middle region is higher than in apical region. Thus, it means that procambial cells in the basal region are much more elongated in comparison to the cells from other regions. Also, the midvein width, and the number of procambial cells per midvein width are higher in the basal

region in comparison with middle and apical regions (**Fig. 4.5D-E**). This indicates that the differentiation of procambial cells in the midvein is more advanced in the basal primordium region than in the apical region. In other words, the direction of procambium differentiation in the midvein is acropetal.

Summarizing, initial procambium differentiation is related to cell divisions, that leads to the generation of slightly elongated cells. Subsequently, procambial cells become much more elongated with a high ratio of cell length and width. This extremely elongated cell shape is a result of anisotropic cell growth (maximal along the long cell axis) and cell divisions oriented parallel to the cell axis, which is indicated by increased cell length and increased number of cells, respectively. The procambial cell width is constant, likely because cell divisions compensate the cell growth in width (perpendicular to the long cell axis). In addition, analysis of cell morphology indicates that the procambium at the midvein differentiates acropetally in leaf primordia (the most advanced procambial cells are found at the basal midvein region). In turn, the second-order strands are branching and differentiate from the pre-existing strand. The formation of these second-order strands occurs in the basipetal direction in primordia, which means that the first strands are branching at the apical midvein region.

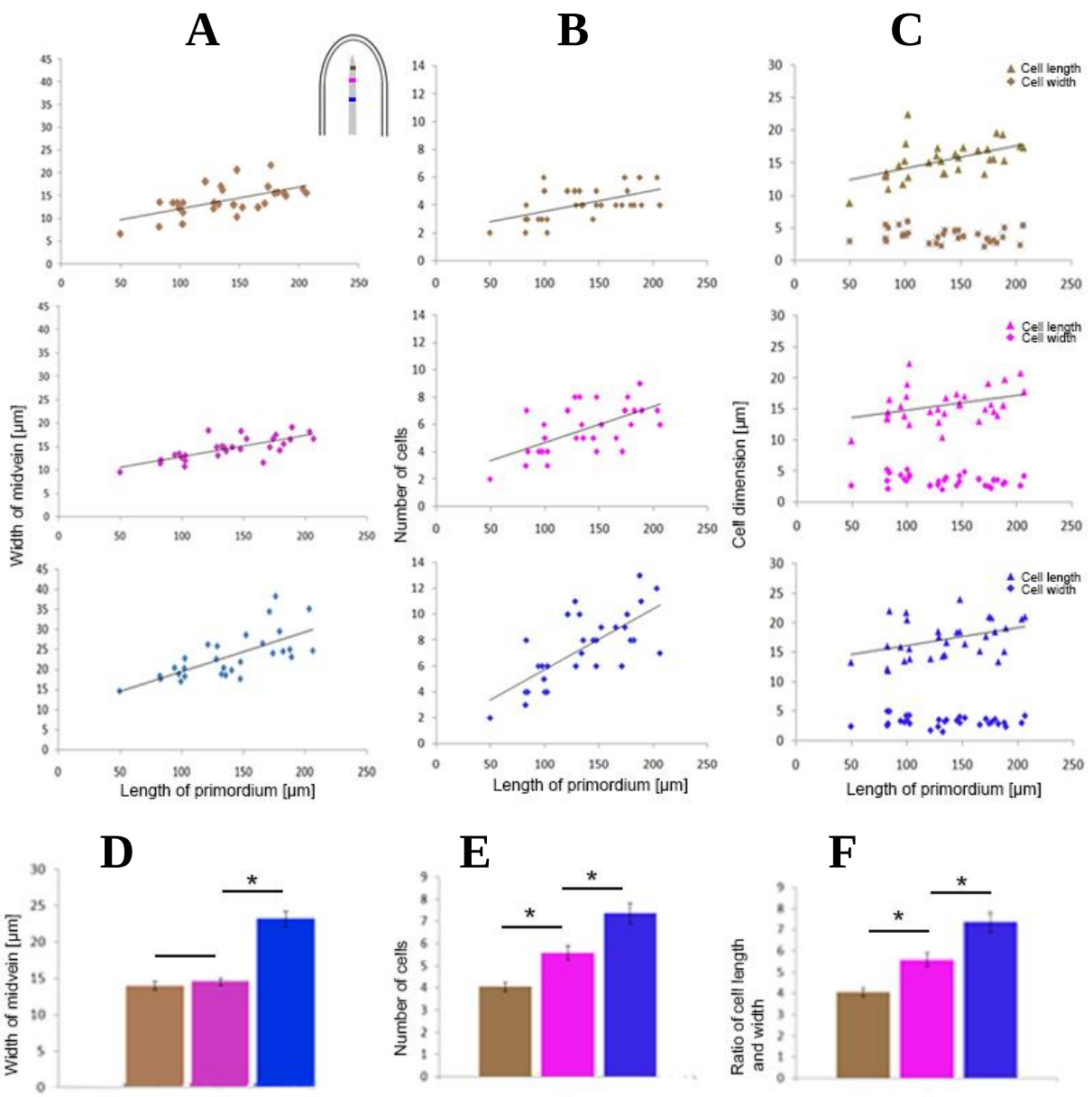

Fig. 4.5. Quantification of procambial cell development in the midvein during primordium growth.

(**A**) The correlation between the midvein width and the primordium length. A scheme at the top indicates measured midvein areas at different primordium regions. (**B**) The correlation between the number of procambial cells per midvein width and the primordium length. The cells from regions indicated in the scheme at (**A**) were counted. (**C**) The correlation between the length or the width of procambial cells in the midvein and the primordium length. Cell length (triangles); cell width (diamonds). Mean values computed for procambial cells in each primordium region are shown. (**D**) The midvein width at different primordium regions. (**E**) The number of procambial cells per midvein width at different primordium regions. (**F**) The ratio of procambial cell length and width at different primordium regions. Apical primordium region (brown); middle region (magenta); basal region (blue). Mean values ± SE are shown.

The black line represents the linear regression. All correlations are significant at 0.05 level (Pearson's correlation significance test). Statistically significant differences at 0.05 level are indicated with asterisks (Student's t test). N= 31 primordia.

4.5. Development of procambial strand pattern

To study development of procambial strand pattern during primordium growth, different parameters describing the vein pattern in leaves have been analyzed based on images of fixed cleared primordia.

Since the vein pattern depends on a leaf shape (Nelson and Dengler 1997), first, the primordium shape have been quantified. In particular, the width of left and right primordium sides during primordium growth (determined by the primordium length) was measured in order to assess the lateral primordium growth and to check to what extent primordia are symmetrical (**Fig. 4.6A**). A positive correlation is found between the width of left or right primordium sides and the primordium length at the apical primordium region (**Fig. 4.6A**, brown triangles, Pearson's r = 0.78 for the left side; brown diamonds, r = 0.77 for the right side), the middle region (**Fig. 4.6A**, magenta triangles, Pearson's r = 0.77 for the left side; magenta diamonds, r = 0.80 for the right side), and the basal region (**Fig. 4.6A**, blue triangles, Pearson's r = 0.71 for the left side; blue diamonds, r = 0.68 for the right side). Thus, the primordium width increases during the primordium growth. However, no statistically significant differences in the mean values between left and right sides are found in apical and middle primordium regions (**Fig. 4.6B**, brown and magenta). Only a slight difference is detected in the basal region (**Fig. 4.6B**, blue). Moreover, the width of right and left sides is higher in the basal region in comparison to middle and apical regions of primordia. These observations suggest that generally leaf primordia are symmetrical, and not only the primordium length, but also the width increases during primordium development, especially in the basal region.

To quantify how the pattern of procambial strands develops during primordium growth, the relation between the number of second-order strands and the primordium length has been analyzed (**Fig. 4.6C**). First, measurements were performed separately for the right and left primordium sides to additionally check whether primordia might be symmetrical in this aspects. Generally, for all analyzed 31 primordia, there is no statistically significant differences between the number of strands at the right and left primordium sides (the mean values: 3.48 and 3.51 at right and left side, respectively). Thus, next, the total number of second-order strands was

estimated and plotted against the primordium length (**Fig. 4.6C**). Statistical analysis shows a strong positive correlation between this number and the primordium length (Pearson's r = 0.75).

The other parameters describing the strand pattern are related to the number of branching points and strands density. Branching points were determined based on the presence of new strands (both the second- and higher-order) branching from these points (**Fig. 4.6D**). Statistical analysis shows a strong positive correlation between the number of branching points and the primordium length (**Fig. 4.6D**, Pearson's r = 0.70). In turn, the strand density was measured as the total length of all procambial strands per primordium area (**Fig. 4.6E**). Statistical analysis shows a positive correlation between the strand density and the primordium length (Pearson's r = 0.54). Thus, during primordium growth both the number of branching points and strand density increase.

The last parameter describing procambium pattern is associated with the formation of loops. To check whether loops are formed in relation to lateral growth of primordia, the correlation between the presence of loops and the primordium width was analyzed (**Fig. 4.6F**). The primordium width, in the cases where loops are observed (**Fig. 4.6F**, L), is significantly higher than in the cases without loops (**Fig. 4.6F**, NL) at all designated primordium regions. Thus, these data suggest that generally loops are formed at particular primordium region when its width increases. However, the primordium width of particular regions is not a critical parameter for the loop formation. The mean primordium width at the apical region with loops is approximately 100 μm (**Fig. 4.6F**, an 'x' in the L brown box), and it is similar to the mean primordium width at middle and basal regions without loops (**Fig. 4.6F**, an 'x' in the NL magenta and blue boxes).

Summarizing, the pattern of procambial strand develops during primordium growth with the respect to the formation of second- and higher-order strands, that is manifested in the increased number of strands, branching points, and strand density. Moreover, development of procambial strands is very similar at both primordium sides, which indicates that leaf primordium is symmetrical in this respect.

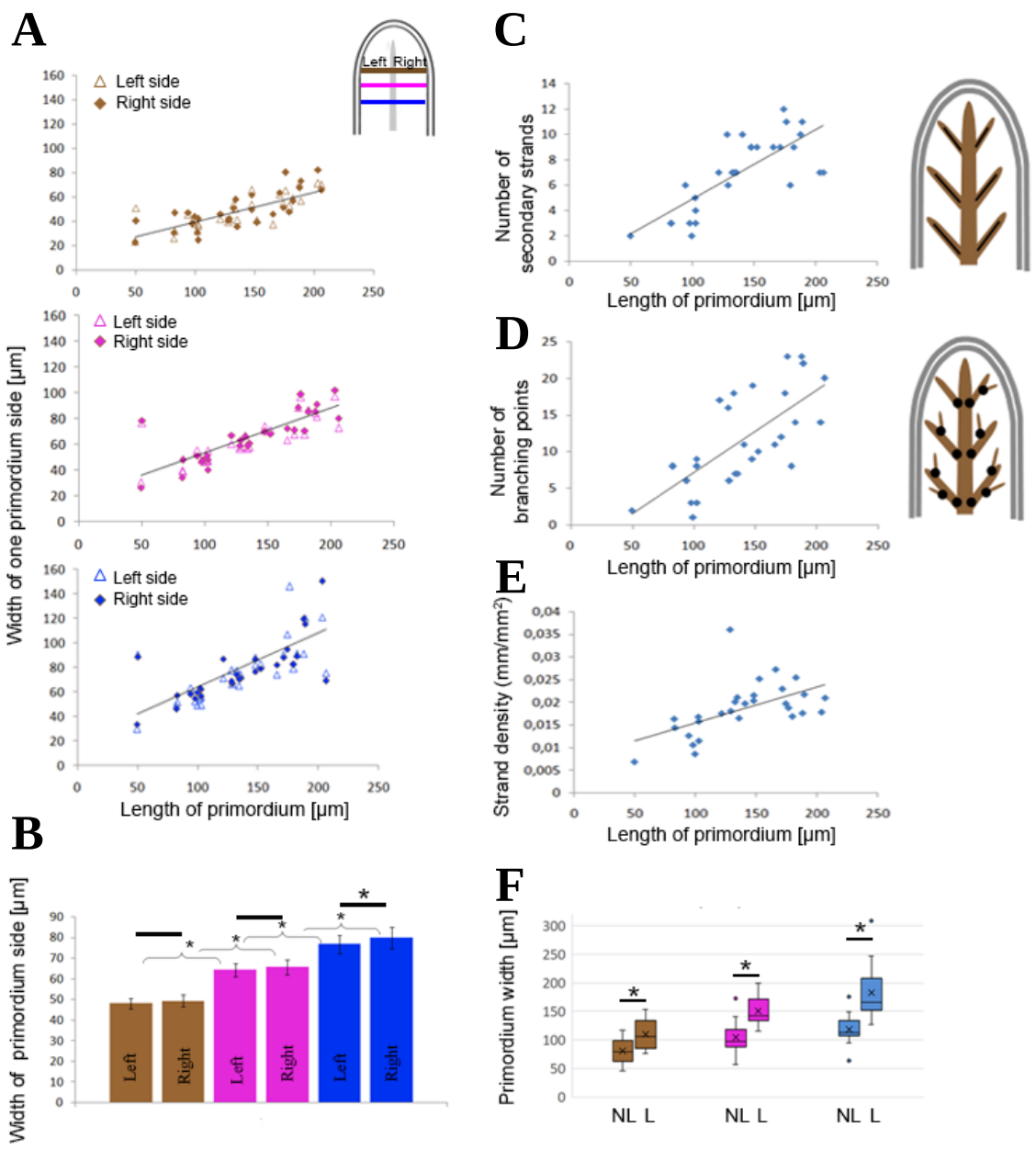

Fig. 4.6. Quantification of procambial strand pattern during primordium growth.

(**A**) The correlation between the width of right or left primordium sides and the primordium length. A scheme at the top indicates measured primordium regions. Left primordium side (triangles); right primordium side (diamonds). (**B**) The width of right and left primordium sides at different primordium regions. Mean values ± SE are shown. (**C-E**) Correlations between the number of second-order strands (**C**), the number of branching points (**D**), strand density (**E**) and the primordium length. Schemes at the right of (**C**) and (**D**) plots indicate counted second-order strands marked by black lines and branching points marked by black ellipses, respectively. (**F**) The relationship between the presence of loops and the primordium width at different regions. No loops (NL); loops (L). The black line represents the linear regression. All correlations are significant at 0.05 level (Pearson's correlation significance test).

Statistically significant differences at 0.05 level are indicated with asterisks (Student's t test). The apical primordium region (brown); the middle region (magenta); the basal region (blue). N= 31 primordia.

4.6. Auxin transcriptional response and the differentiation of procambial cells

To examine the relationship between auxin transcriptional response and the differentiation of procambial cells, leaf primordia were imaged *in vivo* (live imaging) in two time-points (T_{0h} and T_{+48h}) to visualize the DR5v2 expression, and then subsequently fixed (at T_{+48h}), and treated with the clearing solution to visualize procambium cells (see **Materials and Methods**). Next, a program written in the Python has been used to generate 3D reconstructions of strands recognized based on (1) the internal DR5v2 expression and (2) cell morphology (**Fig. 4.7A-D**, red and yellow line segments, respectively). In the latter, procambial cells were identified as at **Fig. 4.4A-D**. In addition, it has been checked whether there is a relation between the progression of procambium strand development and epidermal auxin sources marked by maxima of the DR5v2 expression at primordium tip (apical source) and margins (lateral sources).

In early stages of primordium development, the DR5v2-expressing primary strand extends along the primordium axis and marks the future midvein (**Fig. 4.7A**, T_{0h}). This strand is also connected to the apical auxin source (**Fig. 4.7A**, T_{0h}, bigger red dot). At the same time, a new DR5v2-marked second-order strand is branching at the apical part of the primary strand (**Fig. 4.7A**, T_{0h}, arrow), which next forms the first apical loop with a strand below (**Fig. 4.7A**, T_{48h}, the same second-order strand is indicated by an arrow, the loop – by a hash). Alternatively, the apical loop seems to be also formed independently of the apical auxin source by the extension of the second-order strand either from the primary strand towards lateral primordium region, or from the lateral region towards the primary strand (**Fig. 4.7C**, T_{0h} and T_{+48h}, the same second-order strands are indicated by arrows, loops – by hashes). At the same time, corresponding procambial strands recognized based on cell morphology are observed (**Fig. 47B, D**, yellow line segments), however, they are generally shorter than the DR5v2-marked strands (**Fig. 47B, D**, red line segments). This indicates that the DR5v2 expression precedes the formation of morphologically recognized procambium. For example, while the DR5v2-marked strand already forms a closed loop (**Fig. 4.7B, D**, hash), procambial strands are still free-ending (**Fig. 4.7B, D**, asterisks).

The DR5v2-marked second-order strands extending from the primary strand at the basal primordium region are also connected to lateral auxin sources (**Fig. 4.7A**, T_{+48h}; **Fig. 4.7C**, T_{0h}

and T_{+48h}, arrowheads). Generally, these DR5v2-marked strands overlap with morphologically recognized strands (**Fig. 4.7B, D**), however, the latter are shorter and clearly extend from the primary strand. In later stages of primordium development, the DR5v2-marked third-order strands extend from the strands forming loops (**Fig. 4.7D**, dots). Similarly to the previous cases, the DR5v2 expression also here precedes the formation of corresponding morphologically recognized procambial strands.

Summarizing, the internal DR5v2 expression precedes the formation of morphologically identified procambial cells indicating that auxin response marks also earlier stages of procambium development (pre-procambium). Moreover, the fact that the DR5v2-marked primary strand is connected to the apical auxin source suggests that this epidermal source might play a role in the midvein development. The apical auxin source may be also involved in the formation of the second-order strands and loops at the apical primordium region. The loops, however, can be also initiated by an internal signal at lateral primordium regions. The DR5v2-marked second-order strands at the basal primordium region are in turn connected to the lateral auxin sources which suggests that these epidermal sources (or/and related development of serrations) might regulate the formation second-order strands.

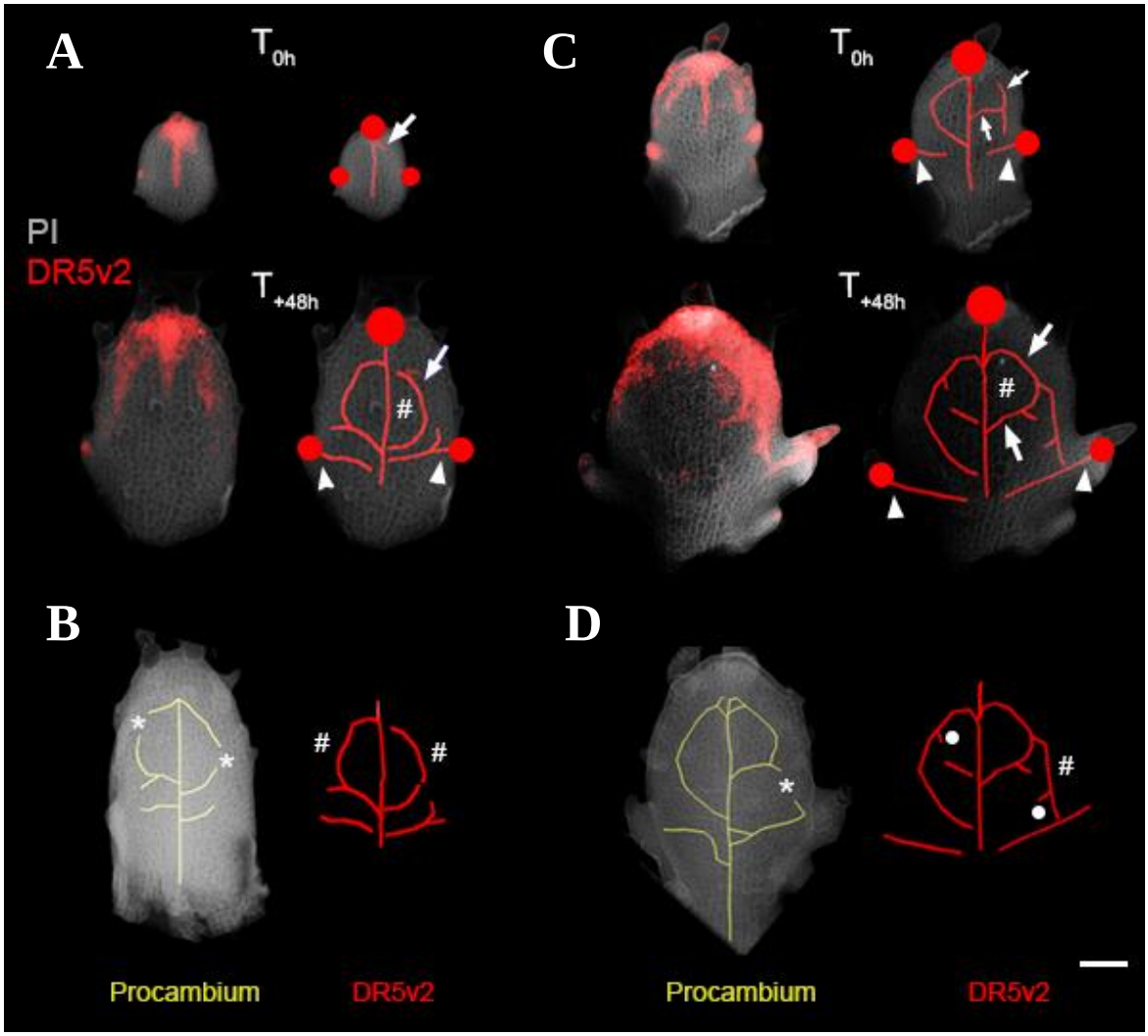

Fig. 4.7. The relation between auxin transcriptional response and the differentiation of procambial cells.

(**A, C**) The visualization of internal DR5v2 expression in two times point (T_{0h} and T_{+48h}) at early stages of primordium development (**A**) and in later stages (**C**), and 3D reconstructions of the DR5v2-marked strands. Red circles indicate apical and lateral epidermal auxin sources. Images show original confocal stacks (obtained from live imaging). Arrows at T_{0h} and T_{+48h} indicate the same DR5v2-marked strands forming apical loops indicated by a hash. Arrowheads indicate the DR5v2-marked strands connected to lateral auxin sources. (**B, D**) The 3D reconstructions of strands recognized based on the internal DR5v2 expression (red) and cell morphology (yellow) at T_{+48h} for primordia shown at (**A**) and (**C**), respectively. Images show original confocal stacks (obtained from clearing method). White dots indicate the third-order DR5v2-marked strands. Loops are indicated by hashes, asterisks show corresponding regions at morphologically recognized procambial strands. Representative primordia are shown (out of 31 analyzed primordia). Scale bar: 50 μm.

4.7. Chemical disturbing of auxin sources – auxin microapplication

To examine what is an impact of epidermal auxin sources on vascular system development, experiments with chemical disturbance of auxin distribution in leaf primordia were carried out. First, the synthetic auxin NAA (1-Naphthaleneacetic acid) in a lanolin paste has been applied at the apical region of primordia at the concentration of 5 mM as in previous studies (Caggiano et al. 2017; Galvan-Ampudia et al. 2020). This local auxin treatment (microapplication) was expected to enhance the strength of the present auxin source at the apical region of primordia.

The first step in the testing effects of the NAA microapplication was the quantification of auxin response by using DR5v2:YFP line and confocal stacks obtained from live imaging (**Fig. 4.8A-D**). The DR5v2 signal intensity has been measured at epidermis based on projection images as described in the previous **4.2** section. Before and after the NAA treatment, apical and lateral auxin sources are clearly distinguishable and marked by locally higher expression of the DR5v2 (**Fig. 4.8A-D**, arrows). After the NAA microapplication, the DR5v2 expression increases in the apical region of primordia in comparison to the mock. Namely, analysis of 10 primordia per treatment shows that the DR5v2 expression in apical auxin source is significantly higher after the NAA microapplication an average by nearly 20 % in comparison to the mock (**Fig. 4.8F**). In addition, the DR5v2 signal intensity is also significantly increased in lateral auxin sources an average by approximately 30 % in comparison to the mock. To check whether the NAA microapplication affects auxin response in pre-existing procambial strands (the midvein and second-order strands), the DR5v2 expression has been also measured at inner tissues (corresponding to procambial strands) based on optical transverse sections across primordia. The NAA microapplication leads to increased DR5v2 expression in procambial strands an average by nearly 40 % in comparison to the mock (**Fig. 4.8G**). Importantly, the effect of NAA microapplication is rather local, since there is no significant differences between the DR5v2 signal intensity measured at the epidermis for whole primordia before and after mock and NAA treatments (**Fig. 4.8E**).

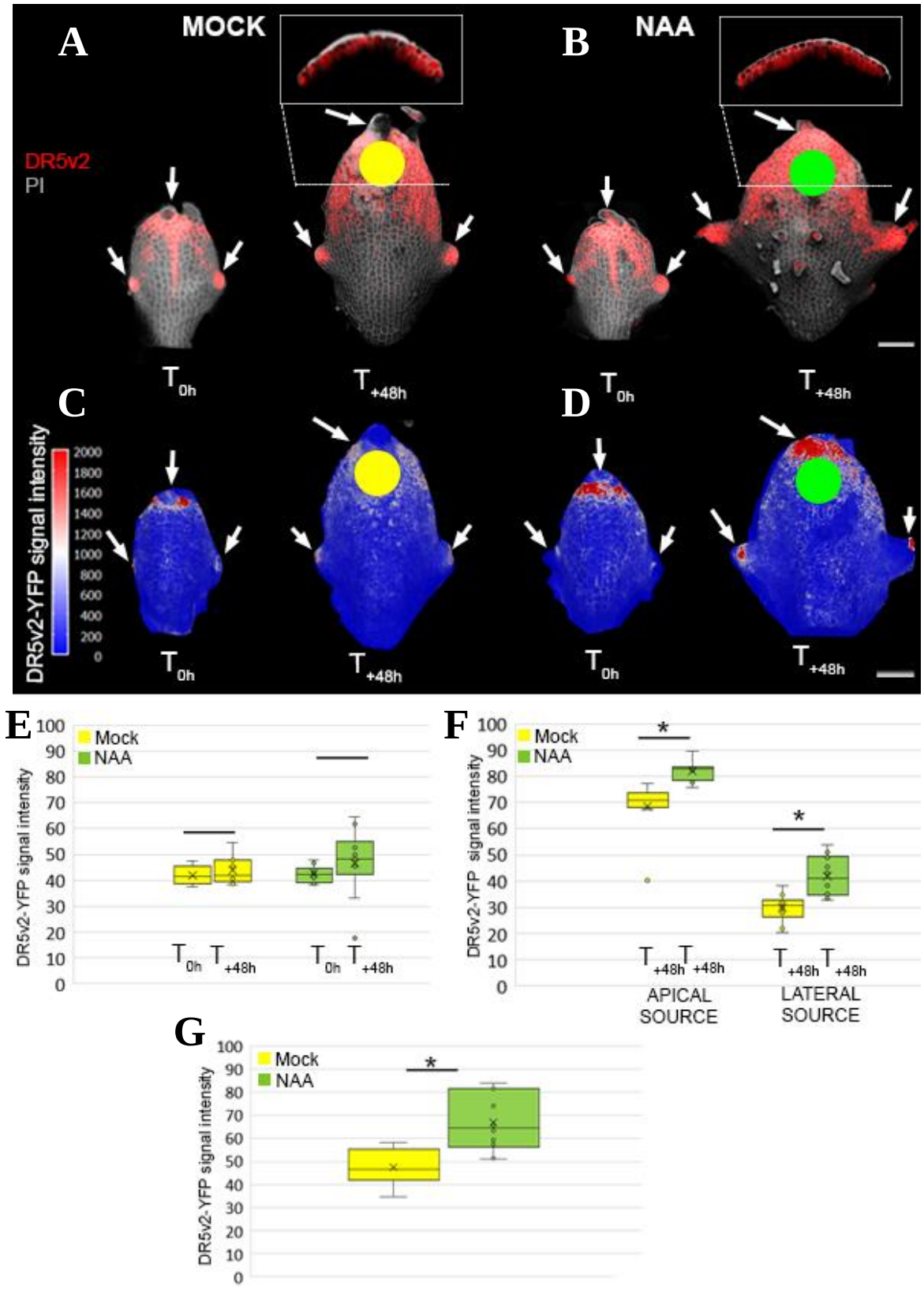

Fig. 4.8. Quantifications of the DR5v2 expression in primordia before and after the mock and NAA microapplication.

(**A-B**) The DR5v2 expression in primordia before (T_{0h}) and after (T_{+48h}) mock (**A**) and NAA (**B**) treatments shown at original confocal stacks (obtained from live imaging). Cell walls were stained with propidium iodide (PI). Inserts (framed) show optical transverse sections across primordia indicated by a dashed line. (**C-D**) The projection of the DR5v2 expression from the epidermis onto the surface before (T_{0h}) and after (T_{+48h}) mock (C) and NAA (D) treatments obtained from the MGX software. The color scale indicates the DR5v2 signal intensity. Sites of the mock and NAA microapplication are indicated by yellow and green dots, respectively. Apical and lateral auxin sources (arrows). Scale bars: 50 μm. (**E**) The DR5v2-YFP signal intensity averaged for whole primordia before (T_{0h}) and after (T_{+48h}) mock and NAA treatments. The signal from the epidermis was measured. (**F**) The DR5v2-YFP signal intensity at the epidermis measured at apical and lateral auxin sources after (T_{+48h}) mock and NAA treatments. (**G**) The DR5v2-YFP signal intensity measured in procambial strands after (T_{+48h}) mock and NAA treatments. The mock treatment (yellow boxes); the NAA treatment (green boxes). Mean values of measured parameters were indicated by „x". Statistically significant differences at 0.05 level are indicated with asterisks (U Mann-Whitney's test). N=10 primordia per treatment.

Since auxin is known to be a major regulator of cell growth (Majda and Robert 2018), primordium growth has been also analyzed. To estimate the growth, the width and length of primordia were measured before and after mock and NAA treatments (**Fig. 4.9A-B**). Based on these parameters, primordium growth rate in width and length has been computed as a relative change of primordium width and length per 48 h (**Fig 4.9C-D**). Analysis of 6 primordia per treatment shows no significant differences in the growth rate both in width and length between mock and NAA-treated primordia.

Further, it has been investigated whether the NAA-induced changes of auxin response at auxin sources and procambial strands affect the pattern of strands. This analysis was based on confocal images of cleared primordia (**Fig. 4.10A-B**). First, the number of second-order strands and the number of branching points (**Fig. 4.10C-D**) were measured in mock- and NAA-treated primordia. Analysis of 6 primordia per treatment shows no significant differences in the number of second-order strands (**Fig. 4.10C**) and branching points (**Fig. 4.10D**) between mock and NAA treatments. Further, the effect of NAA treatment on the formation of loops was checked. Namely, 6 primordia per treatment were analyzed for the occurrence of loops. The analysis shows that the number of loops per primordium is similar in mock and NAA treated primordia and there are usually 2-3 loops in both treatments (data not shown). The NAA microapplication also does not affect the midvein (**Fig. 4.10A-B**, inserts). Analysis of 6 primordia per treatment shows that the midvein width and the number of cells per midvein width increase basipetally

both in mock- and NAA-treated primordia (**Fig. 4.10E-F**). However, no statistically significant differences between both treatments are found.

Summarizing, quantitative analysis of the DR5v2 expression shows that auxin microapplication to the apical primordium region enhances auxin response not only at the apical, but also at lateral auxin sources and inner tissues. This suggests that lateral auxin sources can be supplied with auxin form other primordium regions, and procambial strands are supplied with auxin from auxin sources. Nonetheless, these changes neither significantly affect primordium growth nor the pattern of procambial strands including the midvein development.

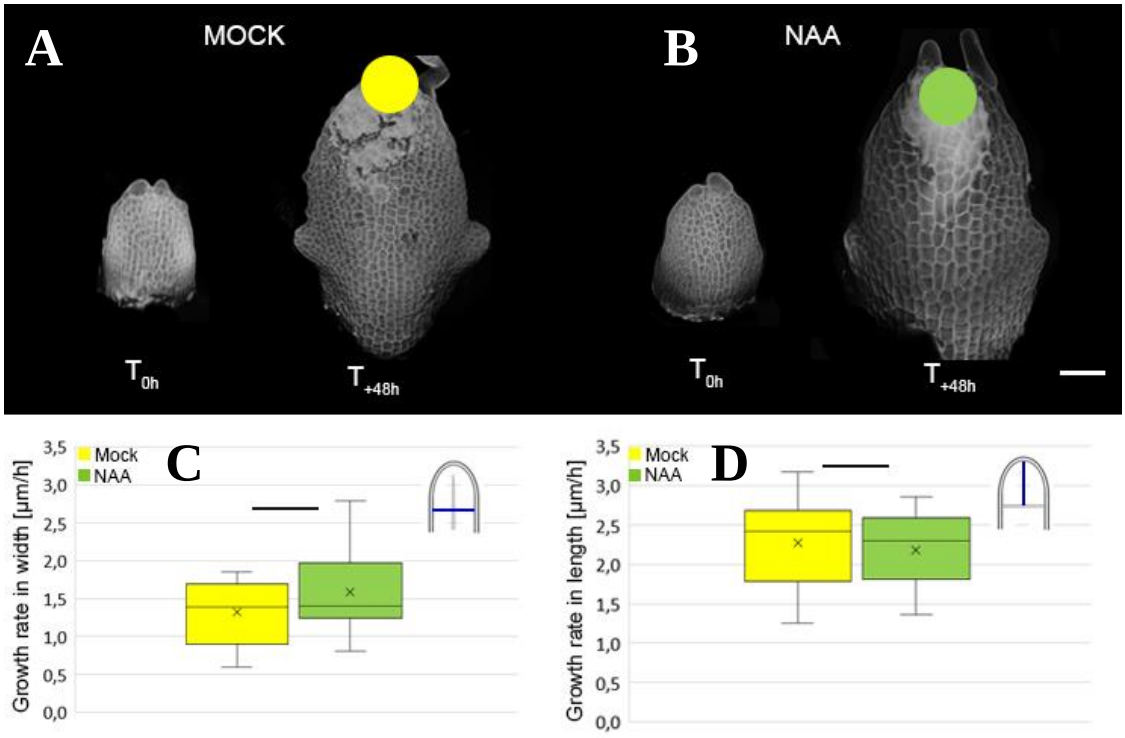

Fig. 4.9. The growth of leaf primordia after the mock and NAA microapplication.

(**A-B**) Primordia before (T_{0h}) and after (T_{+48h}) mock (**A**) and NAA (**B**) treatments shown at original confocal stacks (obtained from live imaging). Cell walls were stained with propidium iodide (PI). Sites of the mock and NAA microapplication are indicated by yellow and green dots, respectively. Scale bar: 50 µm. (**C-D**) The growth rate in primordium width (**C**) and length (**D**). A scheme at the top right corner indicates measured primordium areas. The mock treatment (yellow boxes); the NAA treatment (green boxes). Mean values of measured parameters were indicated by „x". Statistically significant differences at 0.05 level are indicated with asterisks (U Mann-Whitney's test). N=9 primordia per treatment.

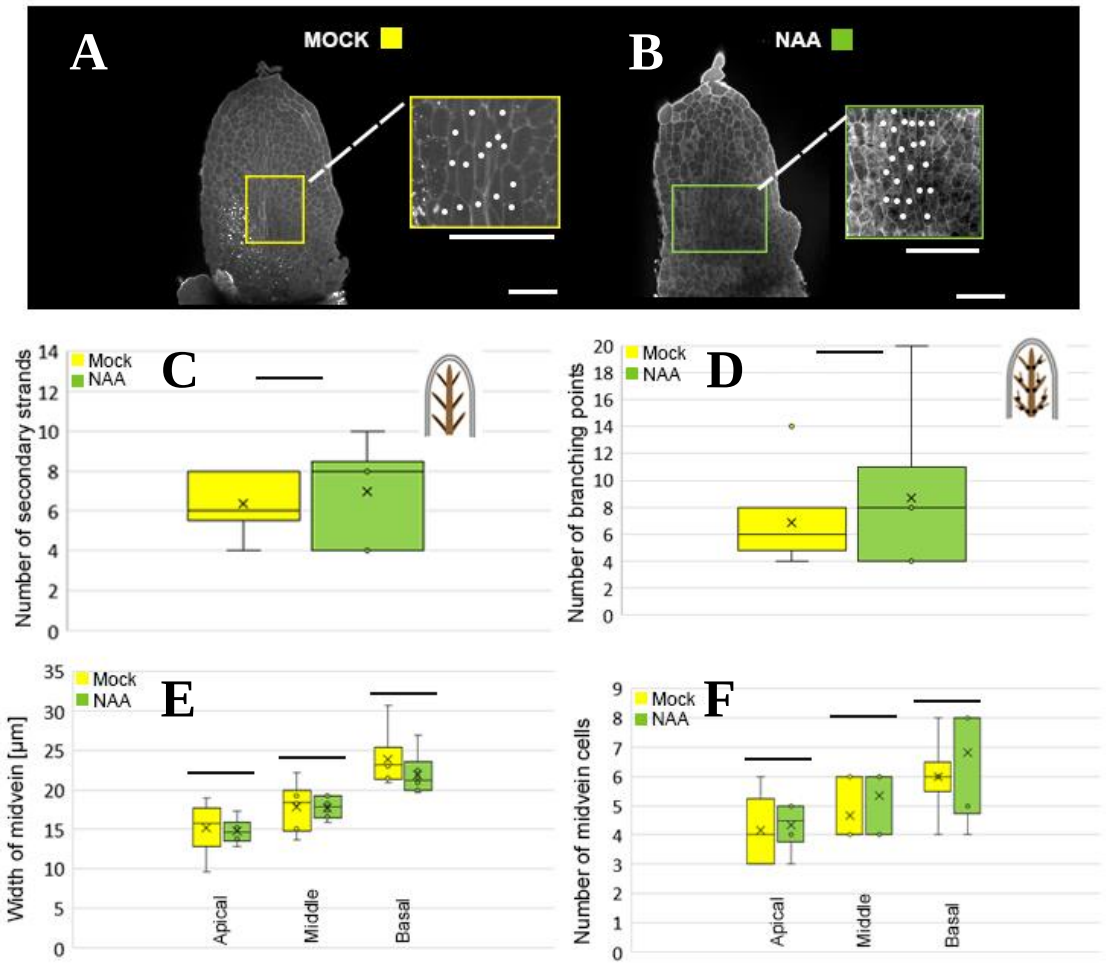

Fig. 4.10. Development of procambial strand pattern after the mock and NAA microapplication.

(**A**-**B**) Images of procambium in primordia after mock (**A**) and NAA (**B**) treatments. Images show original confocal stacks (obtained from clearing method). Insertions show the magnification of framed (yellow and green) regions in primordia. Dots indicate procambial cells at the midvein. Scale bar: 50 µm. (**C**) The number of second-order strands in primordia after mock and NAA treatments. A scheme at the top right corner indicates counted second-order strands marked by black lines. (**D**) The number of branching points in primordia after mock and NAA treatments. A scheme at the top right corner indicates counted branching points marked by black ellipses. (**E**) The width of the midvein after mock and NAA treatmentsat different primordium regions. (**F**) The number of cells per midvein width after mock and NAA treatmentats different primordium regions. The mock treatment (yellow boxes); the NAA treatment (green boxes). Mean values of measured parameters were indicated by „x". Statistically significant differences at 0.05 level are indicated with asterisks (U Mann-Whitney's test). N=6 primordia per treatment.

4.8. Chemical disturbing of auxin sources – global auxin treatment

Since auxin microapplication and resulting changes in auxin response does not affect the pattern of procambial strands, auxin has been applied globally to leaf primordia. In particular, the natural auxin IAA (indole acetic acid) solved in water has been applied to apices isolated from rosettes at the concentration of 5 mM. This auxin concentration was selected based on preliminary experiments (not shown) as the higher concentration had a suppressive effect on primordium growth in agreement with a previous study (Collett et al. 2000). This global auxin treatment was expected to reinforce the strength of pre-existing auxin sources in primordia, or/and lead to the generation of new sources.

To check how auxin sources are affected by the IAA treatment, auxin response in primordia has been quantified (**Fig. 4.11A-D**). In particular, the DR5v2 signal intensity has been measured at epidermis based on projection images (**Fig. 4.11C-D**) and at inner tissues (corresponding to procambial strands) based on optical transverse sections across primordia (**Fig. 4.11A-B**, inserts). Before any treatment, apical and lateral auxin sources are clearly distinguishable from other primordium regions by locally higher DR5v2expression (**Fig. 4.11A-D**, T_{0h}, arrows). After the IAA treatment, the DR5v2 expression strongly increases in the whole primordia in comparison to the mock (**Fig. 4.11A-D**, T_{48h}). Locally increased expression of the DR5v2 after the IAA treatment is also present in procambial strands (**Fig 4.11A-B**, inserts, asterisks). Specifically, analysis of 10 primordia per treatment shows that after the IAA treatment, the DR5v2 signal intensity measured at the epidermis and averaged for whole primordia significantly increases (an average by nearly 100% in comparison to primordia before the treatment) (**Fig. 4.11E**). For comparison, there is no significant differences between the DR5v2 signal intensity in primordia before and after the mock treatment. Furthermore, the DR5v2 expression at the lateral auxin sources is significantly higher after the IAA treatment an average by nearly 70% in comparison with the mock (**Fig. 4.11F**). However, in case of the IAA treatment, these auxin sources are no easily distinguishable in primordia due to almost uniformly high DR5v2 expression along primordium margins (**Fig. 4.11B, D**, $T_{48h,}$ arrowheads). The DR5v2 signal intensity is also slightly increased in apical auxin source, but differences between the mean values for mock and IAA treatments are not statistically significant (**Fig. 4.11F**). The IAA treatment as well leads to increased DR5v2 expression in procambial strands an average by 200 % in comparison with the mock (**Fig. 4.11G**), but due to high DR5v2 expression in other surrounding cells (**Fig. 4.11B**, insert), locally increased DR5v2 expression marking these strands is not clearly distinguished.

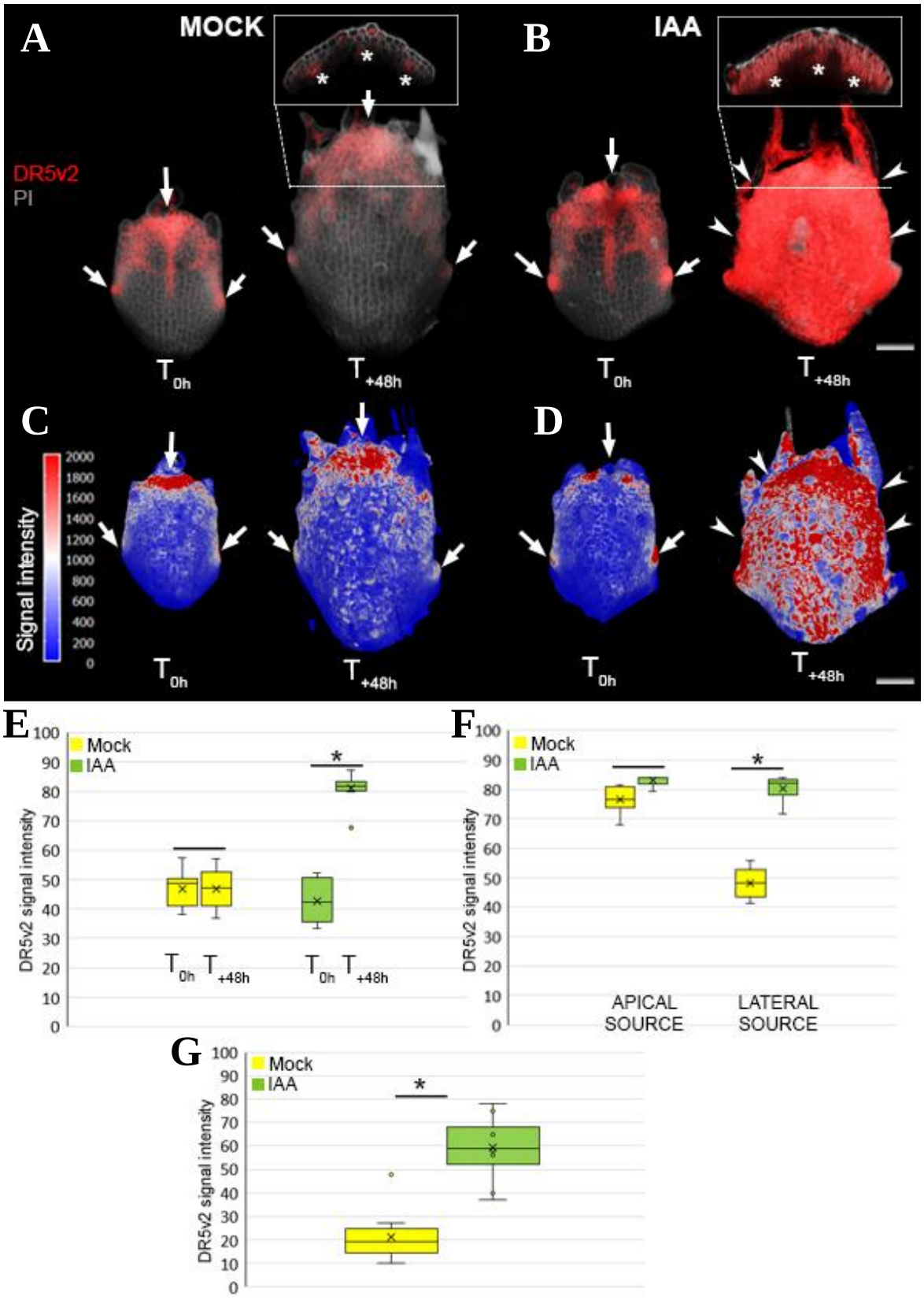

Fig. 4.11. Quantifications of the DR5v2 expression in primordia before and after mock and IAA global treatments.

(**A**-**B**) The DR5v2 expression in primordia before (T_{0h}) and after (T_{+48h}) mock (**A**) and IAA (**B**) treatments shown at original confocal stacks (obtained from live imaging). Inserts (framed) show optical transverse sections across primordia indicated by a dashed line. Cell walls were stained with propidium iodide (PI). (**C**-**D**) The projection of the DR5v2 expression from the epidermis onto the surface before (T_{0h}) and after (T_{+48h}) the mock (**C**) and IAA (**D**) treatments obtained from the MGX software. The color scale indicates the DR5v2 signal intensity. Apical and lateral auxin sources are indicated by arrows; procambial strands by asterisks; the high DR5v2 expression along primordium margins by arrowheads. Scale bars: 50 μm. (**E**) The DR5v2 signal intensity averaged for whole primordia before (T_{0h}) and after (T_{+48h}) mock and IAA treatments. The signal from the epidermis was measured. (**F**) The DR5v2 signal intensity at the epidermis measured in apical and lateral auxin sources after (T_{+48h}) mock and IAA treatments. (**G**) The DR5v2 signal intensity measured at procambial strands after (T_{+48h}) mock and IAA treatments. The mock treatment (yellow boxes); the IAA treatment (green boxes). Mean values of measured parameters were indicated by „x". Statistically significant differences at 0.05 level are indicated with asterisks (U Mann-Whitney's test). N=10 primordia per treatment.

To check how global auxin treatment affects primordium growth, the width and length of primordia were measured before (T_{0h}) and after (T_{+48h}) mock and IAA treatments (**Fig. 4.12A-B**). Based on these measurements, primordium growth rate in width and length was computed. Analysis of 6 primordia per treatment shows no significant differences in the growth rate in width between mock- and IAA-treated primordia (**Fig. 4.12C**). On the other hand, statistically significant differences are observed in the growth rate in length (**Fig. 4.12D**). Accordingly, primordia after the IAA treatment elongate faster in comparison to the mock.

Further, it has been checked how observed changes in auxin response and primordium growth induced by auxin global treatment impact on vascular patterning (**Fig. 4.13A-J**). This analysis was based on confocal images cleared leaf primordia. First, the number of second-order strands and the number of branching points were counted in mock- and IAA-treated primordia. Analysis of 6 primordia per treatment shows no significant differences in the number of second-order strands between mock and IAA treatments (**Fig. 4.13C**). Also, there are no statistically significant differences in the number of branching points between mock and IAA treatments (**Fig. 4.13D**). However, branching point number is higher than the average (15) in more cases of IAA-treated primordia in comparison to the mock. This is reflected by the higher median value for the IAA treatment (18) in comparison with the mock (15).

Second, an impact of the IAA treatment on the formation of loops was checked. Specifically, 6 primordia per treatment were analyzed for the occurrence of loops in relation to the length of

primordia reflecting their developmental stage (**Fig. 4.13E**). Analysis showed that loops are observed at the earlier stages of primordium development after the IAA treatment in comparison to the mock. In particular, loops after the IAA treatment are formed in primordia that attained an average length of 161.3 µm, while after the mock treatment loops are observed in primordia which average length is 195.3 µm. However, generally, the number of loops per primordium is similar in the mock and IAA treated primordia, i.e. usually there are 2-3 loops in both treatments.

Third, since the IAA treatment leads to strongly increased auxin response in primordia, changes in the midvein are expected. Indeed, significant differences in the width of the midvein at its basal region are observed between mock- and IAA-treated primordia (**Fig. 4.13A-B**, dots, **4.13F**). Specifically, after the IAA treatment, the midvein is wider an average by 7 µm in comparison to the mock in the basal region (**Fig. 4.13F**). However, there is no statistically significant differences in the midvein width in apical and middle regions between mock- and IAA-treated primordia. The wider midvein in the basal region can be explained by the higher number of procambial cells per midvein width. Accordingly, a significant difference in the cell number is observed at the basal region of the midvein, where the number of cells is higher (an average by one cell) in IAA-treated primordia than in the mock (**Fig. 4.13G**). There is no statistically significant differences in the cell number in apical and middle midvein regions. Further, significant differences are observed in shape parameters (width, length) of individual midvein cells between mock- and IAA-treated primordia (**Fig. 4.13H, I**). In particular, midvein cells are longer in IAA-treated primordia than in the mock in all three regions (**Fig. 4.13H**). Also, midvein cells in the basal region are wider in IAA-treated primordia than in the mock (**Fig. 4.13I**). However, cells in apical and middle regions are narrower in IAA-treated primordia than in the mock. Although, the effect of the IAA treatment on cell width seems to depend on the midvein region, the ratio of cell length and width is higher in IAA-treated primordia in all three regions, suggesting that after the IAA treatment the midvein cells grow much more in length than in width (**Fig. 4.13J**).

Summarizing, quantitative analysis of auxin response reveals that the global auxin treatment significantly reinforces the strength of lateral auxin sources. However, as the DR5v2 expression is also strongly upregulated in surrounding cells, auxin sources are not clearly defined. Instead, whole primordium margins might function as auxin source. In addition, the auxin treatment increases auxin response in procambial strands. The auxin treatment leads also to faster primordium growth in the length (but not in the width), and accelerated formation of the loops.

Furthermore, the auxin treatment has an impact on the midvein increasing its width in the basal region by rising the cell number. In agreement with auxin effect on primordium growth, it has been observed that midvein cells grow more in the length than in the width along the whole midvein. Auxin treatment does not change significantly the pattern of procambial strands, although some slight increase in the number of branching points can be observed.

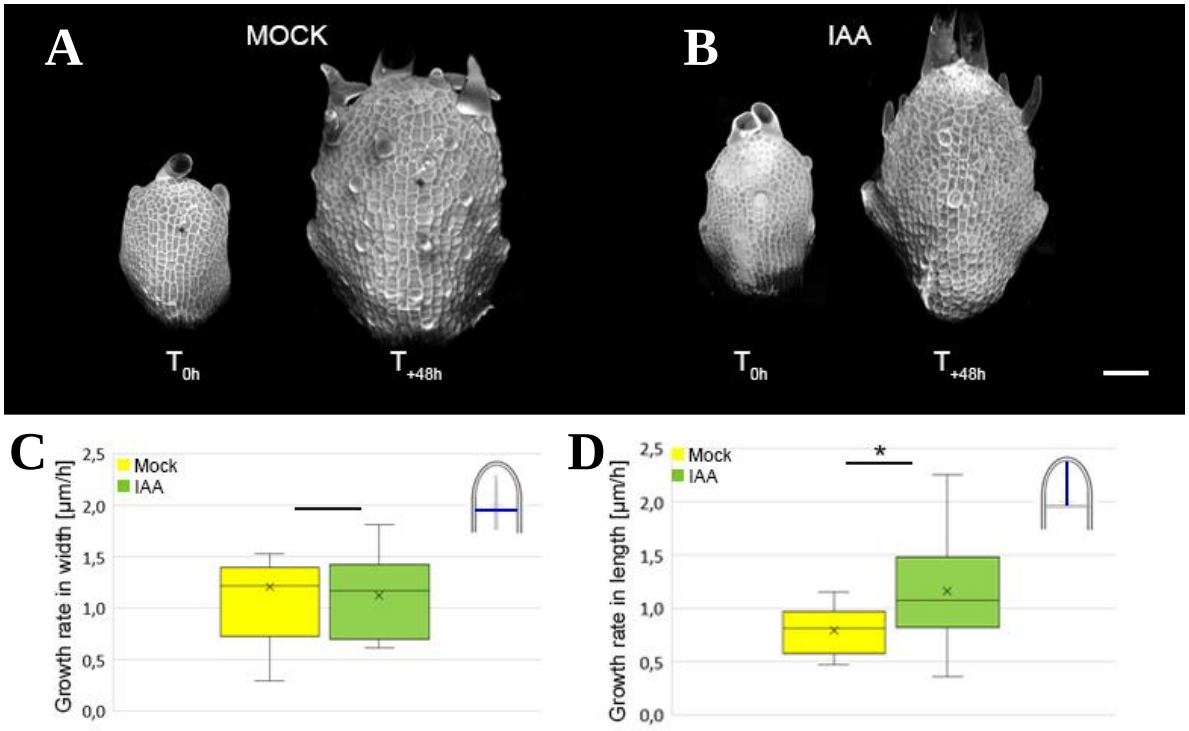

Fig. 4.12. The growth of leaf primordia after mock and IAA treatments.

(**A-B**) Primordia before (T_{0h}) and after (T_{+48h}) mock (**A**) and IAA (**B**) treatments shown at original confocal stacks (obtained from live imaging). Cell walls were stained with propidium iodide (PI). Scale bar: 50 µm. (**C-D**) The growth rate in primordium width (**C**) and length (**D**). A scheme at the top right corner indicates measured primordium areas. The mock treatment (yellow boxes); the IAA treatment (green boxes). Mean values of measured parameters were indicated by „x". Statistically significant differences at 0.05 level are indicated with asterisks (U Mann-Whitney's test). N=9 primordia per treatment.

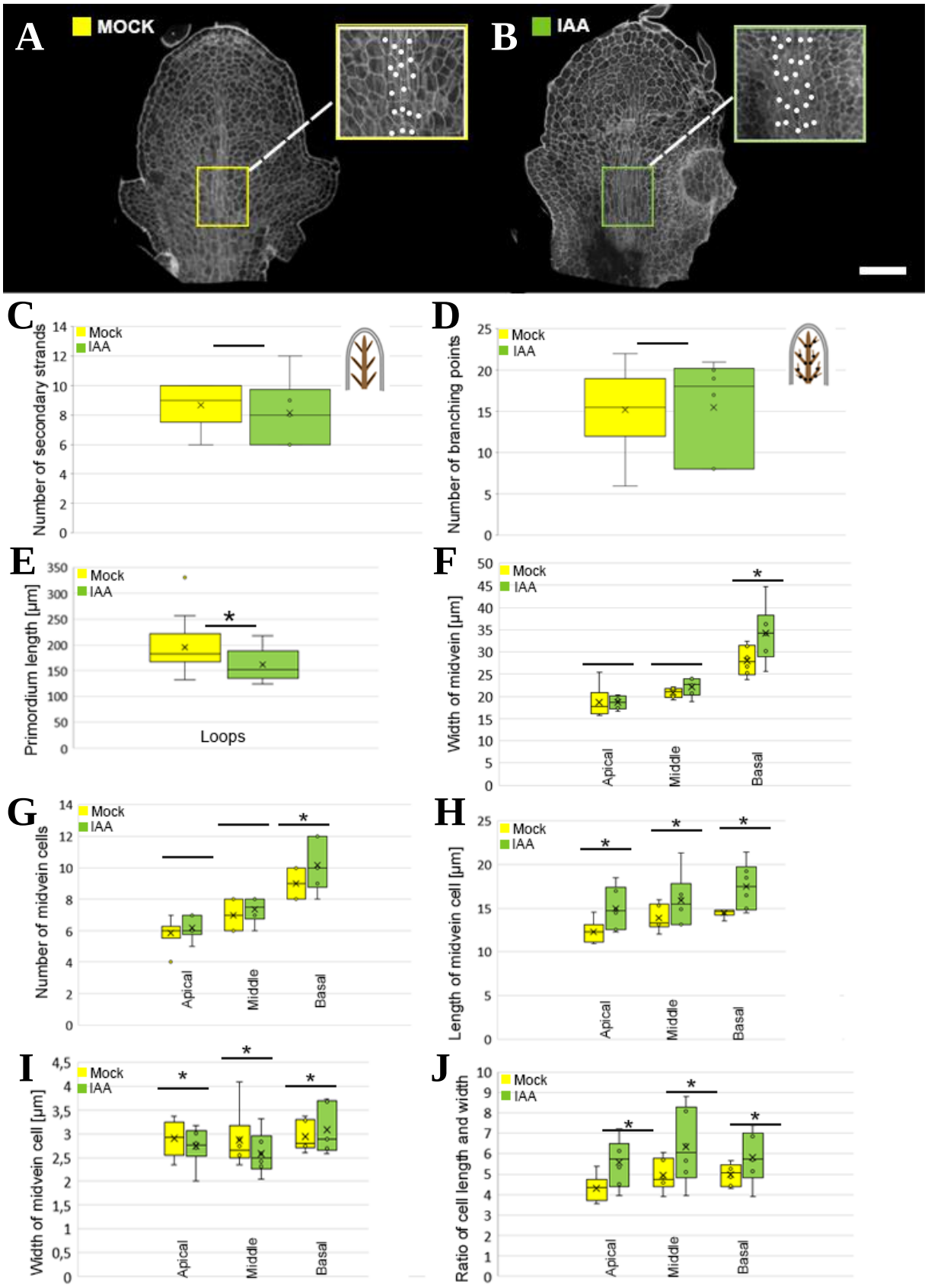

Fig. 4.13. Development of procambial strand pattern after mock and IAA treatments.

(**A**-**B**) Images of procambium in primordia after mock (**A**) and IAA (**B**) treatments. Images show original confocal stacks (obtained from clearing method). Insertions show the magnification of framed (yellow and green) regions in primordia. Dots indicate procambial cells at the future midvein. Scale bar: 50 μm. (**C**) The number of second-order strands in primordia after mock and IAA treatments. A scheme at the top right corner indicates counted second-order strands marked by black lines. (**D**) The number of branching points in primordia after mock and IAA treatments. A scheme at the top right corner indicates counted branching points marked by black ellipses. (**E**) The occurrence of loops after mock and IAA treatments in relation to the primordium length. (**F**) The width of the midvein after mock and IAA treatments at different primordium regions. (**G**) The number of cells per the midvein width after mock and IAA treatments at different primordium regions. (**H**-**I**) The length (**H**) and width (**I**) of cells in the midvein after mock and IAA treatments at different primordium regions. (**J**) The ratio of cell length to widthin the midvein after mock and IAA treatments at different primordium regions. The mock treatment (yellow boxes); the IAA treatment (green boxes). Mean values of measured parameters were indicated by „x". Statistically significant differences at 0.05 level are indicated with asterisks (U Mann-Whitney's test). N=6 primordia per treatment.

4.9. Suppression of polar auxin transport – NPA treatment

In the previous series of experiments, the NAA microapplication and global IAA treatment lead to an increase of auxin response in auxin sources. In other words, auxin treatment affects the strength of auxin sources. The source strength may be also affected by suppressing polar auxin transport, for example by a treatment of chemical inhibitors such as NPA (N-(1-naphthyl) phthalamic acid) (Mattsson et al. 2003). Two effects of the auxin transport suppression are possible: either (1) it would lead to auxin accumulation and consequently to increased DR5v2 expression at auxin sources due to hampered auxin flow from the source; or (2) the DR5v2 expression would be reduced at auxin sources, if only the strength of auxin source depends on auxin transport from other primordium regions. Thus, it has been checked how the NPA-induced suppression of auxin polar transport affects the strength of auxin sources, the pattern of procambium strands, and primordium growth.

The NPA at the concentration of 100 mM has been applied to leaf primordia at partially dissected rosettes and the imaging was performed 5 days later (see **Materials and Methods**) (**Fig. 4.14A-D**). To quantify auxin response, the DR5v2 signal intensity has been measured at epidermis based on projection images (**Fig. 4.14B, D**) and in internal tissues (corresponding to procambial strands) based on transverse sections across primordia (**Fig. 4.14A, C**, inserts). Apical and lateral auxin sources are clearly distinguishable and marked by locally higher

expression of DR5v2 in mock-treated primordia (**Fig. 4.14A-B**, T_{+120h}, arrows). In contrast, after the NPA treatment the apical source is less pronounced (**Fig. 4.14C-D**, T_{+120h}, arrows), the lateral sources are no more visible and the formation of serrations is inhibited (**Fig. 4.14C-D**, T_{+120h}, arrowheads). Furthermore, the analysis of 8 primordia per treatment shows that the DR5v2 signal intensity at the epidermis measured in whole primordia (**Fig. 4.14E**) and at the apical source (**Fig. 4.14F**) is lower after the NPA treatment in comparison to the mock. In addition, the difference in the DR5v2 expression in procambial strands between mock and NPA treatments is no statistically significant (**Fig. 4.14G**). Although, the DR5v2 signal intensity is slightly higher after the NPA treatment than in the mock. On the other hand, in NPA-treated primordia the internal DR5v2 expression is focused at the 4 procambial strands, while in the mock there only 3 strands marked by DR5v2 expression (**Fig. 4.14A, C**, inserts, asterisks).

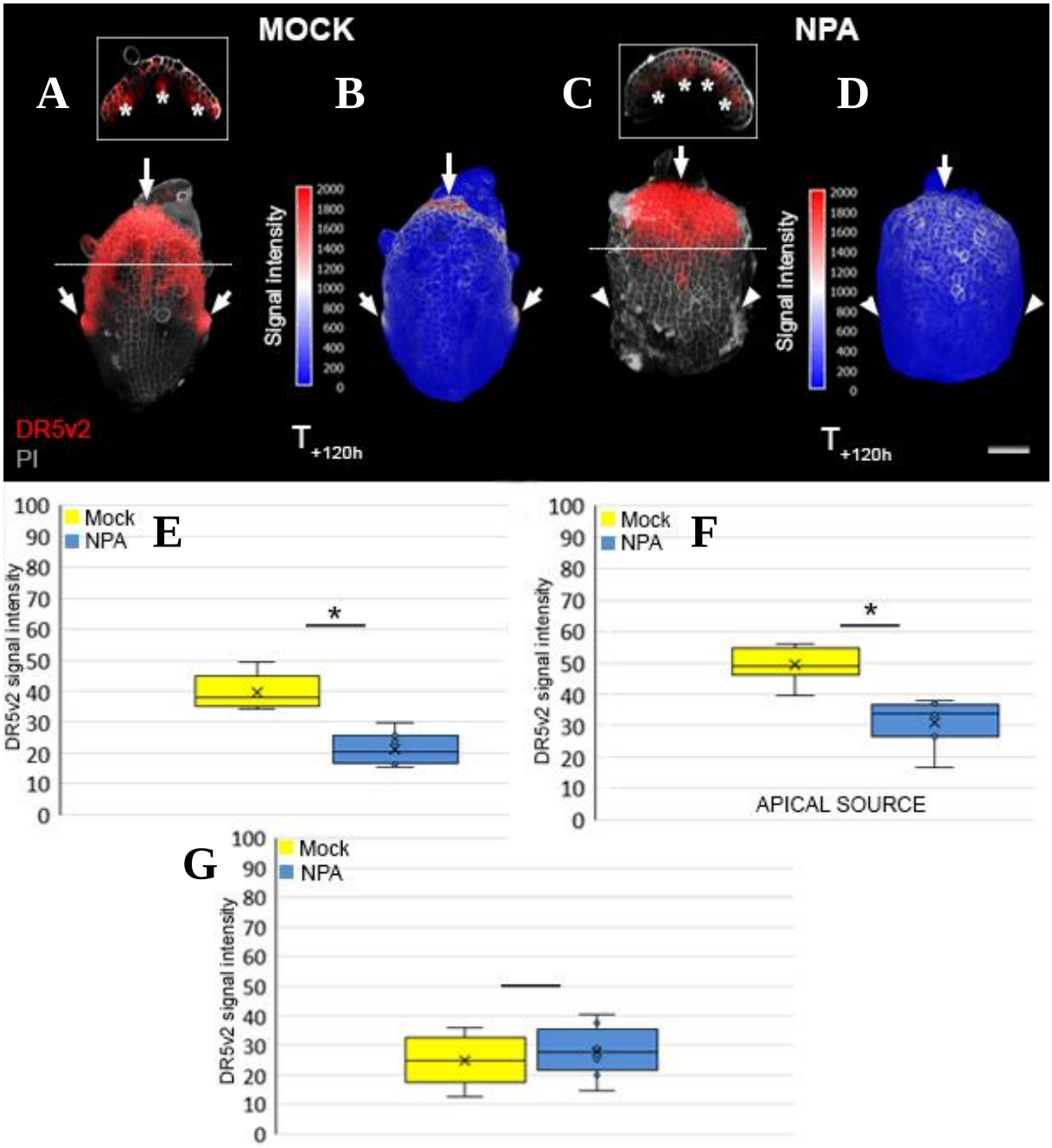

Fig. 4.14. Quantifications of the DR5v2 expression in primordia after mock and NPA treatments.

(**A, C**) The DR5v2 expression in primordia after (T_{+120h}) the mock (**A**) and NPA treatments (**C**) shown at original confocal stacks. Inserts show optical transverse sections throughout the indicated primordium region (dashed line). Cell walls were stained with propidium iodide (PI). (**B, D**) The projection of the DR5v2 expression from the epidermis onto the surface after (T_{+120h}) mock (**B**) and NPA treatments (**D**). The color scale indicates the DR5v2 signal intensity. The present apical and lateral auxin sources are indicated by arrows; procambial strands at transverse sections by asterisks. The lack of lateral sources is marked by arrowheads. Scale bar: 50 μm. (**E**) The DR5v2 signal intensity measured and averaged for

whole primordia after (T_{+120h}) mock and NPA treatments. The signal from the epidermis was measured. (**F**) The DR5v2 signal intensity at the epidermis measured in apical auxin source after (T_{+120h}) mock and NPA treatments. (**G**) The DR5v2 signal intensity measured in procambial strands after (T_{+120h}) mock and NPA treatments. The mock treatment (yellow boxes); the NPA treatment (blue boxes). Mean values of measured parameters were indicated by „x". Statistically significant differences at 0.05 level are indicated with asterisks (U Mann-Whitney's test). N=8 primordia per treatment.

Next, the impact of the NPA-suppressed auxin transport on the primordium growth was analyzed. The width of primordia at apical, middle, and basal regions has been measured after mock and NPA treatments (**Fig. 4.15C**). The analysis of 6 primordia per treatment shows that in all the regions, the width is significantly higher in NPA-treated primordia than in the mock an average by 28%, 37%, and 25% in apical, middle, and basal regions, respectively.

To check how the lack of lateral auxin sources, the formation of additional strands marked by the DR5v2 expression, and increased primordium width at NPA-treated primordia affect the overall pattern of procambial strands, different parameters were analyzed based on images of cleared leaf primordia (**Fig. 4.15A-B)**. First, the number of second-order strands and the number of branching points were measured (**Fig. 4.15D-E)**. The analysis of 6 primordia per treatment shows significant differences in the number of second-order strands between mock and NPA treatments (**Fig. 4.15D**). In particular, this number is lower in NPA treated primordia than in the mock. However, there are no significant differences between mock and NPA treatments in the number of branching points (**Fig. 4.15E**). Another feature of the pattern of procambial strands in NPA-treated primordia is the lack of loops (in 5/6 analyzed primordia), while usually 2 or 3 loops are observed in primordia after the mock treatment (data not shown). Thus, these data suggest that the higher number of DR5v2-marked procambial strands apparent at transverse sections of NPA-treated primordia (**Fig. 4.14C**, insert) can be rather regarded as primary strands. Indeed, these strands extend from the basal region of the midvein, and the midvein is clearly wider in comparison with the mock (**Fig. 4.15A-B**).

To confirm this observation, the width of the midvein was measured in apical, middle and basal regions (**Fig. 4.15F**). The significant differences in the midvein width are observed between mock and NPA treated primordia in all analyzed regions. In particular, the midvein is more than twice wider (i.e. on average by 24 µm) in NPA treated primordia in comparison to the mock. The wider midvein can be explained by the higher number of cells per midvein width in NPA treated primordia, because there are approximately 4 cells more than in the mock (**Fig. 4.15G**).

Then, shape parameters of midvein cells (cell width and length) were measured (**Fig 4.15H-I**). In NPA treated primordia, midvein cells are significantly longer an average by 28% and 30% in middle and basal regions, respectively, in comparison to the mock (**Fig 4.15H**). Even higher difference is observed in the case of cell width (**Fig 4.15I**). Namely, midvein cells in NPA-treated primordia are wider an average by 50% and 60% in middle and basal regions, respectively, in comparison to the mock. In a consequence, the ratio of cell length and width is lower in the NPA-treated primordia than in the mock suggesting that after the NPA treatment cells grow much more in the width than in the length (**Fig. 4.15J**). However, there is no significant differences in midvein cell length and width, or the ratio between mock and NPA treated primordia in the apical region (**Fig. 4.15H-J**).

To summarize, the NPA-induced suppression of polar auxin transport leads to a disappearance of the auxin lateral sources, the lack of serrations, and reduced auxin response in the apical source. Thus, these data suggests that epidermal auxin sources are supplied by auxin flow from other primordium regions. However, auxin response is not reduced at procambial strands indicating that theses strands are more autonomous with regard to auxin supplies. Furthermore, the NPA treatment clearly increases primordium growth in the width, and leads to the formation of wider midvein extending into several strands towards primordium margins. Despite wider midvein and the higher number of midvein cells, the formation of loops and second-order strands is suppressed.

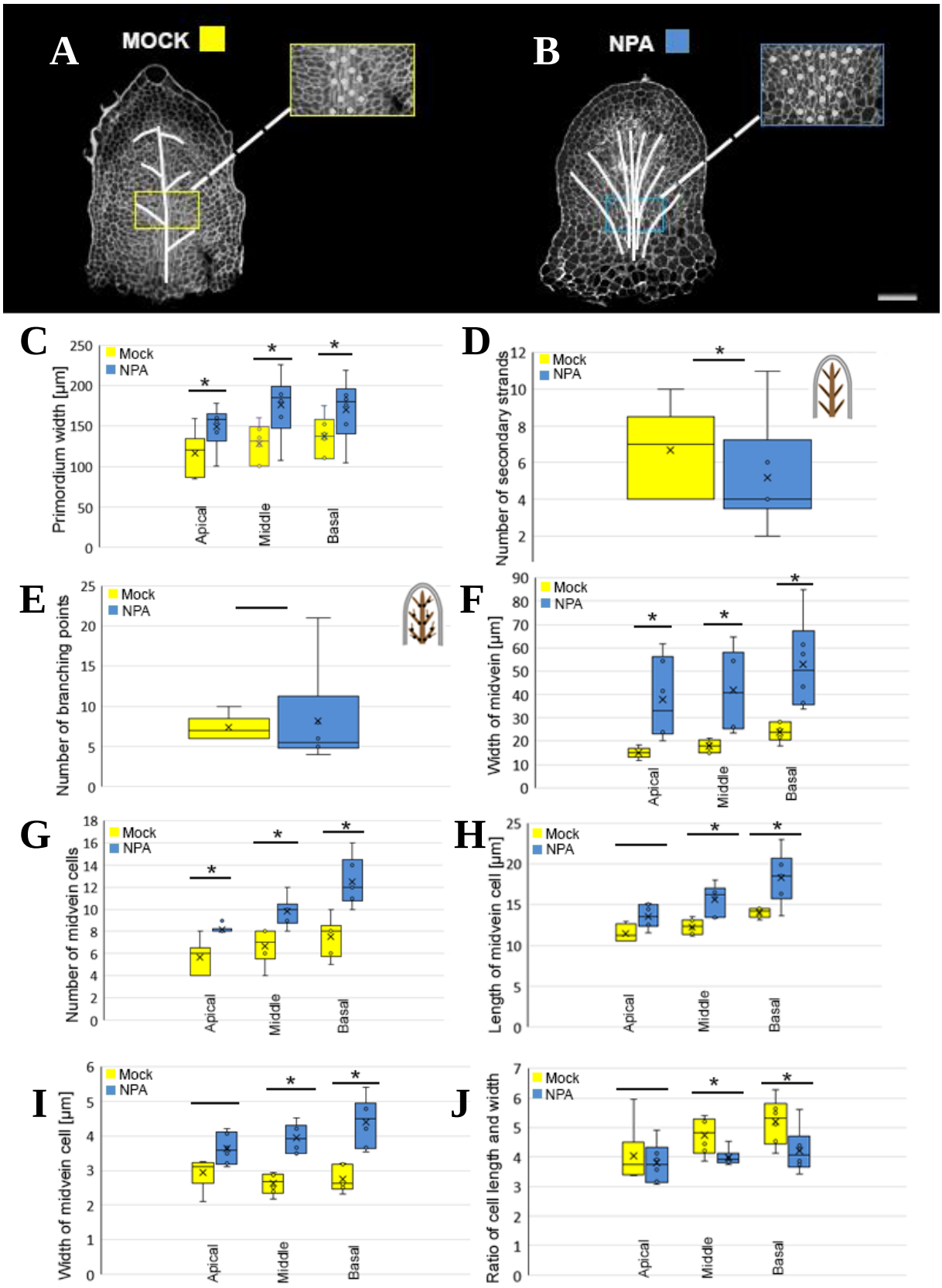

Fig. 4.15. Development of procambial strand pattern after mock and NPA treatments.

(**A, B**) Images of procambium in primordia after mock (**A**) and NPA (**B**) treatments. Images show original confocal stacks (obtained from clearing method). Insertions show the magnification of framed (yellow and blue) regions in primordia. Dots indicate procambial cells at the future midvein. White line segments represents the arrangement of procambial strands (only their basal parts). Scale bar: 50 μm. (**C**) The primordium width at different primordium regions after mock and NPA treatments. (**D**) The number of second-order strands in primordia after mock and NPA treatments. A scheme at the top right corner indicates counted second-order strands marked by black lines. (**E**) The number of branching points in primordia after mock and NPA treatments. A scheme at the top right corner indicates counted branching points marked by black ellipses. (**F**) The width midvein after mock and NPA treatments at different primordium regions. (**G**) The number of cells per midvein width after mock and NPA treatments at different primordium regions. (**H-I**) The length (**H**) and width (**I**) of cells in the midvein after mock and NPA treatments at different primordium regions. (**J**) The ratio of cell length to width in the midvein after mock and NPA treatments at different primordium regions. The mock treatment (yellow boxes); the NPA treatment (blue boxes). Mean values of measured parameters were indicated by „x". Statistically significant differences at 0.05 level are indicated with asterisks (U Mann-Whitney's test). N=6 primordia per treatment.

4.10. Genetic disturbance of auxin sources – *pin1* and *cuc2 cuc3* mutants

After chemical disturbance of auxin distribution and transport, the role of auxin sources in the pattern of vascular system has been examined in *pin1* and *cuc2 cuc3* mutants with impaired polar auxin transport and leaf morphology. In both mutants the most striking feature of leaves is the lack of serrations, which were believed to be associated with the formation of underlying second-order procambial strands (Scarpella et al. 2006). To examine effects of these mutations in the vascular system initiation, auxin response was visualized by DR5v2:YFP reporter (live imaging) and the pattern of procambial strands was analyzed in cleared primordia.

In the *pin1* mutant, a local maximum of the DR5v2 expression is localized at the apical region of primordia similarly to the WT (**Fig. 4.16A-D**, asterisks). However, the DR5v2 expression is more spread along *pin1* primordium margins including the lateral region of primordia (**Fig. 4.16C-D**, arrowheads). Nonetheless, in comparison to the WT (**Fig. 4.16A**, arrows, see also other examples in **Fig. 4.1I-L**), there are no apparent lateral DR5v2 maxima at the basal region of *pin1* primordia, which would mark the formation of serrations (**Fig. 4.16C-D**). The *pin1* mutation also affects the pattern of procambial strands. In particular, the midvein is much wider in *pin1* primordia in comparison to the WT. There are about 8 cells across the midvein width in *pin1* primordia, while there are only 4 cells in the WT (data not shown). Despite lacking of

lateral DR5v2 maxima and serrations (**Fig. 4.16C-D**), several (5-7) second-order procambial strands are observed in *pin1* primordia. However, these strands are branching from the midvein at more sharp angle (40-60 deg.) in comparison with the WT, where the angle between second-order strands and the midvein is nearly 90 deg. (**Fig. 4.16A-B** and **C-D**, yellow line segments). Another feature of procambium pattern in *pin1* primordia is the lack of loops (**Fig. 4.16D**), which are present in older WT primordia (**Fig. 4.16B,** hash).

In the *cuc2 cuc3* mutant, apical maximum of the DR5v2 expression is established similarly to the WT (**Fig. 4.16A-B** and **E-F**, asterisks). At older *cuc2 cuc3* primordia, the DR5v2 expression extends also along primordium margins (**Fig. 4.16F**, arrowheads), but it is clearly absent at the basal region of primordia. Consequently, serrations are not formed in *cuc2 cuc3* primordia. Another morphological feature of *cuc2 cuc3* primordia is their slightly more rounded shape in comparison with the WT primordia (**Fig. 4.16B**, **F**). The pattern of procambium strands in *cuc2 cuc3* primordia is similar to the WT in regard to the midvein structure and the formation of second-order strands (**Fig. 4.16B**, **F**, yellow line segments). However, in the mutant second-order strands form loops much faster than in the WT, because they are observed already in primordia at younger stage of development (**Fig. 4.16A-B** and **E-F**, hash). In the WT, second-order strands at the most basal primordium region can form loops by connecting to upper strands, but they can also extend toward serrations and form short free-ending strands (**Fig. 4.16A-B**, dots). In *cuc2 cuc3* mutant, basal second-order strands are only connecting to upper strands forming loops (**Fig. 4.16E-F**, hash).

Summarizing, analysis of *pin1* and *cuc2 cuc3* mutant primordia shows that the formation of second-order procambial strands is independent of lateral maxima of the DR5v2 expression and subsequent development of serrations. Thus, it is likely that they do not depend on epidermal lateral auxin sources. However, if present, lateral auxin sources can locally guide the extension second-order procambial strands. The disruption of polar auxin transport in the *pin1* mutant, in turn, affects the midvein thickness and the branching of second-order strands.

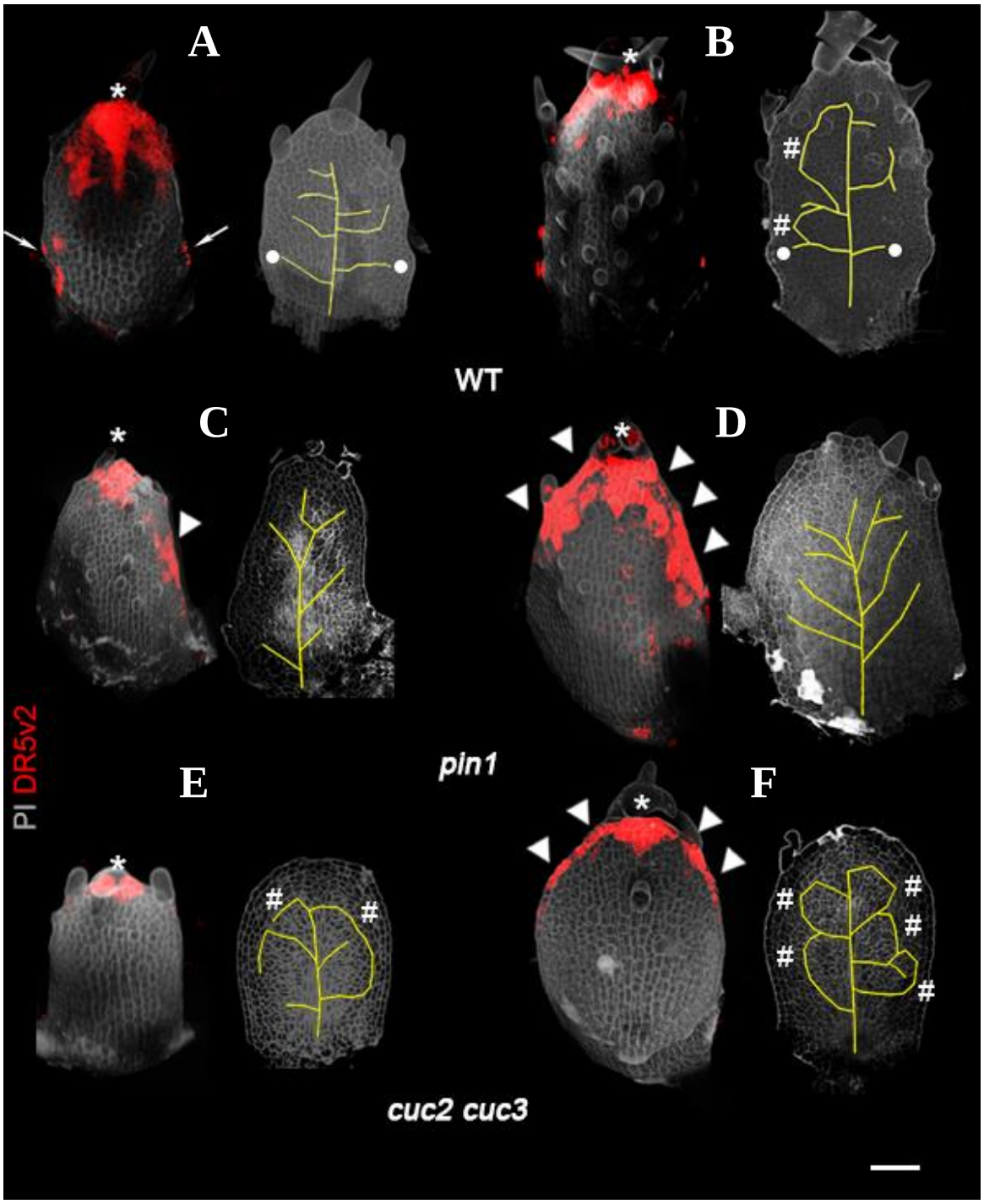

Fig. 4.16. Auxin response and the pattern of procambial strands in *pin1* and *cuc2 cuc3* mutants.

(**A-B**) The expression of DR5v2:YFP (left) and the reconstruction of procambial strands (yellow line segments, right) in younger (**A**) and older (**B**) WT primordia. (**C-D**) The expression of DR5v2:YFP (left) and the reconstruction of procambial strands (right) in younger (**C**) and older (**D**) *pin1* primordia.

(**E-F**) The expression of DR5v2:YFP (left) and the reconstruction of procambial strands (right) in younger (**E**) and older (**F**) *cuc2 cuc3* primordia. Images show original confocal stacks obtained from live imaging (left) or clearing method (right). Cell walls were stained with propidium iodide (PI).

Asterisks indicate apical DR5v2 expression; arrowheads – the extended DR5v2 expression at primordium margins. Hashes mark loops; dots - basal free-ending second-order procambial strands extending towards serrations. N = 6 WT and *cuc2cuc3* primordia, and N= 4 *pin1* primordia . Scale bar: 50 μm.

4.11. Mechanical disturbance of auxin sources and pre-existing strands – cell ablations

Finally, to test a role of auxin sources and pre-existing strands on development of procambial strand pattern, a series of cell ablation experiment have been performed. Specifically, to disrupt auxin sources, apical and lateral regions of primordia were damaged by a precise puncture with a very fine needle. Moreover, to disrupt the midvein, the puncture was done at the middle region of primordia deep enough to ablate midvein cells and to interrupt its continuity. To check how ablations affect the auxin response marking auxin sources, the DR5v2:YFP line was used in the experiments. Leaf primordia were imaged at two time points (just after the ablation and 2 days later), and then primordia were incubated in the clearing solution to examine the pattern of procambial strands.

In the first type of ablation experiments, the very apical region of primordia containing a local maximum of the DR5v2 expression was punctured (**Fig. 4.17A-C**, inserts). Interestingly, after this apical ablation the shape of primordia has been changed and the wounding is displaced either into left (3/9 primordia) or right (6/9 primordia) primordium side (**Fig. 4.17B-C**, T_{+48h}), despite the fact that the ablation has been done symmetrically (**Fig. 4.17B-C**, T_{0h}). The asymmetry is also apparent in the localization of DR5v2 expression. Namely, the DR5v2 expression is scattered over the apical region of primordia, but it is more extended at the opposite region of the wounding (**Fig. 4.17B**, T_{+48h}, arrowheads, observed in 7/9 primordia).

Generally, the pattern of procambial strands in ablated primordia is similar to control primordia (**Fig. 4.17A, B**, left), however, it has been observed that the apical ablation leads to a delay in loop formation. Namely, there are 1-4 loops per primordium in the control (**Fig. 4.17A**, hash), while either no loops or only 1-2 loops are observed in ablated primordia (**Fig. 4.17B**). Furthermore, analysis of 9 primordia per treatment shows no significant differences in the number of secondary strands, branching points, and strand density between control and ablated primordia (**Fig. 4.18A-C**). On the other hand, a more detailed analysis of procambial strands revealed a significant effect of the apical ablation on the width of the midvein (**Fig. 4.19A-C**). In the control, the midvein width at three regions (apical, middle, basal) is similar (**Fig. 4.19C**). However, in ablated primordia the midvein width is significantly different in all regions in

comparison with the control, and it increases basipetally. In particular, the midvein in ablated primordia is wider an average by 20%, 30%, and by more than 100% in apical, middle, and basal regions, respectively, in comparison to the control. Despite wider midvein in ablated primordia, the shape of procambial cells is similar to the control (**Fig. 4.19A-B**, inserts). In ablated primordia not only the midvein is wider, but also primordia themselves. Ablated primordia were wider an average by 20%, 30%, and 40% in apical, middle, and basal regions, respectively in comparison with the control (**Fig. 4.19D**). Therefore, the increase in the midvein width in the basal region of ablated primordia is disproportionally higher than the increase in primordium width. Moreover, there are differences in differentiation level of procambial cells in second-order strands, which may explain a delay in the formation of loops. In ablated primordia, procambial cells in these strands are much less developed, which is manifested in their less elongated shape in comparison to the control, where procambial cells are nearly 3-4 times long than wide (**Fig. 4.20A,B**, dots).

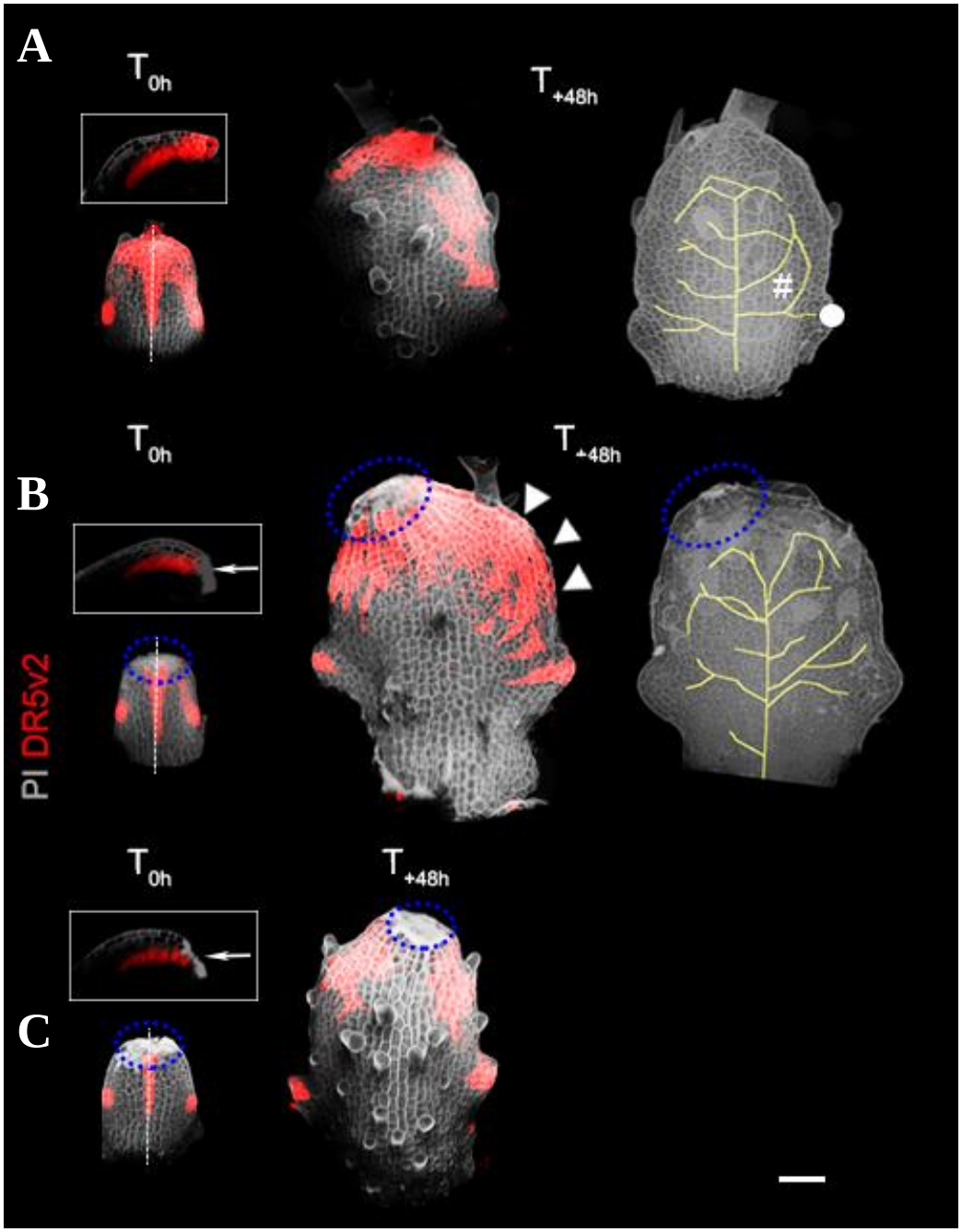

Fig. 4.17. Auxin response and the pattern of procambial strands after the apical ablation.

(**A**-**C**) The expression of DR5v2:YFP (left and middle) and the reconstruction of procambial strands (yellow line segments, right) in control primordia (**A**) and in primordia after the apical ablation (**B, C**) at two time points T_{0h} (just after the ablation) and T_{+48h} (48 h later). Inserts (framed) show optical longitudinal sections across the primordium indicated below by a dashed line. Arrows at inserts indicate the ablation site (**B, C**). Loops are marked by a hash, a dot indicate a free-ending procambial strand extending towards a serration. Blue dotted ellipses at primordia mark the ablation site. Arrowheads indicate extended DR5v2 expression at apical primordium region after the ablation. Images show

original confocal stacks obtained from live imaging (left and middle) or clearing method (right). Cell walls were stained with propidium iodide (PI). N = 9 primordia per treatment (control and ablation). Scale bar: 50 μm.

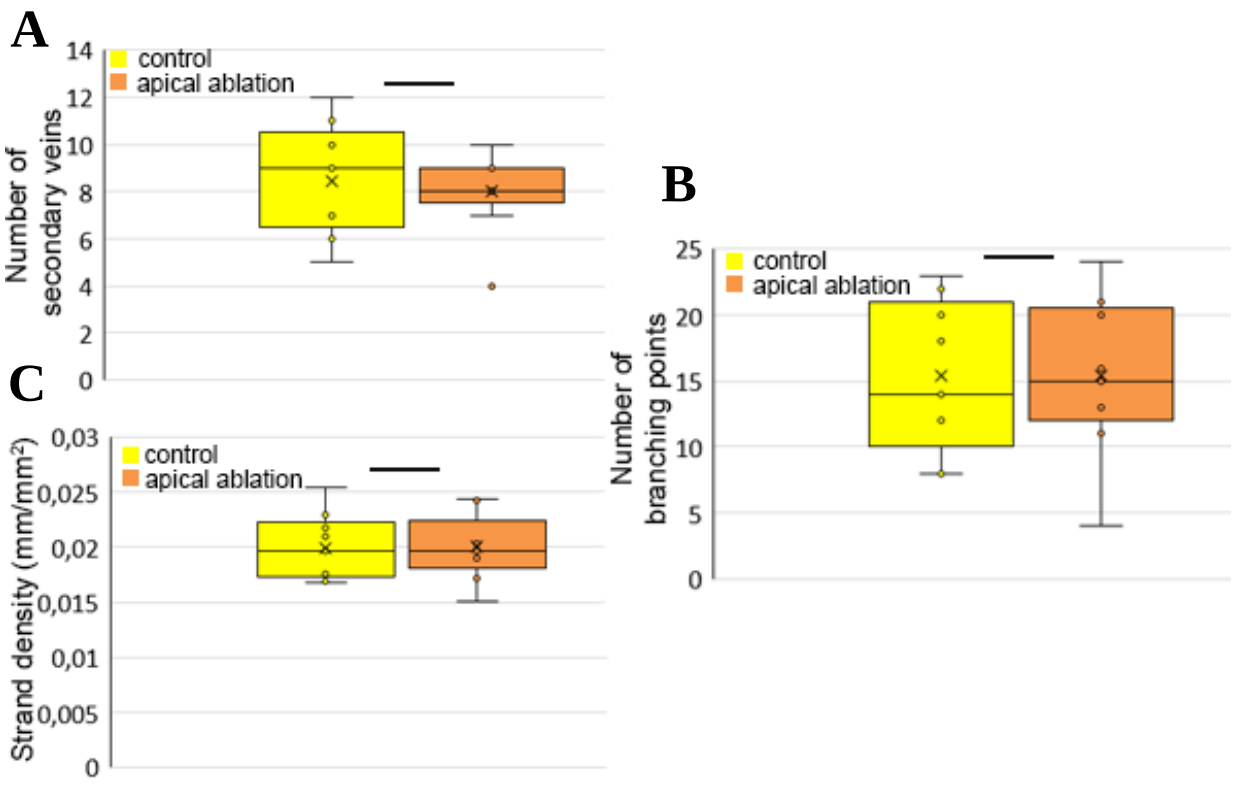

Fig. 4.18. Analysis of procambial strand pattern 48 h after the apical ablation.

(**A**) The number of second-order procambial strands in the control and after the apical ablation. (**B**) The number of branching points in primordia in the control and after the apical ablation. (**C**) The strand density in the control and after the apical ablation. Control primordia (yellow boxes); primordia after apical ablation (orange boxes). Mean values of measured parameters were indicated by „x". Statistically significant differences at 0.05 level are indicated with asterisks (U Mann-Whitney's test). N=9 primordia per treatment (control and ablation).

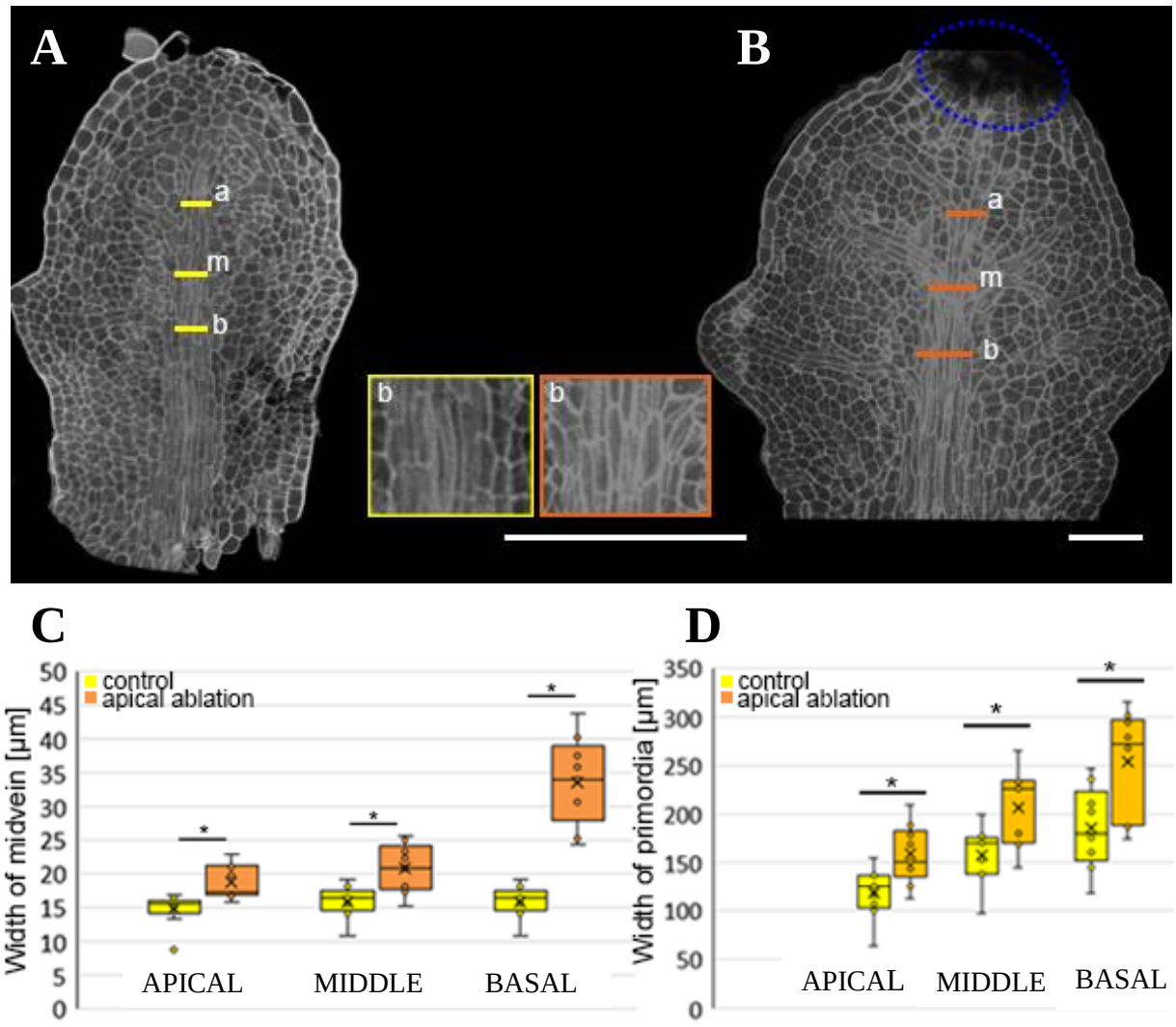

Fig. 4.19. The midvein 48 h after the apical ablation.

(**A, B**) The midvein in control primordium (**A**) and in ablated primordium (**B**). Images show original confocal stacks obtained from clearing method. Yellow and orange line segments indicate particular midvein regions (a, apical; m, middle; b, basal) where the midvein width has been measured. Inserts (framed) show a magnification of the midvein at the basal primordium region. Cell walls were stained with propidium iodide (PI). Scale bar: 50 µm. (**C**) The midvein width at different regions of control and ablated primordia. (**D**) The width of primordium at different regions of control and ablated primordia. Control (yellow boxes), apical ablation (orange boxes); the ablation site (blue dotted ellipse). Mean values of measured parameters were indicated by „x". Statistically significant differences at 0.05 level are indicated with asterisks (U Mann-Whitney's test). N=9 primordia per treatment (control and ablation).

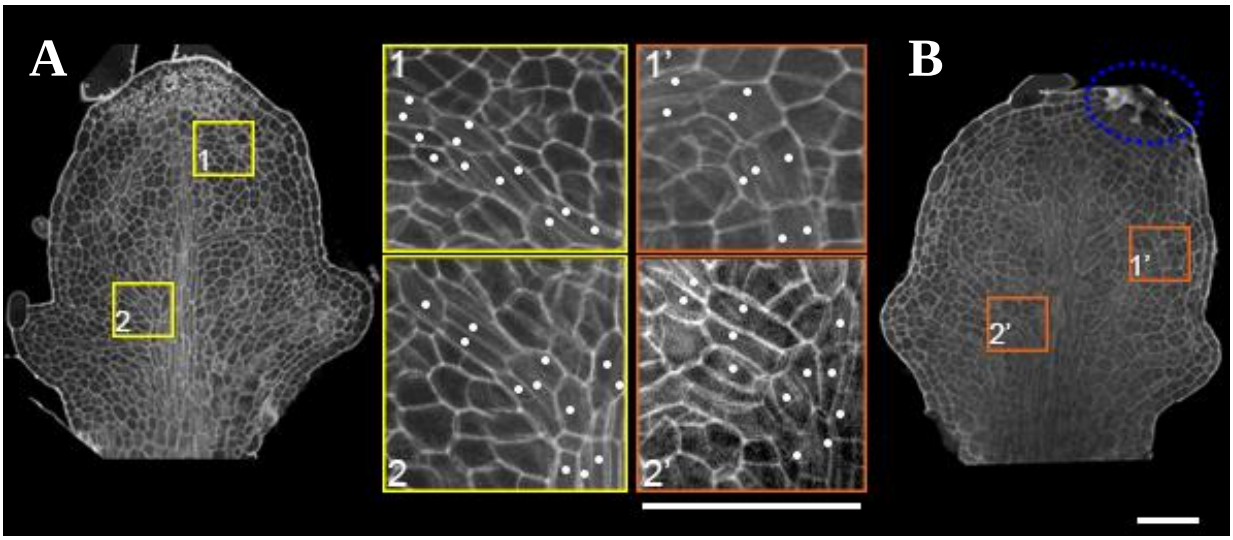

Fig. 4.20. Procambium morphology in second-order strands 48 h after the apical ablation.

(**A, B**) Second-order procambial strands in control primordium (**A**) and in ablated primordium (**B**). Images show original confocal stacks obtained from clearing method. Inserts (framed) show a magnification of procambium strands from two different primordium regions (numbered by 1, 2 and 1',2' in control and ablated primordia, respectively). Procambial cells are marked by dots, the ablation site by blue dotted ellipse. Cell walls were stained with propidium iodide (PI). Scale bar: 50 μm.

In the second type of ablation experiments, cells at the lateral-basal region of primordia were punctured to disrupt the lateral auxin source (**Fig. 4.21A-C**, inserts). After the lateral ablation, a shape of primordia has been changed into more rounded than in the control due to the induction of growth at the site of wounding (**Fig. 4.21B**, T_{48h}, **Fig. 4.22A-B**, blue ellipses, observed in 4/5 primordia). Despite the growth induction, a serration is not formed and the DR5v2 is not expressed at the wounding site (**Fig. 4.21C**, arrowhead), or it is locally downregulated (**Fig. 4.21B**, arrowhead). However, the lateral ablation does not disturb the DR5v2 expression in the apical primordium region and in the opposite lateral region of not ablated primordium side, where the serration is formed.

The lateral ablation locally affects the pattern of procambial strands. It has been observed that in the presence of serrations, the most basal second-order procambial strands form loops with the upper strands, but they are also extend toward the serration as free-ending strands (**Fig. 4.17A**, **Fig. 4.21B**, dots, **Fig. 4.22A**, insert 2). The lateral ablation abolishes the formation of a serration, and the second-order strand branching from the midvein at the level, where a serration should be formed, immediately extends upwards to create a loop with another strand (**Fig.**

4.21B, T_{48h}, **Fig. 4.22A**, compare strands at the primordium side with the ablation indicated by a blue ellipse (insert 1) and at not ablated side (insert 2); observed in 4/5 primordia). Generally, in the most of analysed primordia the lateral ablation and resulting local outgrowth do not affect the formation of secondary procambial strand. However, in one case (1/5 primordia), where the ablation has been performed in a very young primordium, a branching of few elongated cells from the midvein towards a wounding site has been observed, which might account for the induction of a new secondary procambial strand (**Fig. 4.22B**, dots, insert1). This might indicate that a local tissue outgrowth may induce procambium branching.

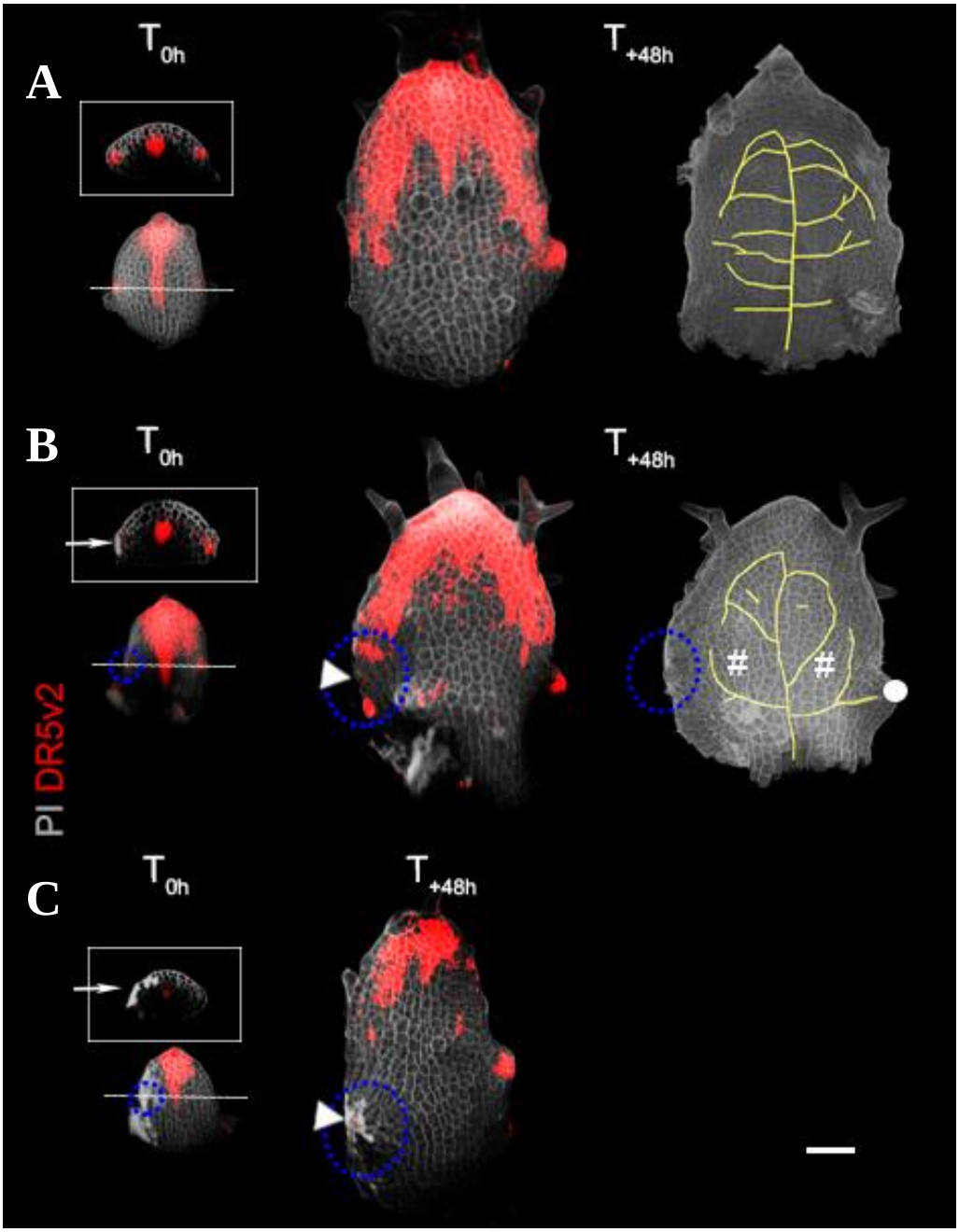

Fig. 4.21. Auxin response and the pattern of procambial strands after the lateral ablation.

(**A-C**) The expression of DR5v2:YFP (left and middle) and the reconstruction of procambial strands (right) in control primordia (**A**) and in primordia after the lateral ablation (**B, C**) at two time points T_{0h} (just after the ablation) and T_{+48h} (48 h later). Inserts (framed) show optical transverse sections across the primordium indicated below by a dashed line. Arrows at inserts indicate the ablation site (**B, C**). Procambial strands after or just before the formation of loops are marked by a hash, a dot indicate a free-ending procambial strand extending towards a serration. Blue dotted ellipses at primordia mark the ablation site. Arrowheads indicate the downregulation of the DR5v2 expression at wounding site. Images show original confocal stacks obtained from live imaging (left and middle) or clearing method (right). Cell walls were stained with propidium iodide (PI). N = 5 primordia per treatment (control and ablation). Scale bar: 50 μm.

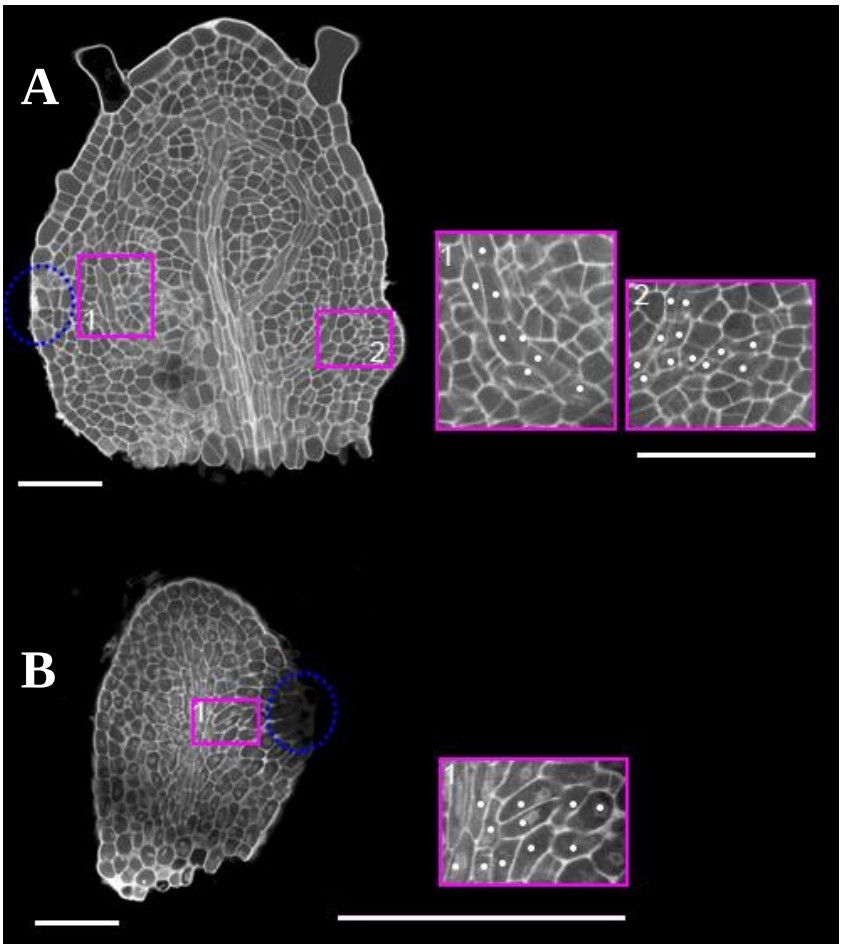

Fig. 4.22. Procambium morphology in second-order strands 48h after lateral ablation.

(**A, B**) Second-order procambial strands in ablated primordia at older (**A**) and younger (**B**) leaf primordia. Images show original confocal stacks obtained from clearing method. Inserts (framed) show a magnification of the procambium strands from framed primordium regions (numbered by 1, 2). Procambial cells are marked by dots, the ablation site by blue dotted ellipse. Cell walls were stained with propidium iodide (PI). Scale bar: 50 μm.

In the third type of ablation experiments, midvein cells at the middle region of primordia together with the above lying parenchyma and epidermal cells were punctured to disrupt potential signals coming from this pre-existing strand (**Fig. 4.23A-D**, inserts). This midvein ablation does not change significantly the primordium shape or the DR5v2 expression. In the most of analysed primordia (7/9), the DR5v2 expression at the apical primordium region and at serrations is similar to the control primordia (**Fig. 4.23A-C**, T_{48h}, asterisks and arrows, respectively). Only in some ablated primordia (2/9), the DR5v2 expression at the apical region is lower (**Fig. 4.23D**, T_{48h}, asterisks).

However, the midvein ablation leads to a dramatic rearrangement of procambial strand pattern. First, the midvein development is disrupted. Either procambial cells at the midvein above the ablation site are less differentiated in comparison to the control, which is manifested in their less elongated shape (**Fig. 4.24A, B**, inserts 3, arrowheads, observed in 7/9 primordia), or these procambial cells disappear and instead nearly isodiametric cells are generated due to transverse cell divisions (**Fig. 4.24C**, insert 3, arrows, observed in 2/9 primordia). On the other hand, procambial cells at the midvein below the ablation site are undisrupted when comparing to control primordia (**Fig. 4.24A-C**, inserts 1).

Second, new procambial strands are formed which bypass the ablated site (**Fig. 4.23B-D**, T_{48h}, arrowheads). These strands seem to emerge from the basal region of the midvein and extend acropetally. It has been observed that bypassing strands in some primordia form an closed pattern as they are already connected at apical primordium region (**Fig. 4.23B-C**, T_{48h}, observed in 6/9 primordia), while in some primordia, these strands are not yet connected (**Fig. 4.23D**, T_{48h}, observed in 3/9 primordia). Moreover, similarly to control primordia, in ablated primordia there are higher-order free-ending procambial strands extending towards serrations branching either form the basal midvein or from bypassing strands (**Fig. 4.23A-D**, T_{48h}, dots, **Fig. 4.24A-C**, inserts 2 and 4). Thus, the extending of procambial strands in relation to serration is not disrupted in ablated primordia.

Summarizing, cell ablations, which aimed at apical and lateral auxin sources, change the DR5v2 expression as well the shape of primordia, that suggests that these auxin sources are important for the growth regulation. Moreover, the displacement of the wounding after the apical ablation and more pronounced DR5v2 expression at non-ablated site imply that the damaged apical source or/and the primordium tip may be regenerated. The apical ablation also affects the midvein development and play a role in the formation of loops, because after the apical ablation the formation of loops and the differentiation of procambial cells is delayed. In turn, the lateral

ablation does not significantly affects the formation of loops, instead, it changes locally the extension of second-order strands, and at the ablation side free-ending strands are not formed. Thus, lateral auxin sources can locally organize the procambium pattern. The most dramatic changes leading to the rearrangement of whole procambial strand pattern occurs after the ablation of several cells at the midvein that disrupts its continuity. These changes include delayed differentiation and in some cases even de-differentiation of procambial cells of the midvein, but only at the region above the ablation site. The region below the ablation seems to be unaffected. This suggests that the midvein development depends on signals from underlying vasculature of a shoot. Moreover, new strands are formed bypassing the ablation site. Thus, the midvein play a major role in the organization of procambial strand pattern.

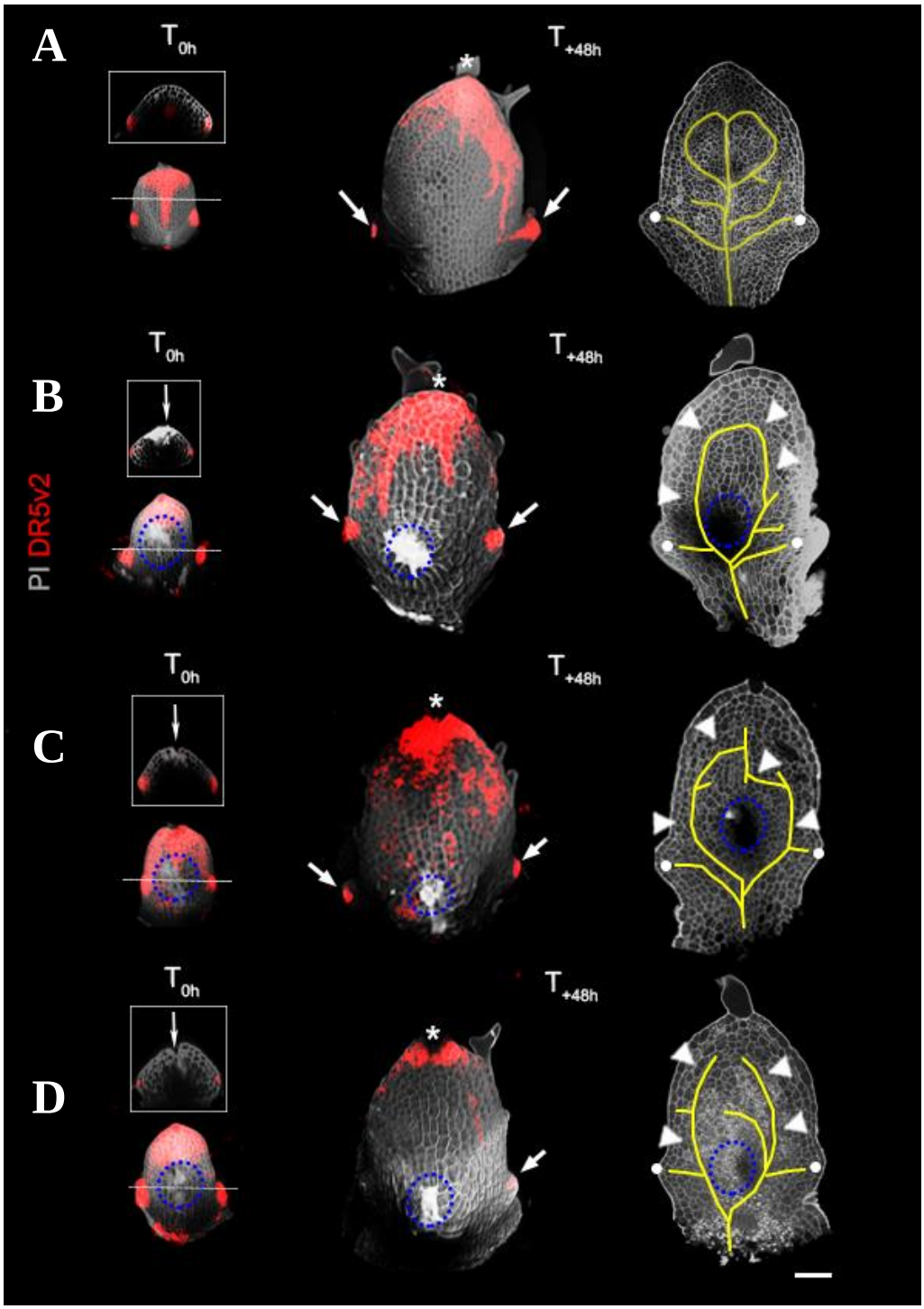

Fig. 4.23. Auxin response and the pattern of procambial strands after the midvein ablation.

(**A-D**) The expression of DR5v2:YFP (left and middle) and the reconstruction of procambial strands (yellow line segments, right) in control primordia (**A**) and in primordia after the midvein ablation (**B-D**) at two time points T_{0h} (just after the ablation) and T_{+48h} (48 h later). Inserts (framed) show optical transverse sections across the primordium indicated below by a dashed line. Arrows at inserts indicate the ablation site (**B-D**). Asterisks indicate the DR5v2 expression at apical primordium region, arrows –

the DR5v2 expression at serrations. Dots indicate free-ending procambial strands extending towards a serration. Blue dotted ellipses at primordia mark the ablation site. Procambial strands which bypass the ablation site are marked by arrowheads. Images show original confocal stacks obtained from live imaging (left and middle) or clearing method (right). Cell walls were stained with propidium iodide (PI). N = 9 primordia per treatment (control and ablation). Scale bar: 50 μm.

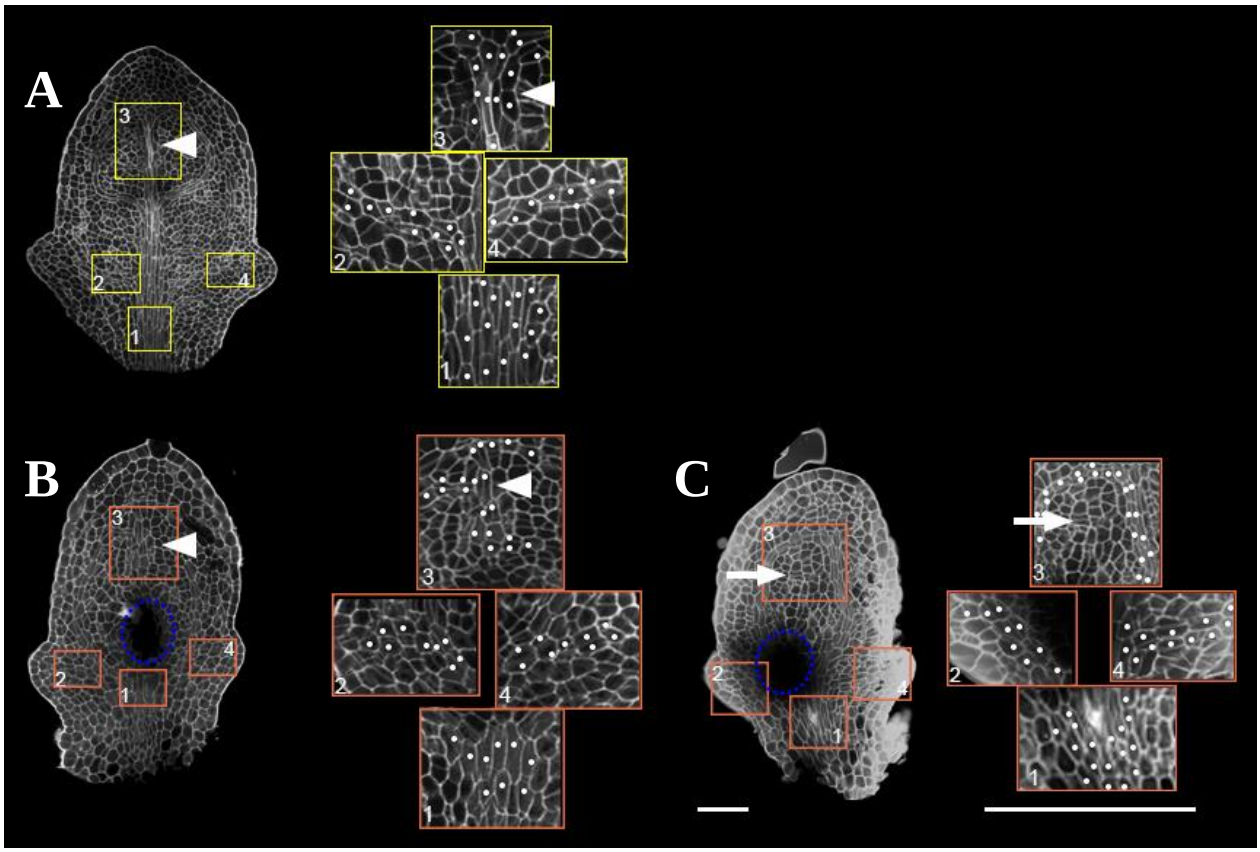

Fig. 4.24. Procambium morphology in the midvein and other procambial strands 48 h after the apical ablation.

(**A-C**) The midvein in control primordium (**A**) and in ablated primordium (**B-C**). Images show original confocal stacks obtained from clearing method. Inserts (numbered from 1 to 4) show a magnification from the framed region of primordia. Images show original confocal stacks obtained from clearing method. Procambial cells are marked by dots, the ablation site by blue dotted ellipse. Arrowheads indicate procambial cells at the midvein above the ablation site, arrows – cells without procambium morphology above the ablation site. Cell walls were stained with propidium iodide (PI). Scale bar: 50 μm.

5. DISCUSSION

5.1. Methods in studying the formation of leaf vasculature in *Arabidopsis*

The formation of leaf vein patterns has been fascinated biologists for many years. Most of studies at this field were focused on *Arabidopsis thaliana*. Using this model plant, development of the vascular system has been studied in cotyledons (Busse and Evert 1999; Sieburth 1999; Berleth et al. 2000; Tsukaya et al. 2000; Kastanaki et al. 2022), in adult rosette leaves (Kang and Dengler 2002; 2004; Aloni et al. 2003), however, current knowledge on the vascular patterning is mainly based on studies on the first true rosette leaves (Candela et al. 1999; Mattson et al. 1999; Scarpella et al. 2004; 2006; Tsukaya et al. 2000; Sawchuk et al. 2007; 2013; Donnet et al. 2009; Gardiner et al. 2011; Wenzel et al. 2012; Verna et al. 2015; 2019; Marcos and Berleth 2014; Govindaraju et al. 2020; Krishna et al. 2021; Linh and Scarpela 2022).

The advantage of using cotyledons is the simplicity of their structure (no trichomes, no serrations) and repetitive character of the vascular pattern (only second-order vascular strands and two pairs of loops) (Sieburth 1999). On the other hand, the fact that cotyledons and their vasculature are formed during embryogenesis makes experimental manipulations (e.g. chemical or mechanical) difficult. It also hampers the imaging over time the initiation of vascular strands. That's why all studies on cotyledons are based on imaging of either fixed material with using standard light microscope (Busse and Evert 1999; Sieburth 1999; Berleth et al. 2000; Tsukaya et al. 2000) or live imaging with laser confocal microscope, but only at one time-point (Kastanaki et al. 2022).

The first true rosette leaves are more advanced in their structure and vasculature. They have in total three hydathodes (the structures that are directly connected to leaf vasculature and responsible for water release), the one localized at the leaf tip and two others at serrations at the basal region of a leaf (Tsukaya et al. 2000). The vasculature contains both second-order vascular strands forming three pairs of loops and higher-order strands (either connected or free-ending) (Scarpella et al. 2004). This enables to study mechanisms of the generation of different local vascular patterns, for example closed *versus* open patterns. Since the first true leaves are initiated during post-embryonic development, the advantage of this model system is a possibility of *in vivo* imaging in a time-lapse sequence with laser confocal microscope (see below). Another advantage is that plants used in these studies grows under the continuous light and the leaves were examined after relatively short time since the germination (quantified in

days). In particular, the formation of vasculature was monitoring usually at 3-7 days after the germination (DAG), which reduced the time needed for consecutive experiments (Scarpella et al. 2004; 2006; Sawchuk et al. 2007; 2013; Marcos and Berleth 2014).

The studies on adult rosette leaves are much more limited nowadays, and there were only few of studies, which relied on fixed material, where leaf vasculature was visualized with standard light microscope (Kang and Dengler 2002; 2004; Aloni et al. 2003). However, these leaves exhibit the most elaborated patterns of the vasculature with several higher-order vascular strands, which are organized in several loops or stay free-ending, and connect to several hydathodes or serrations at the leaf margin. Thus, this system seems to be better to capture the variability of vascular patterns with possible different mechanisms of their formation. However, due to this variability, studying the pattern of vascular strands is challenging. The exact position of the formation of vascular strands is unpredictable, thus, experiments needs a high number of repetitions (Scarpella and Meijer 2004). The other disadvantage is related with a relatively long time needed to obtain a material, as the plants used to study adult leaves are supposed to grow for 4-5 weeks in the short-day conditions that prolong the vegetative phase of plant development.

Most of earlier studies on leaf vascular system were based on fixed material and the auxin-related reporters (e.g. DR5) with GUS (β-glucuronidase) system (Sieburth 1999; Tsukaya et al. 2000; Kang and Dengler 2002; 2004; Aloni et al. 2003; Mattson et al. 2003). These studies provided useful information on auxin spatial distribution (indirectly) and vascular patterns at early and later levels of differentiation in leaves at different developmental stages. However, these methods cannot provide reliable knowledge about the dynamics (a sequence of events) of vascular formation process. Also, the GUS expression cannot be easily quantified in leaves. On the other hand, methods based on the fixed material are still currently using in the combination with clearing procedures and laser confocal microscope (Truernit at l. 2008; Wuyts et al. 2010; Ursache et al. 2018). Such methods enables detailed visualization inner cells in an organ with a very good resolution, that is especially important is studying of the vascular system in leaves. In addition, clearing methods eliminate the need of tissue thin sectioning, thus, can provide information on the 3D organ structure.

In turn, in non-invasive *in vivo* imaging of leaves (mostly used nowadays) different auxin-related (PIN1, MP, DR5) and vascular-specific (ATHB8, ET1335, Q0990) reporters with fluorescence proteins (such as GFP or YFP) are used, which mark the earliest stages of vascular strand formation. Also, the expression of fluorescent-tagged genes can be quantified providing

important information on a gene activity or auxin distribution at different regions of leaves. To get a comprehensive view of the dynamic aspects of vascular patterning and direct visualization of its critical events, a leaf can be imaged over time at several time-points, for example, at lower resolution - over 4 days (Sawchuk et al. 2007), or with a high subcellular resolution - over 36 hours (Marcos and Berleth, 2014). However, as the time-lapse imaging of leaf primordia is still challenging, most of the studies on vascular system initiation take advantage from one time-point live imaging of leaves at different developmental stages (Gardiner et al. 2011; Verna et al. 2015; 2019; Govindaraju et al. 2020; Krishna et al. 2021; Linh and Scarpella 2022).

In this study, primordia of adult rosette leaves have been examined from plants growing in the short-day conditions. To image growing leaf primordia at earliest possible developmental stages (when primordia were already clearly separated from the meristem, and the midvein has been specified), plants were dissected, shoot apices were isolated, and moved to the *in vitro* culture. The rosettes growing at these conditions are larger and they are easier to dissect then seedlings or young rosettes, and leaf primordia are more accessible for experimental manipulations. Due to the fact, that the vascular pattern in leaves is to some extend unpredictable (Scarpella and Meijer 2004), a high number of control (untreated) primordia at different stages were analyzed (N = 40). The timing of imaging (two time-points with 48 h time interval) was adjusted after several preliminary experiments, from one hand, to minimize the side effects of organ isolation, culturing in non-sterilized conditions, staining of cell walls by propidium iodide, and laser exposure, but to other hand, to let effects of experimental manipulations (chemical treatment, cell ablations) to be expressed in the DR5v2 signal intensity, initiating vasculature, and primordium growth. Visualization of the primordia at different developmental stages at two time-points allowed for the analysis of a sequence of events during the initiation of procambium strands, although, it was more challenging manually and more time-consuming. Also, the imaging itself with using the inverted confocal microscope caused some difficulties, due to the fact that the primordia were scanned with long-working distance objectives in a drop of water, which very often flowed down extending the scanning time.

The combination of live imaging with pseudo-Schiff-propidium iodide-based clearing method enabled the analysis of the effects of experimental manipulations with the respect to the DR5v2 expression, cell morphology reflecting procambium differentiation, and other parameters of the vascular pattern (strand branching, density). The obtained images were analyzed by dedicated computer software (MGX, Python), not only qualitatively (the reconstruction of DR5-expressing or procambial strands), but also quantitatively, for example, by the quantification of

the expression of genes related to auxin biosynthesis and the DR5v2 expression reflecting the strength of auxin sources.

5.2. The generation and maintenance of auxin sources at leaf primordia

Using the DR5v2:YFP line in this study allowed to visualize and analyze not only early stages of the initiation of vascular strands, but also possible epidermal auxin sources at *Arabidopsi*s leave primordia. Auxin sources can play the role in the organization of vascular pattern (Sachs 1981; Aloni 2001, 2003; Rolland-Lagan and Prusinkiewicz 2005; Runions et al. 2005; Scarpella et al. 2006), as they are the sites of high auxin concentration from which auxin is polarly transported initiating the future vascular strands. In this scenario, the strength of auxin source could be proportional to the auxin concentration. The auxin concentration, in turn, may affect the width or/and the amount of related vascular strands.

The source strength was measured in this study based on the intensity of the DR5v2 expression. From one hand, the DR5v2 expression shows auxin levels indirectly, because its expression depends also on other factors in auxin signaling pathway (TIR1/AFB, AUX/IAAs, ARFs) (Vernoux et al. 2011). But on the other hand, the DR5v2 expression is sensitive to different auxin concentrations (Liao et al. 2014; Galvan-Ampudia et al. 2020), thus, it can be used for a detection of higher auxin levels. Indeed, the quantitative analysis of the DR5v2 expression in this study showed that both local auxin microapplication to the apical primordium region and global auxin treatment lead to a significant enhancement of the DR5v2 expression in the apical and lateral auxin sources indicating an increase of their strength.

To answer the question how primordium development affects the auxin sources, the epidermal DR5v2 expression was quantified in the apical and lateral (marginal) primordium regions at different developmental stages. Such a detailed analysis of auxin sources has not been the subject of any previous researches. In agreement to previous studies (Aloni 2003; Scarpella et al. 2006), this study shows that the DR5v2 expression related to apical auxin source is present in primordia from their earliest stages. The first DR5v2-marked lateral sources appear at primordium margin in the relation to the formation of the first pairs of serrations localized closer to the basal primordium region and below the region where the first apical loops are formed. Subsequent lateral sources are formed above the first ones. Although, the consecutive serrations are usually formed basipetally (Nikovics et al. 2006; Kawamura et al. 2010; Kierzkowski et al. 2019), sometimes serrations can be formed in the acropetal direction (Daniel Kierzkowski,

personal communication). Thus, observed in this study lateral DR5v2-marked auxin sources are formed in the relation to the serrations. Also, this study shows that the strength of apical auxin source does not change from the earliest stages of primordia (with smooth margins) at least until the formation of well outgrow first pair of serrations and the initiation of the second pair of serrations. The same applies to lateral auxin sources: once they appear at primordium margin before any morphological signs of the serration formation, the source strength is constant. In addition, the strength of apical and lateral sources is similar. This indicates that just after their establishment, the strength of auxin sources reaches the maximum, which is further maintained.

Thus, the question arises, what is the mechanism of auxin source generation and maintenance? Locally elevated auxin levels might by a consequence of the PIN1-mediated polar auxin transport (Scarpella et al. 2006) or/and local auxin biosynthesis (Aloni 2003; Kneuper et. al 2021). Indeed, the overlapping local upregulation of the *YUC4* and *TAA1* expression at primordium margins shown in this study suggests, that the generation of lateral auxin sources is related to the localized auxin biosynthesis. This observation is in agreement to the previous study of Kneuper et al. (2021), where a detailed map of auxin biosynthesis genes has been presented. In contrast, no local upregulation of either *YUC4* or *TAA1* genes has been observed in this study at apical primordium region. However, in the Kneuper et al. (2021) study, a local *YUC4* upregulation has been found at apical primordium overlapping with a more broad *TAA1* expression. The reason of this discrepancy is unclear. It might be a result of using different transgenic constructs (especially in the case of *YUC4*, where the transgenic lines come from different labs) or/and the sensitivity of detectors in the laser confocal microscope used in this study and those of Kneuper et al. (2021). Thus, data in this study suggests that auxin biosynthesis is not specifically localized at apical primordium region and it unlikely explains the generation or/and maintenance of apical auxin source. However, it cannot be excluded that by using other transgenic lines or tools such localized biosynthesis might be observed.

In turn, increased strength of lateral auxin sources after local auxin microapplication to apical primordium region implies, that auxin supplying these sources at leaf margins can also derive from other primordium regions, for example by the PIN1-mediated polar transport. Interestingly, the suppressing polar auxin transport by the NPA treatment and the mutation in the *PIN1* lead to the disappearance of lateral auxin sources. This means that despite the presence of local auxin biosynthesis at these sites, polar auxin transport is a crucial process responsible for high auxin concentrations in lateral sources. In addition, this observation also implies that

there might be a link between the polar auxin transport and auxin biosynthesis: any disruption of the first component negatively affects the other.

Apical auxin source as well relies on the polar auxin transport, but this source seems to be more resistant to the transport perturbations in comparison to lateral sources. Namely, the NPA treatment leads to reduced auxin response in the apical source, but some DR5v2 expression is still observed at apical primordium region. Similarly, the local maxima of the DR5v2 expression at the apical region in *pin1* primordia are still maintained, however, they are more spread along primordium margin in comparison to the WT. This means that the PIN1-mediated polar auxin transport significantly participates in the maintenance of apical auxin source, however, also other unknown mechanisms are likely involved. The apical source seems to be also more plastic. After the ablation of cells at the site of apical source, the DR5v2 expression becomes to be more extended towards the opposite non-wounding region. In contrast, after the ablation of cells at lateral auxin source, the DR5v2 expression is reduced at nearby cells at primordium margin, and no signs of local upregulation of auxin response have been observed at this region.

5.3. The midvein development

The midvein is initiated before the emergence of leaf primordia and is associated with the auxin canal formed by basipetal auxin transport from the SAM surface into inner tissues (Bayer et al. 2009). The auxin canal extends and ultimately joins the pre-existing vasculature of the stem. Even after the initiation, the basipetal auxin transport in the future midvein is maintained (Scarpella et al. 2006; Kneuper et al. 2020). However, this and previous studies show that the differentiation of vascular cells in the midvein proceeds acropetally, which is manifested in the length of procambial cells and their number per the midvein width (Dengler 2006).

The DR5 fused with either GUS or GFP/YFP fluorescent proteins is a useful reporter that marks the earliest stages of vascular strand development including the midvein (Mattsson et al. 2003; Scarpella et al. 2006; Marcos and Berleth 2014; Biedroń and Banasiak 2018). The only disadvantage, shown in all these previous studies and also confirmed in this study, is that the DR5 or DR5v2 expression is decreasing upon vascular cell differentiation. Thus, in the case of the midvein, the DR5v2 expression gradually disappears from the basal region of the midvein at older leaf primordia. This may indicate that during the progression of vascular differentiation auxin levels are decreasing or/and the ARF-dependent auxin signalling is suppressing.

In this study, leaf primordia with already initiated midvein were analysed, where in the youngest primordia, the future midvein consists of cells just after the first round of cell divisions, which results in their slight elongated shape. Detailed analysis of older primordia shows, that from its initiation the midvein undergoes developmental changes: procambial cell length and the midvein width increase during primordium growth, the latter parameter - mostly due to procambial cell divisions (there is an increase in the number of procambial cells per midvein width). The fact that the midvein is connected to the apical auxin source (there is a continuity of the DR5v2 expression) suggests that this source might play a role in the midvein development.

However, the reinforcement of apical auxin source by about 20 % by local auxin microapplication does not affect the midvein. It is possible, that this reinforcement is not strong enough to significantly affects the differentiation of the midvein. However, global auxin treatment leads to the midvein widening in the basal region by an increase in the number of procambial cells per midvein width. On the other hand, global auxin treatment does not lead to the significant upregulation of the DR5v2 expression at the apical source. Instead, the expression in the whole primordium (including epidermis and inner tissues) is strongly upregulated.

The midvein is also wider after the suppression of polar auxin transport by the NPA treatment or *pin1* mutation in agreement with other studies (Mattsson et al. 2003; Verna et al. 2015; 2019; Kneuper et al. 2020). Interestingly, the NPA treatment significantly decreased the DR5v2 expression at apical auxin source, but not at inner tissues. This suggests that the midvein might be supplied by auxin from inner sources. Indeed, the study of Kneuper et al. (2021) strongly suggests that vascular tissues might be sites of auxin biosynthesis. Although, in this study the expression of neither *YUC4* or *TAA1* was detected in inner tissues, however, this might result from using different transgenic lines or technical issues related to the confocal microscopy. Nonetheless, auxin biosynthesis in inner tissues might explain why the DR5v2 expression is not decreasing after the suppression of polar auxin transport. It needs to be also noted, that the level of inner DR5v2 expression might be underestimated in this study: the laser penetration across tissues decreases, especially in older leaf primordia such as those analyzed after the NPA treatment.

The midvein development can be also affected by mechanical disruption of the apical auxin source, however, in this case the interpretation of obtained results is not straightforward. After the cell ablation at the apical source, the DR5v2 expression is more extended, which might

indicate that paradoxically, the ablation leads to the source regeneration and at least its transient reinforcement. Such a scenario would explain the midvein widening observed in this study at the basal midvein region.

Altogether, although the epidermal apical auxin source may somehow affects the midvein, results obtained in this study suggests that the auxin source is not crucial factor shaping the post-initiation development of the midvein. There was a similar conclusion of theoretical work of Rolland-Lagan and Prusinkiewicz (2005). Instead, the midvein development might depend on auxin concentration (and associated auxin signalling) in the midvein. This and other studies (Mattsson et al. 2003; Scarpella et al. 2006; Wenzel et al. 2012; Kneuper et al. 2021; Linh and Scarpella 2022) show that the increased auxin concentration or/and auxin signalling, independently of how they were achieved (by auxin treatment or by the suppression of polar auxin transport), would promote the vascular differentiation by either increasing the number of parallel cell divisions or/and recruiting more cells from ground tissue. This would also suggest that the midvein is more autonomous with regard to the factors which control its development. Since the midvein development is acropetal, it may also depend on signals from connected pre-existing vasculature of the stem (Banasiak and Gola 2023). Such an idea is supported by an experiment in this study, where the cell ablation was performed in the middle region of the midvein. This cell ablation, which disrupts the midvein continuity with stem vasculature, leads to a delay of the vascular differentiation at the midvein region above the wounding, or in the most extreme cases – to de-differentiation of procambial cells in this region. However, the basal midvein region, which maintained the connection with underlying vasculature, is unaffected by the cell ablation. Thus, without the connection of the midvein to the stem vasculature, the normal procambium differentiation in the midvein is inhibited.

5.4. Development of higher-order strands and loops

After the establishment of the midvein, higher-order vascular strands are initiated. In the first rosette leaves of *Arabidopsis*, the second-order strands branch from the midvein and form the first, second, and third pairs of loops, so that the first loops are formed at the apical primordium region, and subsequent loops appear in the basipetal direction. It has been proposed that the initiation of second-order strands and associated loops is closely related to the epidermal PIN1-convergence points at primordium margins (reviewed in Banasiak and Biedroń 2018; Perico et al. 2022). In theory, these convergence points should be also sites of local auxin concentration,

thus, they might be regarded as auxin sources. However, the exact role of these putative auxin sources is unclear.

The first convergence points are observed at primordium margins at half-way from the primordium tip and are connected to the second-order PIN1-expressing strands ultimately forming the first loops (Scarpella et al. 2006). The below second-order strands, which give rise the second loops, are shown to be formed also in relation to the epidermal PIN1-convergence points. However, the contribution of the PIN1-convergence points in the initiation of second-order vascular strands and the first and second loops is controversial since these convergence points are transient and not correlated with the local DR5 maxima (Scarpella et al. 2010). In contrast, the second-order strands forming the third loops at basal primordium region are connected the PIN1-convergence points at primordium margins, where the *PIN1* expression clearly extends into subepidermal cells. Importantly, these points are associated with local DR5 maxima indicating high auxin levels, and mark the position of future serrations or hydathodes (Scarpella et al. 2006). Thus, it has been proposed, that only third loops are formed in association with lateral auxin sources, while the formation of first and second loops is related to the internal auxin sources localized close to the midvein (Scarpella et al. 2010).

In the agreement with previous studies (Scarpella et al. 2006; Marcos and Berleth 2014), this study shows that the second-order strands, which subsequently form loops, are initiated first at apical primordium region either close to the apical auxin source or lateral primordium region. However, no epidermal DR5v2 local maxima corresponding to lateral auxin sources were found at apical and middle primordium margins. Instead, DR5v2-marked lateral auxin sources are connected to the second-order strands at basal primordium region. Thus, the vascular strands (including loops) at apical and middle primordium regions might be regulated by apical source or/and internal signals, while those at basal primordium region - by lateral auxin sources related to the serrations. However, such scenario would assume that there are different mechanisms for the vascular pattern formation within the same organ. Also, any disruption of apical or lateral auxin sources should affect the vascular pattern at corresponding primordium region. Observations and experiments performed in this study suggest rather that it is not a case.

For example, the local auxin microapplication, which reinforced the strength of apical and lateral auxin sources (by 20 % and 30%, respectively), does not affect the formation second-order strands or loops. In turn, global auxin treatment led to the dispersion of auxin sources and the DR5v2 expression was strongly upregulated in the whole primordium including inner

tissues. However, the number of second-order strands, loops and vascular branching points does not significantly increase after the auxin treatment (although some slight increase in the number of branching points has been observed). On the other hand, auxin seems to promote the extension of vascular strands, since the loops in the treated primordia develop earlier in comparison to the control.

The impact of lateral auxin sources has been also tested by the NPA treatment, which suppresses of polar auxin transport. This treatment decreases the strength of auxin sources, in particular at the margins of primordium basal region, where no local DR5v2 maxima are observed. The NPA treatment leads to clear changes in the vascular pattern. There are less second-order strands, which would branch from the midvein. Instead, several procambial strands extend parallel to the midvein at the basal primordium region, and they extend towards the primordium margins only at more distal primordium regions. No loops were formed. Thus, the NPA treatment affected mostly branching of the higher-order strands and patterning, not really the initiation of the strands.

Similar effects have been observed in *pin1* mutant primordia, which also lack the lateral auxin sources (and serrations), however, these effects are weaker in comparison to the NPA treatment as previously reported (Mattson et al. 1999). Namely, as in the case of NPA treatment, no loops are found in *pin1* leaf primordia. Moreover, the branching of second-order strands in *pin1* mutant is disrupted as these strands extend from the midvein a lower (more sharp) angle in comparison to the WT. It appears that this effect is much more pronounced after the NPA treatment, where the vascular strands extend parallel at basal primordium region. Changes in the vascular pattern observed after the NPA treatment and in the *pin1* mutant might be a consequence of disturbed auxin sources, however, they might result as well from lower auxin flux in vascular strands due to the suppression of auxin transport. In other word they might be related with auxin sink.

The lack of lateral auxin sources (and serrations) reflected by the disappearance of local DR5v2 maxima at primordium margins characterizes also leaf primordia in double *cuc2cuc3* mutant. However, in contrast to the NPA-treated or *pin1* leaf primordia, auxin flux in the *cuc2cuc3* vasculature seems to be not affected. Although, it has been proposed that *CUC*2 gene promotes the PIN1-mediated generation of local auxin maxima in leaf margins, the PIN1 still exhibits its polar cellular localization in the *cuc2* mutant (Bilsborough et al. 2011), and no direct genetic interaction was reported between *CUC*s and *PIN1*. Instead, *CUC* genes are known to act as

repressors of cell growth and divisions (Zadnikova and Simon 2014; Burian et al. 2015). Thus, it is unlikely that the polar auxin transport in leaf vascular strands is significantly suppressed in *cuc2 cuc3* mutant. Accordingly, potential changes in the vascular pattern in *cuc2 cuc3* mutant can be interpreted as the effect of the absence of lateral sources, while in *pin1* and NPA -treated primordia – as an effect of lower auxin flux in the vasculature or/and source loss.

In this study, it has been shown that despite the lack of lateral auxin sources and serrations, the vascular pattern in the *cuc2 cuc3* mutant is generally similar to the WT. In addition, an accelerated formation of loops in *cuc2 cuc3* primordia is observed. More importantly, there is no free-ending vascular strands at the basal primordium region that would terminate in serrations (while such strands occur in the WT). Similar changes were reported previously in the *cuc2* single mutant: the vascular pattern is normal with regard to the number of second-order veins, their branching, and loop formation, but no vascular strands were terminated at primordium margins (Bilsborough et al. 2011).

Interestingly, this effect has been also observed in leaf primordia after the cell ablation at lateral auxin source in this study. Even though the ablation leads to local growth induction, the second-order strands form loops, but they do not extend towards the wounding site and form free-ending strands, like in undisturbed primordium in the presence of serrations. The only exception was the case, when at very early stage of primordium development, lateral ablation and resulting local outgrowth induces vascular branching directly from the midvein, however, at the same time no local DR5v2 upregulation at primordium margin was observed. Thus, still it is possible that at some circumstances, new strands can be formed in relation to a tissue outgrowth. Cell ablation at apical auxin source performed in this study leads to a slight delay in the loop formation, probably related to slower procambium differentiation in the second-order strands. However, it is unclear if such effects are associated with the disruption of apical auxin source or with the wounding itself, which changes the primordium growth especially at the apical region.

Concluding, it can be proposed that the epidermal lateral auxin sources and corresponding local auxin maxima are not necessary for the proper development of leaf vascular pattern. It is in agreement with the recent study that shows that epidermal PIN1 expression in not requiring for the development of proper vascular pattern including the formation of second-order strands and loops (Govindaraju et al. 2020). Instead, lateral auxin sources at primordium margins are necessary for the formation of serrations (Bilsborough et al. 2011). The formation of serrations,

in turn, can be associated with the induction of free-ending vascular strands, which ultimately terminate at hydathodes. In this case, the initiation of serrations would be involved with the generation of epidermal PIN1 convergence points and local auxin maxima. Subsequent basipetal auxin transport from the primordium margin towards underlying pre-existing vascular strands would generate auxin canal inducing free-ending strands.

Thus, changes in the vascular pattern observed in the NPA-treated or *pin1* leaf primordia (the inhibition of loop formation, the disruption of strand branching, strand widening) result rather from lower auxin flux or/and related auxin concentration in the vascular strands. However, it is hard to predict what are auxin levels under these conditions. From one hand, lower auxin flux might lead to auxin accumulation in the vasculature. But on the other hand, lower auxin flux might affect the auxin biosynthesis, and lead to auxin level decrease (Burian et al. 2019). Obviously, more studies are necessary to check auxin concentrations in vasculature, for example with using more advanced laser microscopes (e.g. bi-photon or LigthSheet), and the reporters which would show auxin levels more directly such as R2D2 (Liao et al. 2015).

Strikingly, experiments where a continuity of the midvein has been disrupted by the cell ablation show that the midvein acts as organizer of the vascular pattern in a leaf, provided its connection to the stem vasculature. The procambium differentiation in the midvein above the ablation site is suppressing, while the differentiation of cells below the ablation, where the midvein is connected to the underlying stem vasculature, proceeds normally. In addition, new strands bypassing the wound emerge from this undisturbed basal region of the midvein. Altogether, this suggests that signals inducing the formation of vascular strands might derive from pre-existing vasculature. Thus, the vascular system in this regard would be autonomous. However, at the same time, development of vascular strands is plastic and responds to local environment, which is reflected, for example in the induction of new strands after the tissue wounding which bypass the wound and restore vascular continuity, or strands which terminate at hydathodes.

5.5. The relation between vascular pattern development and primordium growth

Several studies suggest that that there is a relationship between the vascular patterning and leaf growth. Indeed, as leaves are growing, there is a continuous addition of new vascular strands and an increase in the vasculature complexity (Candela et al. 1999; Kang and Dengler 2004). These observations have been conformed in this study: during subsequent stages of primordium

development, the vascular pattern becomes more complex, that is manifested in the increased number of higher-order strands and loops, branching points, and strand density. Thus, the older the leaf, the more advanced the vascular system. Moreover, it has been reported that leaf shape and vascular pattern defects can be coupled in mutants (Dengler and Kang 2001; Petricka et al. 2008). Thus, the same factors which regulate the vascular pattering might also affect the primordium growth, and *vice versa*.

Although, in this study no clear correlation has been found between overall vascular pattern and primordium shape after chemical or mechanical disturbances, it seems that some features of the midvein might be coupled with primordium growth. Namely, after global auxin treatment leaf primordia grow faster in length in comparison to untreated primordia, which is in agreement with the fact that auxin stimulates cell elongation (Majda and Robert 2018). Strikingly, procambial cells in the midvein are longer along whole primordium in IAA-treated primordia than in untreated primordia. Conversely, after the NPA treatment leaf primordia are wider in comparison to untreated primordia, which indicates that they grow more in width. Accordingly, in NPA-treated primordia procambial cells are wider at middle and basal midvein regions in comparison to the untreated primordia. Although, these cells are also longer in NPA-treated primordia, the ratio of cell length and width shows that after the NPA treatment procambial cells grow much more in the width than in the length. Thus, it seems that the growth of leaf primordia can be reflected in the growth of procambial cells in the midvein which determine the midvein shape. However, to study more deeply the relation between organ growth and vascular pattern, more advanced methods of growth computations would be needed (for example, the computation of cell growth rate and anisotropy in individual cells) together with microscopy enabling to follow over time cell behaviour in inner tissues.

The other cellular aspect of leaf vasculature development is procambium differentiation. The expression of procambial differentiation markers suggests that procambium cell features (elongated shape) appear simultaneously along entire strands (Scarpella et al. 2010). Moreover, characteristic elongated shape of procambium cells was proposed to result from coordinated elongation (highly anisotropic cell growth), rather than from synchronized cell divisions (Donnelly et al. 1999; Kang and Dengler 2002; Sawchuk et al. 2007).

However, in this study, the using clearing protocol for the visualization of details of cell morphology in initiating vascular strands enabled to detect a gradient of procambium differentiation along a strand. Namely, procambium in newly formed second-order strands differentiates from the branching point, i.e. from the pre-existing strand, and the loops are

formed by joining two second-order strands. Thus, the most differentiated procambial cells in the new strand are close to pre-existing strands, while the less differentiated - at distal strand position. Moreover, the earliest stages of procambial differentiation recognized in this study based on the morphology (slightly elongated cells) emerge due to cell divisions oriented parallel to the axis of future vascular strand. This suggests that the initial shape of procambium cells is generated due to cell divisions rather than from anisotropic growth. But in the course of subsequent development, procambial cells becoming more elongated due to both anisotropic growth and parallel cell divisions.

Interestingly, there are two gradients related to the formation of leaf vasculature. From one hand, the midvein develops in acropetal direction (the most differentiated cells are at basal or proximal primordium region), and every second-order strands develop from pre-existing strands (the most differentiated cells are at proximal region of a strand, while less differentiated – at distal region). Since the midvein is formed in the continuity with pre-existing vasculature of the stem, it might be generalize that all vascular strands differentiate form the pre-existing strands. This implies that the signals regulating procambium differentiation derive from pre-existing vasculature.

On the other hand, new second-order strands and loops appear in basipetal direction (first strands branch at apical and middle primordium region, and the next ones - below). This gradient, in turn, is likely associated with growth and differentiation gradients in leaf primordia (Donnelly et al. 1999). Namely, after primordium emergence at the SAM, primordium expands along proximal-distal axis (Echevin et al. 2019). Soon after, the cell growth and cell division frequency occur mostly close to primordium margins, and then they are more dispersed within primordium. In *Arabidopsis* (but not in all plant species), a basipetal gradient of cell growth and divisions develops with faster cell differentiation in more distal primordium regions. Altogether, these data suggest that procambium differentiation and the initiation of new vascular strands is regulated by separate mechanisms, the former is related to pre-existing vasculature, while the latter - with overall developmental program in a leaf.

6. CONCLUSIONS

• The locally elevated DR5v2 expression in *Arabidopsis* leaf primordia marks not only the initiation of vascular strands, but also plausible auxin sources at apical and lateral primordium regions. The strength of these sources remains constant during primordium development. Lateral sources appear in relation to the formation of serrations at primordium margin.

• Analysis of *TAA1* and *YUC4* expression suggests that the generation of lateral auxin sources at primordium margins is related to the localized auxin biosynthesis. However, it is the PIN1-mediated polar auxin transport, which is crucial for the high auxin response in lateral sources. Accordingly, chemical or genetic suppression of auxin transport leads to the disappearance of lateral auxin sources.

• Apical auxin source does not depend on auxin biosynthesis since no local upregulation of neither *TAA1* and *YUC4* has been found at apical primordium region. However, both chemical and genetic suppression of the polar auxin transport partially disrupts the auxin response at apical primordium region indicating that the maintenance of the apical source relies on the auxin transport.

• In contrast to lateral auxin sources, the apical source is more plastic. After cell ablation at apical primordium region, the auxin response is more extended towards non-wounding region. This may indicate the regeneration of the source or/and primordium tip.

• The midvein in leaf primordia undergoes developmental changes. Namely, procambial cell length and the midvein width increase during primordium growth. The differentiation of cells in the midvein proceeds acropetally, which is manifested in more elongated procambial cells and their higher number at the basal primordium region.

• Despite the fact that the midvein is connected to the epidermal apical auxin source, this source is not crucial in the midvein shaping. Global auxin treatment and the NPA treatment increase the midvein width, although these treatments have different effects on the source strength. However, still the apical auxin source may affects the midvein since its getting wider after the cell ablation the at apical primordium region. It is proposed that development of the midvein depends mostly on its internal auxin concentration or/and signals from connected pre-existing vasculature of the stem. Accordingly, the disruption of the midvein continuity by the cell ablation, does affect the procambium differentiation at the midvein region above the ablation site, but not at the below region connected to the underlying stem vasculature.

• The midvein development is coupled with primordium growth. Auxin-induced increased primordium growth in length is correlated with more elongated procambial cells in the midvein. Conversely, NPA-induced increased primordium growth in width correlates with wider procambial cells.

• During leaf primordium development, the vascular pattern becomes more complex, that is manifested in the increased number of higher-order strands and loops, branching points, and strand density. The first second-order procambial strands and loops are formed at apical primordium region without any apparent relation to lateral auxin sources. Only strands and loops which appear in the basal primordium region are connected to lateral sources.

• Epidermal auxin sources are not necessary for the proper development of leaf vascular pattern. Neither local auxin microapplication nor auxin global treatment affects significantly the vascular pattern. Although, the NPA treatment and *pin1* mutation inhibit the formation of loops and disrupt branching of higher-order strands, these effects result rather from lower auxin flux or/and related auxin levels in the vascular strands. The lack of lateral auxin sources in *cuc2cuc3* mutant or the ablation of these sources is not associated with serious disruption in the vascular pattern. However, the presence of epidermal lateral sources is necessary for the induction of free-ending vascular strands which normally would terminate in serrations.

• There are two gradients related to the formation of leaf vasculature. The first gradient concerns the procambium differentiation in new strands which proceeds from branching points at pre-existing strands. This applies to both the primary (the midvein) and second-order strands. The second gradient concerns the formation of new second-order strands and loops which occurs in the basipetal direction in a leaf primordium. The first gradient likely depends on signals from pre-existing vasculature, while the second gradient is associated with growth and differentiation gradients in leaf primordia.

7. REFERENCES

Adamowski, Maciek, and Jiří Friml. 2015. “PIN-Dependent Auxin Transport: Action, Regulation, and Evolution.” *The Plant Cell* 27 (1): 20–32. https://doi.org/10.1105/tpc.114.134874.

Aloni, Roni. 2001. “Foliar and Axial Aspects of Vascular Differentiation: Hypotheses and Evidence.” *Journal of Plant Growth Regulation* 20 (1): 22–34. https://doi.org/10.1007/s003440010001.

Aloni, Roni, Katja Schwalm, Markus Langhans, and Cornelia I. Ullrich. 2003. “Gradual Shifts in Sites of Free-Auxin Production during Leaf-Primordium Development and Their Role in Vascular Differentiation and Leaf Morphogenesis in Arabidopsis.” *Planta* 216 (5): 841–53. https://doi.org/10.1007/s00425-002-0937-8.

Banasiak, Alicja, and Edyta M. Gola. 2023. “Organ Patterning at the Shoot Apical Meristem (SAM): The Potential Role of the Vascular System.” *Symmetry* 15 (2): 364. https://doi.org/10.3390/sym15020364.

Barbez, Elke, Martin Kubeš, Jakub Rolčík, Chloé Béziat, Aleš Pěnčík, Bangjun Wang, Michel Ruiz Rosquete, et al. 2012. “A Novel Putative Auxin Carrier Family Regulates Intracellular Auxin Homeostasis in Plants.” *Nature* 485 (7396): 119–22. https://doi.org/10.1038/nature11001.

Barbier de Reuille, Pierre, Anne-Lise Routier-Kierzkowska, Daniel Kierzkowski, George W Bassel, Thierry Schüpbach, Gerardo Tauriello, Namrata Bajpai, et al. 2015. “MorphoGraphX: A Platform for Quantifying Morphogenesis in 4D.” *ELife* 4 (May). https://doi.org/10.7554/eLife.05864.

Bayer, Emmanuelle M, Richard S Smith, Therese Mandel, Naomi Nakayama, Michael Sauer, Przemyslaw Prusinkiewicz, and Cris Kuhlemeier. 2009. “Integration of Transport-Based Models for Phyllotaxis and Midvein Formation.” *Genes & Development* 23 (3): 373–84. https://doi.org/10.1101/gad.497009.

Benková, Eva, Marta Michniewicz, Michael Sauer, Thomas Teichmann, Daniela Seifertová, Gerd Jürgens, and Jiří Friml. 2003. “Local, Efflux-Dependent Auxin Gradients as a Common Module for Plant Organ Formation.” *Cell* 115 (5): 591–602. https://doi.org/10.1016/S0092-8674(03)00924-3.

Berleth, Thomas, Jim Mattsson, and Christian S Hardtke. 2000. “Vascular Continuity and Auxin Signals.” *Trends in Plant Science* 5 (9): 387–393. https://doi.org/10.1016/S1360-1385(00)01725-8.

Biedroń, Magdalena, and Alicja Banasiak. 2018. "Auxin-Mediated Regulation of Vascular Patterning in Arabidopsis Thaliana Leaves." *Plant Cell Reports* 37 (9): 1215–29. https://doi.org/10.1007/s00299-018-2319-0.

Bilsborough, Gemma D., Adam Runions, Michalis Barkoulas, Huw W. Jenkins, Alice Hasson, Carla Galinha, Patrick Laufs, Angela Hay, Przemyslaw Prusinkiewicz, and Miltos Tsiantis. 2011. "Model for the Regulation of *Arabidopsis Thaliana* Leaf Margin Development." *Proceedings of the National Academy of Sciences* 108 (8): 3424–29. https://doi.org/10.1073/pnas.1015162108.

Brackmann, Kalus, Jiyan Qi, Michaela Gebert, Virginie Jouannet, Theresa Schlamp, Karin Grunwald, Eva-Sophie Wallner, Daia Novikova, Victor Levitsky, Javier Agusti, Pablo Sanchez, Jan U. Lohmann, and Thomas Greb. 2018. "Spatial specificity of auxin responses coordinates wood formation." *Nature Communications* 9: 875. https://doi.org/10.1038/s41467-018-03256-2.

Burian, Agata. 2021. "Does Shoot Apical Meristem Function as the Germline in Safeguarding Against Excess of Mutations?" *Frontiers in Plant Science* 12 (August). https://doi.org/10.3389/fpls.2021.707740.

Burian, Agata, Magdalena Raczyńska-Szajgin, and Wojtek Pałubicki. 2021. "Shaping Leaf Vein Pattern by Auxin and Mechanical Feedback." *Journal of Experimental Botany* 72 (4): 964–67. https://doi.org/10.1093/jxb/eraa499.

Burian, Agata, Magdalena Raczyńska-Szajgin, Dorota Borowska-Wykręt, Agnieszka Piatek, Mitsuhiro Aida, and Dorota Kwiatkowska. 2015. "The CUP-SHAPED COTYLEDON2 and 3 Genes Have a Post-Meristematic Effect on Arabidopsis Thaliana Phyllotaxis." *Annals of Botany* 115 (5): 807–20. https://doi.org/10.1093/aob/mcv013.

Busse, James S., and Ray F. Evert. 1999. "Vascular Differentiation and Transition in the Seedling of *Arabidopsis Thaliana* (Brassicaceae)." *International Journal of Plant Sciences* 160 (2): 241–51. https://doi.org/10.1086/314117.

Candela, Héctor, Antonio Martínez-Laborda, and José Luis Micol. 1999. "Venation Pattern Formation InArabidopsis ThalianaVegetative Leaves." *Developmental Biology* 205 (1): 205–16. https://doi.org/10.1006/dbio.1998.9111.

Cao, Xu, Honglei Yang, Chunqiong Shang, Sang Ma, Li Liu, and Jialing Cheng. 2019. “The Roles of Auxin Biosynthesis YUCCA Gene Family in Plants.” *International Journal of Molecular Sciences* 20 (24): 6343. https://doi.org/10.3390/ijms20246343.

Carland, Francine, Andrew Defries, Sean Cutler, and Timothy Nelson. 2016. “Novel Vein Patterns in Arabidopsis Induced by Small Molecules.” *Plant Physiology* 170 (1): 338–53. https://doi.org/10.1104/pp.15.01540.

Chen, Yiru, Yordan S. Yordanov, Cathleen Ma, Steven Strauss, and Victor B. Busov. 2013. “DR5 as a Reporter System to Study Auxin Response in Populus.” *Plant Cell Reports* 32 (3): 453–63. https://doi.org/10.1007/s00299-012-1378-x.

Chitwood, Daniel H., Lauren R. Headland, Aashush Ranjan, Ciera Martinez, Siobhan A. Braybrook, Daniel P. Koenig, Cris Kuhlemeier, Richard S. Smith, and Neelima R. Sinha. 2012. “Leaf asymmetry as a developmental constraint imposed by auxin-dependent phyllotactic patterning.” *Th e Plant Cell* 24: 2318–2327. https://doi.org/10.1105/tpc.112.098798.

Collett, Clare E., Nicholas P. Harberd, and Ottoline Leyser. 2000. “Hormonal interactions in the control of Arabidopsis hypocotyl elongation.” *Plant Physiology* 124: 553–61.

Corson, Francis, Mokhtar Adda-Bedia, and Arezki Boudaoud. 2009. “In Silico Leaf Venation Networks: Growth and Reorganization Driven by Mechanical Forces.” *Journal of Theoretical Biology* 259 (3): 440–48. https://doi.org/10.1016/j.jtbi.2009.05.002.

Couder, Y., L. Pauchard, C. Allain, M. Adda-Bedia, and S. Douady. 2002. “The Leaf Venation as Formed in a Tensorial Field.” *The European Physical Journal B* 28 (2): 135–38. https://doi.org/10.1140/epjb/e2002-00211-1.

Dengler, Nancy G. 2006. “The Shoot Apical Meristem and Development of Vascular ArchitectureThis Review Is One of a Selection of Papers Published on the Special Theme of Shoot Apical Meristems.” *Canadian Journal of Botany* 84 (11): 1660–71. https://doi.org/10.1139/b06-126.

Donner, Tyler J., Ira Sherr, and Enrico Scarpella. 2009. “Regulation of Preprocambial Cell State Acquisition by Auxin Signaling in *Arabidopsis* Leaves.” *Development* 136 (19): 3235–46. https://doi.org/10.1242/dev.037028.

Du, Fei, Chunmei Guan, and Yuling Jiao. 2018. “Molecular Mechanisms of Leaf Morphogenesis.” *Molecular Plant* 11 (9): 1117–34. https://doi.org/10.1016/j.molp.2018.06.006.

Echevin, Emilie, Constance Le Gloanec, Nikolina Skowrońska, Anne-Lise Routier-Kierzkowska, Agata Burian, and Daniel Kierzkowski. 2019. “Growth and Biomechanics of Shoot Organs.” *Journal of Experimental Botany* 70 (14): 3573–85. https://doi.org/10.1093/jxb/erz205.

Endrizzi, Karin, Bernard Moussian, Achim Haecker, Joshua Z. Levin, and Thomas Laux. 1996. “The SHOOT MERISTEMLESS Gene Is Required for Maintenance of Undifferentiated Cells in Arabidopsis Shoot and Floral Meristems and Acts at a Different Regulatory Level than the Meristem Genes WUSCHEL and ZWILLE.” *The Plant Journal* 10 (6): 967–79. https://doi.org/10.1046/j.1365-313X.1996.10060967.x.

Evert, Ray F. 2006. “Frontmatter.” In *Esau’s Plant Anatomy*, i–xx. Hoboken, NJ, USA: John Wiley & Sons, Inc. https://doi.org/10.1002/0470047380.fmatter.

Feller, Chrystel, Etienne Farcot, and Christian Mazza. 2015. “Self-Organization of Plant Vascular Systems: Claims and Counter-Claims about the Flux-Based Auxin Transport Model.” Edited by Miguel A Blazquez. *PLOS ONE* 10 (3): e0118238. https://doi.org/10.1371/journal.pone.0118238.

Feugier, Francois G., A. Mochizuki, and Y. Iwasa. 2005. “Self-Organization of the Vascular System in Plant Leaves: Inter-Dependent Dynamics of Auxin Flux and Carrier Proteins.” *Journal of Theoretical Biology* 236 (4): 366–75. https://doi.org/10.1016/j.jtbi.2005.03.017.

Friml, Jiří, and Justyna Wiśniewska. 2018. “Auxin as an Intercellular Signal.” In *Annual Plant Reviews Online*, 1–26. Chichester, UK: John Wiley & Sons, Ltd. https://doi.org/10.1002/9781119312994.apr0153.

Galvan-Ampudia, Carlos S, Guillaume Cerutti, Jonathan Legrand, Géraldine Brunoud, Raquel Martin-Arevalillo, Romain Azais, Vincent Bayle, et al. 2020. “Temporal Integration of Auxin Information for the Regulation of Patterning.” *ELife* 9 (May): 1–65. https://doi.org/10.7554/eLife.55832.

Gardiner, Jason, Tyler J. Donner, and Enrico Scarpella. 2011. “Simultaneous Activation of SHR and ATHB8 Expression Defines Switch to Preprocambial Cell State in Arabidopsis Leaf Development.” *Developmental Dynamics* 240 (1): 261–70. https://doi.org/10.1002/dvdy.22516.

Govindaraju, Priyanka, Carla Verna, Tongbo Zhu, and Enrico Scarpella. 2020. “Vein Patterning by Tissue-Specific Auxin Transport.” *Development* 147 (13). https://doi.org/10.1242/dev.187666.

Guenot, Bernadette, Emmanuelle Bayer, Daniel Kierzkowski, Richard S. Smith, Therese Mandel, Petra Žádníková, Eva Benková, and Cris Kuhlemeier. 2012. “PIN1-Independent Leaf Initiation in Arabidopsis .” *Plant Physiology* 159 (4): 1501–10. https://doi.org/10.1104/pp.112.200402.

Ha, Chan Man, Ji Hyung Jun, and Jennifer C. Fletcher. 2010. “Shoot Apical Meristem Form and Function.” In *Current Topics in Developmental Biology*, 91:103–40. Academic Press Inc. https://doi.org/10.1016/S0070-2153(10)91004-1.

Heidstra, Renze, and Sabrina Sabatini. 2014. “Plant and Animal Stem Cells: Similar yet Different.” *Nature Reviews. Molecular Cell Biology* 15 (5): 301–12. https://doi.org/10.1038/nrm3790.

Holloway, David M, and Carol L Wenzel. 2021. “Polar Auxin Transport Dynamics of Primary and Secondary Vein Patterning in Dicot Leaves.” Edited by Amy Marshall-Colon. *In Silico Plants* 3 (2): 1–17. https://doi.org/10.1093/insilicoplants/diab030.

Husbands, Aman Y., Anna H. Benkovics, Fabio T.S. Nogueira, Mukesh Lodha, and Marja C.P. Timmermans. 2016. “The ASYMMETRIC LEAVES Complex Employs Multiple Modes of Regulation to Affect Adaxial-Abaxial Patterning and Leaf Complexity.” *The Plant Cell* 27 (12): 3321–35. https://doi.org/10.1105/tpc.15.00454.

Jedličková, Veronika, Shekoufeh Ebrahimi Naghani, and Hélène S Robert. 2022. “On the Trail of Auxin: Reporters and Sensors.” *The Plant Cell* 34 (9): 3200–3213. https://doi.org/10.1093/plcell/koac179.

Jönsson, Henrik, Marcus G. Heisler, Bruce E. Shapiro, Elliot M. Meyerowitz, and Eric Mjolsness. 2006. “An Auxin-Driven Polarized Transport Model for Phyllotaxis.” *Proceedings of the National Academy of Sciences* 103 (5): 1633–38. https://doi.org/10.1073/pnas.0509839103.

Kang, Julie, and Nancy Dengler. 2004. “Vein Pattern Development in Adult Leaves of *Arabidopsis Thaliana*.” *International Journal of Plant Sciences* 165 (2): 231–42. https://doi.org/10.1086/382794.

Kastanaki, Elizabeth, Noel Blanco-Touriñán, Alexis Sarazin, Alessandra Sturchler, Bojan Gujas, Francisco Vera-Sirera, Javier Agustí, and Antia Rodriguez-Villalon. 2022a. “A Genetic Framework for Proximal Secondary Vein Branching in the *Arabidopsis Thaliana* Embryo.” *Development* 149 (12). https://doi.org/10.1242/dev.200403.

Kastanaki, Elizabeth, Noel Blanco-Tourinãán, Alexis Sarazin, Alessandra Sturchler, Bojan Gujas, Francisco Vera-Sirera, Javier Agustı, and Antia Rodriguez-Villalon. 2022b. “A Genetic

Framework for Proximal Secondary Vein Branching in the Arabidopsis Thaliana Embryo." *Development (Cambridge)* 149 (12). https://doi.org/10.1242/dev.200403.

Kawamura, Eiko, Gorou Horiguchi, and Hirokazu Tsukaya. 2010. "Mechanisms of Leaf Tooth Formation in Arabidopsis." *The Plant Journal* 62 (3): 429–41. https://doi.org/10.1111/j.1365-313X.2010.04156.x.

Kierzkowski, Daniel, Adam Runions, Francesco Vuolo, Sören Strauss, Rena Lymbouridou, Anne-Lise Routier-Kierzkowska, David Wilson-Sánchez, et al. 2019. "A Growth-Based Framework for Leaf Shape Development and Diversity." *Cell* 177 (6): 1405-1418.e17. https://doi.org/10.1016/j.cell.2019.05.011.

Kneuper, Irina, William Teale, Jonathan Edward Dawson, Ryuji Tsugeki, Eleni Katifori, Klaus Palme, and Franck Anicet Ditengou. 2021. "Auxin Biosynthesis and Cellular Efflux Act Together to Regulate Leaf Vein Patterning." Edited by Daniel Gibbs. *Journal of Experimental Botany* 72 (4): 1151–65. https://doi.org/10.1093/jxb/eraa501.

Kubeš, Martin, and Richard Napier. 2019. "Non-Canonical Auxin Signalling: Fast and Curious." *Journal of Experimental Botany* 70 (10): 2609–14. https://doi.org/10.1093/jxb/erz111.

Kuhlemeier, Cris. 2007. "Phyllotaxis." *Trends in Plant Science* 12 (4): 143–50. https://doi.org/10.1016/j.tplants.2007.03.004.

Kwiatkowska, D. 2004. "Structural Integration at the Shoot Apical Meristem: Models, Measurements, and Experiments." *American Journal of Botany* 91 (9): 1277–93. https://doi.org/10.3732/ajb.91.9.1277.

Laguna, Maria F, Steffen Bohn, and Eduardo A Jagla. 2008. "The Role of Elastic Stresses on Leaf Venation Morphogenesis." Edited by Philip E. Bourne. *PLoS Computational Biology* 4 (4): e1000055. https://doi.org/10.1371/journal.pcbi.1000055.

Leyser, Ottoline. 2018. "Auxin Signaling." *Plant Physiology* 176 (1): 465–79. https://doi.org/10.1104/pp.17.00765.

Liao, Che-Yang, Wouter Smet, Geraldine Brunoud, Saiko Yoshida, Teva Vernoux, and Dolf Weijers. 2015. "Reporters for Sensitive and Quantitative Measurement of Auxin Response." *Nature Methods* 12 (3): 207–10, 2 p following 210. https://doi.org/10.1038/nmeth.3279.

Lièvre, Maryline, Christine Granier, and Yann Guédon. 2016. "Identifying Developmental Phases in the *Arabidopsis Thaliana* Rosette Using Integrative Segmentation Models." *New Phytologist* 210 (4): 1466–78. https://doi.org/10.1111/nph.13861.

Linh, Nguyen Manh, and Enrico Scarpella. 2022. “Leaf Vein Patterning Is Regulated by the Aperture of Plasmodesmata Intercellular Channels.” Edited by Mark Estelle. *PLOS Biology* 20 (9): e3001781. https://doi.org/10.1371/journal.pbio.3001781.

Linh, Nguyen Manh, Carla Verna, and Enrico Scarpella. 2018. “Coordination of Cell Polarity and the Patterning of Leaf Vein Networks.” *Current Opinion in Plant Biology* 41 (February): 116–24. https://doi.org/10.1016/j.pbi.2017.09.009.

Louveaux, Marion, Jean-Daniel Julien, Vincent Mirabet, Arezki Boudaoud, and Olivier Hamant. 2016. “Cell Division Plane Orientation Based on Tensile Stress in *Arabidopsis Thaliana*.” *Proceedings of the National Academy of Sciences* 113 (30): E4294–4303. https://doi.org/10.1073/pnas.1600677113.

Lucas, William J., Andrew Groover, Raffael Lichtenberger, Kaori Furuta, Shri-Ram Yadav, Ykä Helariutta, Xin-Qiang He, et al. 2013. “The Plant Vascular System: Evolution, Development and Functions [F].” *Journal of Integrative Plant Biology* 55 (4): 294–388. https://doi.org/10.1111/jipb.12041.

Lyndon, R. F. 1990. “Root and Shoot Meristems: Structure and Growth.” In *Plant Development*, 19–38. Dordrecht: Springer Netherlands. https://doi.org/10.1007/978-94-011-7979-9_2.

Majda, Mateusz, and Stéphanie Robert. 2018. “The Role of Auxin in Cell Wall Expansion.” *International Journal of Molecular Sciences* 19 (4): 951. https://doi.org/10.3390/ijms19040951.

Mano, Y., and K. Nemoto. 2012. “The Pathway of Auxin Biosynthesis in Plants.” *Journal of Experimental Botany* 63 (8): 2853–72. https://doi.org/10.1093/jxb/ers091.

Marcos, Danielle, and Thomas Berleth. 2014. “Dynamic Auxin Transport Patterns Preceding Vein Formation Revealed by Live-Imaging of Arabidopsis Leaf Primordia.” *Frontiers in Plant Science* 5 (JUN). https://doi.org/10.3389/fpls.2014.00235.

Mattsson, Jim, Wenzislava Ckurshumova, and Thomas Berleth. 2003. “Auxin Signaling in Arabidopsis Leaf Vascular Development.” *Plant Physiology* 131 (3): 1327–39. https://doi.org/10.1104/pp.013623.

Mattsson, Jim, Z. Renee Sung, and Thomas Berleth. 1999. “Responses of Plant Vascular Systems to Auxin Transport Inhibition.” *Development* 126 (13): 2979–91. https://doi.org/10.1242/dev.126.13.2979.

Mayer, Klaus F.X, Heiko Schoof, Achim Haecker, Michael Lenhard, Gerd Jürgens, and Thomas Laux. 1998. “Role of WUSCHEL in Regulating Stem Cell Fate in the Arabidopsis Shoot Meristem.” *Cell* 95 (6): 805–15. https://doi.org/10.1016/S0092-8674(00)81703-1.

Merks, Roeland M.H., Yves Van de Peer, Dirk Inzé, and Gerrit T.S. Beemster. 2007. “Canalization without Flux Sensors: A Traveling-Wave Hypothesis.” *Trends in Plant Science* 12 (9): 384–90. https://doi.org/10.1016/j.tplants.2007.08.004.

Murphy, Angus S, Karen R Hoogner, Wendy Ann Peer, and Lincoln Taiz. 2002. “Identification, Purification, and Molecular Cloning of N-1-Naphthylphthalmic Acid-Binding Plasma Membrane-Associated Aminopeptidases from Arabidopsis.” *Plant Physiology* 128 (3): 935–50. https://doi.org/10.1104/pp.010519.

Nelson, T., and N. Dengler. 1997. “Leaf Vascular Pattern Formation.” *The Plant Cell* 9 (July): 1121–35. https://doi.org/10.1105/tpc.9.7.1121.

Nikovics, Krisztina, Thomas Blein, Alexis Peaucelle, Tetsuya Ishida, Halima Morin, Mitsuhiro Aida, and Patrick Laufs. 2006. “The Balance between the MIR164A and CUC2 Genes Controls Leaf Margin Serration in Arabidopsis.” *The Plant Cell* 18 (11): 2929–45. https://doi.org/10.1105/tpc.106.045617.

Nishimura, Takeshi, Ken-ichiro Hayashi, Hiromi Suzuki, Atsuko Gyohda, Chihiro Takaoka, Yusuke Sakaguchi, Sachiko Matsumoto, et al. 2014. “Yucasin Is a Potent Inhibitor of YUCCA, a Key Enzyme in Auxin Biosynthesis.” *The Plant Journal* 77 (3): 352–66. https://doi.org/10.1111/tpj.12399.

Perico, Chiara, Sovanna Tan, and Jane A. Langdale. 2022. “Developmental Regulation of Leaf Venation Patterns: Monocot versus Eudicots and the Role of Auxin.” *New Phytologist* 234 (3): 783–803. https://doi.org/10.1111/nph.17955.

Petrášek, Jan, and Jiří Friml. 2009. “Auxin Transport Routes in Plant Development.” *Development* 136 (16): 2675–88. https://doi.org/10.1242/dev.030353.

Petricka, Jalean Joyanne, Nicole Kho Clay, and Timothy Mark Nelson. 2008. “Vein Patterning Screens and the *Defectively Organized Tributaries* Mutants in *Arabidopsis Thaliana*.” *The Plant Journal* 56 (2): 251–63. https://doi.org/10.1111/j.1365-313X.2008.03595.x.

Ravichandran, Sree Janani, Nguyen Manh Linh, and Enrico Scarpella. 2020. “The Canalization Hypothesis – Challenges and Alternatives.” *New Phytologist* 227 (4): 1051–59. https://doi.org/10.1111/nph.16605.

Reinhardt, Didier, and Edyta M. Gola. 2022. “Law and Order in Plants – the Origin and Functional Relevance of Phyllotaxis.” *Trends in Plant Science*. 27 (10): 1017–32. https://doi.org/10.1016/j.tplants.2022.04.005.

Reinhardt, Didier, Eva-Rachele Pesce, Pia Stieger, Therese Mandel, Kurt Baltensperger, Malcolm Bennett, Jan Traas, Jiří Friml, and Cris Kuhlemeier. 2003. “Regulation of Phyllotaxis by Polar Auxin Transport.” *Nature* 426 (6964): 255–60. https://doi.org/10.1038/nature02081.

Robert, Helene S., Peter Grones, Anna N. Stepanova, Linda Robies, Annemarie Lokerse, Jose M. Alonso, Dolf Weijers, and Jiri Friml. 2013. “Local auxin sources orient the apical-basal axis in Arabidopsis Embryos.” *Current Biology* 23: 1–7. https://doi.org/10.1016/j.cub.2013.09.039.

Rolland-Lagan, Anne-Gaëlle, and Przemyslaw Prusinkiewicz. 2005. “Reviewing Models of Auxin Canalization in the Context of Leaf Vein Pattern Formation in Arabidopsis.” *The Plant Journal* 44 (5): 854–65. https://doi.org/10.1111/j.1365-313X.2005.02581.x.

Runions, Adam, Martin Fuhrer, Brendan Lane, Pavol Federl, Anne-Gaëlle Rolland-Lagan, and Przemyslaw Prusinkiewicz. 2005. “Modeling and Visualization of Leaf Venation Patterns.” In *ACM SIGGRAPH 2005 Papers*, 702–11. New York, NY, USA: ACM. https://doi.org/10.1145/1186822.1073251.

Runions, Adam, Miltos Tsiantis, and Przemyslaw Prusinkiewicz. 2017. “A Common Developmental Program Can Produce Diverse Leaf Shapes.” *New Phytologist* 216 (2): 401–18. https://doi.org/10.1111/nph.14449.

Sabatini, Sabrina, Dimitris Beis, Harald Wolkenfelt, Jane Murfett, Tom Guilfoyle, Jocelyn Malamy, Philip Benfey, et al. 1999. “An Auxin-Dependent Distal Organizer of Pattern and Polarity in the Arabidopsis Root.” *Cell* 99 (5): 463–72. https://doi.org/10.1016/S0092-8674(00)81535-4.

Sachs, Tsvi. 1969. “Polarity and the Induction of Organized Vascular Tissues.” *Annals of Botany* 33 (2): 263–75. https://doi.org/10.1093/oxfordjournals.aob.a084281.

Sachs, Tsvi. 1981. “The Control of the Patterned Differentiation of Vascular Tissues.” In , 151–262. https://doi.org/10.1016/S0065-2296(08)60351-1.

Sack, Lawren, and Christine Scoffoni. 2013. “Leaf Venation: Structure, Function, Development, Evolution, Ecology and Applications in the Past, Present and Future.” *New Phytologist* 198 (4): 983–1000. https://doi.org/10.1111/nph.12253.

Sauer, Michael, Jozef Balla, Christian Luschnig, Justyna Wiśniewska, Vilém Reinöhl, Jiří Friml, and Eva Benková. 2006. “Canalization of Auxin Flow by Aux/IAA-ARF-Dependent Feedback

Regulation of PIN Polarity." *Genes & Development* 20 (20): 2902–11. https://doi.org/10.1101/gad.390806.

Sawchuk, Megan G., Tyler J. Donner, and Enrico Scarpella. 2008. "Auxin Transport-Dependent, Stage-Specific Dynamics of Leaf Vein Formation." *Plant Signaling & Behavior* 3 (5): 286–89. https://doi.org/10.4161/psb.3.5.5345.

Sawchuk, Megan G., Philip Head, Tyler J. Donner, and Enrico Scarpella. 2007. "Time-lapse Imaging of Arabidopsis Leaf Development Shows Dynamic Patterns of Procambium Formation." *New Phytologist* 176 (3): 560–71. https://doi.org/10.1111/j.1469-8137.2007.02193.x.

Scarpella, E., M. Barkoulas, and M. Tsiantis. 2010. "Control of Leaf and Vein Development by Auxin." *Cold Spring Harbor Perspectives in Biology* 2 (1): a001511–a001511. https://doi.org/10.1101/cshperspect.a001511.

Scarpella, Enrico. 2017. "The Logic of Plant Vascular Patterning. Polarity, Continuity and Plasticity in the Formation of the Veins and of Their Networks." *Current Opinion in Genetics & Development* 45 (August): 34–43. https://doi.org/10.1016/j.gde.2017.02.009.

Scarpella, Enrico, Danielle Marcos, Jiří Friml, and Thomas Berleth. 2006. "Control of Leaf Vascular Patterning by Polar Auxin Transport." *Genes & Development* 20 (8): 1015–27. https://doi.org/10.1101/gad.1402406.

Scarpella, Enrico, and Annemarie H. Meijer. 2004. "Pattern Formation in the Vascular System of Monocot and Dicot Plant Species." *New Phytologist* 164 (2): 209–42. https://doi.org/10.1111/j.1469-8137.2004.01191.x.

Schoof, Heiko, Michael Lenhard, Achim Haecker, Klaus F.X Mayer, Gerd Jürgens, and Thomas Laux. 2000. "The Stem Cell Population of Arabidopsis Shoot Meristems Is Maintained by a Regulatory Loop between the CLAVATA and WUSCHEL Genes." *Cell* 100 (6): 635–44. https://doi.org/10.1016/S0092-8674(00)80700-X.

Sieburth, Leslie E. 1999. "Auxin Is Required for Leaf Vein Pattern in Arabidopsis." *Plant Physiology* 121 (4): 1179–90. https://doi.org/10.1104/pp.121.4.1179.

Smith, Richard S., and Emmanuelle M. Bayer. 2009. "Auxin Transport-Feedback Models of Patterning in Plants." *Plant, Cell & Environment* 32 (9): 1258–71. https://doi.org/10.1111/j.1365-3040.2009.01997.x.

Smith, Richard S., Soazig Guyomarc'h, Therese Mandel, Didier Reinhardt, Cris Kuhlemeier, and Przemyslaw Prusinkiewicz. 2006. "A Plausible Model of Phyllotaxis." *Proceedings of the National Academy of Sciences* 103 (5): 1301–6. https://doi.org/10.1073/pnas.0510457103.

Stepanova, Anna N., Joyce Robertson-Hoyt, Jeonga Yun, Larissa M. Benavente, De-Yu Xie, Karel Doležal, Alexandra Schlereth, Gerd Jürgens, and Jose M. Alonso. 2008. "TAA1-Mediated Auxin Biosynthesis Is Essential for Hormone Crosstalk and Plant Development." *Cell* 133 (1): 177–91. https://doi.org/10.1016/j.cell.2008.01.047.

Stepanova, Anna N., Jeonga Yun, Linda M. Robles, Ondrej Novak, Wenrong He, Hongwei Guo, Karin Ljung, and Jose M. Alonso. 2011. "The *Arabidopsis* YUCCA1 Flavin Monooxygenase Functions in the Indole-3-Pyruvic Acid Branch of Auxin Biosynthesis." *The Plant Cell* 23 (11): 3961–73. https://doi.org/10.1105/tpc.111.088047.

Suzuki, Masashi, Chiaki Yamazaki, Marie Mitsui, Yusuke Kakei, Yuka Mitani, Ayako Nakamura, Takahiro Ishii, Kazuo Soeno, and Yukihisa Shimada. 2015. "Transcriptional Feedback Regulation of YUCCA Genes in Response to Auxin Levels in Arabidopsis." *Plant Cell Reports* 34 (8): 1343–52. https://doi.org/10.1007/s00299-015-1791-z.

Swarup, Ranjan, and Benjamin Péret. 2012. "AUX/LAX Family of Auxin Influx Carriers—an Overview." *Frontiers in Plant Science* 3 (OCT). https://doi.org/10.3389/fpls.2012.00225.

Truernit, Elisabeth, Hélène Bauby, Bertrand Dubreucq, Olivier Grandjean, John Runions, Julien Barthélémy, and Jean-Christophe Palauqui. 2008. "High-Resolution Whole-Mount Imaging of Three-Dimensional Tissue Organization and Gene Expression Enables the Study of Phloem Development and Structure in *Arabidopsis*." *The Plant Cell* 20 (6): 1494–1503. https://doi.org/10.1105/tpc.107.056069.

Tsukaya, Hirokazu, Keiko Shoda, Gyung-Tae Kim, and Hirofumi Uchimiya. 2000. "Heteroblasty in Arabidopsis Thaliana (L.) Heynh." *Planta* 210 (4): 536–42. https://doi.org/10.1007/s004250050042.

Ursache, Robertas, Tonni Grube Andersen, Peter Marhavý, and Niko Geldner. 2018. "A Protocol for Combining Fluorescent Proteins with Histological Stains for Diverse Cell Wall Components." *The Plant Journal* 93 (2): 399–412. https://doi.org/10.1111/tpj.13784.

Verna, Carla, Sree Janani Ravichandran, Megan G Sawchuk, Nguyen Manh Linh, and Enrico Scarpella. 2019. "Coordination of Tissue Cell Polarity by Auxin Transport and Signaling." *ELife* 8 (December). https://doi.org/10.7554/eLife.51061.

Verna, Carla, Megan G. Sawchuk, Nguyen Manh Linh, and Enrico Scarpella. 2015a. “Control of Vein Network Topology by Auxin Transport.” *BMC Biology* 13 (1): 94. https://doi.org/10.1186/s12915-015-0208-3.

Vernoux, Teva, Géraldine Brunoud, Etienne Farcot, Valérie Morin, Hilde Van den Daele, Jonathan Legrand, Marina Oliva, et al. 2011. “The Auxin Signalling Network Translates Dynamic Input into Robust Patterning at the Shoot Apex.” *Molecular Systems Biology* 7 (1). https://doi.org/10.1038/msb.2011.39.

Wang, Bing, Jinfang Chu, Tianying Yu, Qian Xu, Xiaohong Sun, Jia Yuan, Guosheng Xiong, Guodong Wang, Yonghong Wang, and Jiayang Li. 2015. “Tryptophan-Independent Auxin Biosynthesis Contributes to Early Embryogenesis in *Arabidopsis*.” *Proceedings of the National Academy of Sciences* 112 (15): 4821–26. https://doi.org/10.1073/pnas.1503998112.

Wenzel, Carol L., Mathias Schuetz, Qian Yu, and Jim Mattsson. 2007. “Dynamics of MONOPTEROS and PIN-FORMED1 Expression during Leaf Vein Pattern Formation in Arabidopsis Thaliana.” *Plant Journal* 49 (3): 387–98. https://doi.org/10.1111/j.1365-313X.2006.02977.x.

Wuyts, Nathalie, Jean-Christophe Palauqui, Geneviève Conejero, Jean-Luc Verdeil, Christine Granier, and Catherine Massonnet. 2010. “High-Contrast Three-Dimensional Imaging of the Arabidopsis Leaf Enables the Analysis of Cell Dimensions in the Epidermis and Mesophyll.” *Plant Methods* 6 (1): 17. https://doi.org/10.1186/1746-4811-6-17.

Yagi, Hiroki, Kentaro Tamura, Tomonao Matsushita, and Tomoo Shimada. 2021. “Spatiotemporal Relationship between Auxin Dynamics and Hydathode Development in *Arabidopsis* Leaf Teeth.” *Plant Signaling & Behavior* 16 (12). https://doi.org/10.1080/15592324.2021.1989216.

Yoshida, Saiko, Therese Mandel, and Cris Kuhlemeier. 2011. “Stem Cell Activation by Light Guides Plant Organogenesis.” *Genes & Development* 25 (13): 1439–50. https://doi.org/10.1101/gad.631211.

Žádníková, Petra, and Rüdiger Simon. 2014. “How Boundaries Control Plant Development.” *Current Opinion in Plant Biology* 17 (1): 116–25. https://doi.org/10.1016/j.pbi.2013.11.013.

Zazímalová, Eva, Angus S Murphy, Haibing Yang, Klára Hoyerová, and Petr Hosek. 2010. “Auxin Transporters--Why so Many?” *Cold Spring Harbor Perspectives in Biology* 2 (3): a001552. https://doi.org/10.1101/cshperspect.a001552.

Zhang, Tian-Qi, Yu Chen, and Jia-Wei Wang. 2021. “A Single-Cell Analysis of the Arabidopsis Vegetative Shoot Apex.” *Developmental Cell* 56 (7): 1056-1074.e8. https://doi.org/10.1016/j.devcel.2021.02.021.

Zhao, Yunde. 2012. “Auxin Biosynthesis: A Simple Two-Step Pathway Converts Tryptophan to Indole-3-Acetic Acid in Plants.” In *Molecular Plant*, 5:334–38. Oxford University Press. https://doi.org/10.1093/mp/ssr104.

8. SUMMARY

The vascular system in plants is necessary for the distribution of water and nutrients, the propagation of signalling molecules, and the mechanical support. The development of vascular system in dicot leaves is hierarchical and occurs in the continuity with the pre-existing stem vasculature. The mechanism of vasculature formation is usually explained in terms of canalization hypothesis, where the newly formed vascular strands are specified by pathways of auxin flow from auxin sources to pre-existing vascular strands (auxin sink). Thus, the aim of this study was to test experimentally a role of epidermal auxin sources and existing vasculature in the formation of the vascular pattern in growing leaf primordia of *Arabidopsis thaliana*. With using auxin-related reporters, the initiation of vascular strands has been monitoring over time in undisturbed conditions and after different (chemical, genetic, mechanical) disturbances of epidermal auxin sources and existing vasculature. The *in vivo* imaging has been coupled with clearing procedure enabling the analysis of procambium differentiation process. It has been found that the auxin source at apical primordium region does not depend on localized auxin biosynthesis, however, the PIN1-dependent polar auxin transport contributes to their maintenance. In contrast, the generation of lateral auxin sources at primordium margins is correlated to the localized auxin biosynthesis, and strongly depends on the polar auxin transport. Experimental manipulations suggest that epidermal auxin sources are not crucial for the development of the midvein in leaf primordia. Instead, it is proposed that midvein development depends on its internal auxin concentration or/and signals from connected pre-existing vasculature of the stem. Also, epidermal auxin sources are not necessary for the proper development of the vascular pattern. It is rather auxin flow or/and related auxin levels in the vascular strands that affects the overall vascular pattern in leaf primordia.

9. STRESZCZENIE

Układ waskularny u roślin jest niezbędny do transportu wody, składników odżywczych, cząsteczek sygnałowych, a także do wsparcia mechanicznego. Rozwój systemu waskularnego w liściach roślin dwuliściennych jest hierarchiczny i przebiega w ciągłości z istniejącym systemem waskularnym łodygi. Mechanizm powstawania waskulatury jest zazwyczaj tłumaczony przez hipotezę kanalizacji która zakłada, że nowo powstałe pasma waskularne są definiowane przez ścieżki przepływu auksyny ze źródła auksyny do wcześniej powstałych pasm waskularnych (zlewni auksyny). Dlatego też celem niniejszej pracy było eksperymentalne sprawdzenie jaką rolę w tworzeniu wzoru waskularnego w rosnących zawiązkach liści *Arabidopsis thaliana* pełnią epidermalne źródła auksyny oraz istniejące pasma waskularne. Inicjacja powstawania systemu waskularnego była monitorowana w czasie przy użyciu reporterów związanych z auksyną w niezaburzanych warunkach jak i po różnych (chemicznych, genetycznych, mechanicznych) zaburzeniach źródeł auksyny oraz istniejącego systemu waskularnego. Obrazowanie *in vivo* zostało połączone z metodą prześwietleniową, która umożliwiła analizę procesu różnicowania komórek prokambium. Stwierdzono, że źródło auksyny w apikalnym regionie zawiązka jest niezależne od zlokalizowanej biosyntezy auksyny, jednak zależny od PIN1 polarny transport auksyny ma wkład w jego utrzymanie. W przeciwieństwie do tego, powstawanie bocznych źródeł auksyny w częściach marginalnych zawiązka jest skorelowane z lokalną biosyntezą auksyny, oraz jest zależne od polarnego transportu auksyny. Z przeprowadzonych manipulacji eksperymentalnych wynika, że źródła auksyny w epidermie nie są kluczowe dla rozwoju nerwu głównego w zawiązkach liści. Natomiast proponuje się, że powstawanie i rozwój nerwu głównego zależy od wewnętrznej koncentracji auksyny i/lub sygnałów z połączonego systemu waskularnego łodygi. Ponadto, epidermalne źródła auksyny nie są niezbędne do prawidłowego rozwoju wzoru waskularnego, a raczej przepływ auksyny i/lub stężenie auksyny w pasmach waskularnych wpływają na kształtowanie ogólnego wzoru waskularnego w zawiązkach liści.